Alma Mater Studiorum · University of Bologna

School of Science
Department of Physics and Astronomy
Master Degree in Physics

MEASUREMENT INDUCED PHASE TRANSITIONS IN FREE-FERMIONIC QUANTUM CIRCUITS

Supervisor:
Dr. Lorenzo Piroli

Submitted by:
Matteo Barbieri

Academic Year 2023/2024

Abstract

The advent of quantum simulation platforms has motivated the study of new theoretical "quantum circuit" models for the dynamics of quantum many-body systems. In recent years, these models have revealed new many-body phenomena of physical interest. A particularly important example is that of the so-called measurement induced phase transitions. In this context, we will study systems that evolve through a unitary circuit, which generates quantum entanglement, interspersed with local projective measurements, which instead tend to destroy it. By increasing the frequency of these measurements, a transition between two phases is observed, in which the entanglement passes from a "volume-law" to an "area-law". The goal of this thesis is to study circuit dynamics that can be mapped onto non-interacting fermions. In this context, recent studies have demonstrated the absence of a phase transition. The objective of the thesis is to investigate whether changes to the standard measurement protocol can lead to the appearance of a transition.

Contents

Introduction

Quantum dynamical phenomena have typically been employed to explore the universal characteristics of quantum condensed matter at low temperatures and near equilibrium. On the other hand, given that quantum coherence is easily disrupted at elevated temperatures, one might assume that quantum matter far from its ground state would not display universal dynamics that are uniquely quantum. However, the study of out-of-equilibrium dynamics in lattice models ([1], [2], [3], [4]) and quantum field theories ([5], [6]) has demonstrated that universal patterns can arise in quantum correlations and the entanglement structures within many-body systems.

These studies have been intensified by the advent of quantum simulation platforms[7]. Nowadays, Quantum Simulation and Quantum Computing have *Noisy Intermediate-Scale Quantum* (NISQ) technology at their disposal [8]. NISQ devices are quantum system that have up to hundreds of qubits, which are affected by noise. In particular, the development of *digital quantum simulators* allow for a greater degree of control of the studied systems' dynamics. Indeed the evolution on digital quantum simulators is discrete in time and it is done via *unitary gates*, *measurements* and *feedback*, which lead to the study new theoretical "quantum circuit" models for the dynamics of quantum many-body systems, which revealed new many-body phenomena [9]. In these models a lattice of spins (qubits) evolve under local unitary gates and measurements and the discrete time structure (the so called "quantum circuit" [10]) recalls the trotterization of continuous time Hamiltonians. A minimally-structured unitary quantum circuit which lacks any symmetries or other special properties will rapidly bring the system into a steady-state that is locally completely disordered, in the sense that local observables reproduce an infinite-temperature statistical ensemble. The study of new quantum phenomena involves quantities typical of theoretical quantum information, such as the entanglement entropy, which is a measure of the correlations that is non linear in the reduce density matrix of a subsystem.

In such models, the application of local unitaries brings the system toward a local thermal equilibrium and the understanding the irreversible nature of this *thermalization* process [11] requires the understanding of the production of quantum many-body entanglement. When measurements are introduced in the discrete evolution of a quantum circuit, new quantum dynamical phenomena appear. In this thesis we will focus

on one of such phenomena, namely *measurement induced phase transitions* ([12], [13]). Indeed, under weak monitoring the wavefunction describing the system is highly entangled, whereas for sufficiently frequent measurements the wavefunction remains close to a product state, which is less entangled. These phase and the transition between them can be mapped to effective classical statistical models ([14], [15]) and many monitored many-body systems have been studied ([16], [17],[18],[19],[20] and more).

However the experimental validation of such studies proves to be challenging ([21], [22]) and means to study large system through classical simulations prove to be necessary for numerical studies of such phenomena. In this context, non interacting fermionic dynamics can be efficiently simulated on classical computers [23]. Therefore we will study free-fermionic dynamics that can be mapped onto quantum circuits and analyze the evolution of the entanglement entropy in such systems under monitored dynamics. In this context it has been proven that simple projective measurements do not allow for a measurement induced phase transition ([24], [25]), therefore we will investigate whether modification to the measurement procedure can instead lead to the appearance of such a transition. The structure of this thesis is outlined below.

In Chap. 1 we review the basic concepts and methods of Quantum Many-Body Physics, Statistical Mechanics and Quantum Information needed to investigate the topic of *measurement induced entanglement phase transitions* [9]. First of all, the concept of entanglement entropy ([10]) is introduced in Sec. 1.1. Then, in Sec. 1.2, we look at the quantum gates that can be mapped onto non-interacting fermions via the *Jordan-Wigner transformation* ([26]). Afterwards, in Sec. 1.3, we describe *fermionic Gaussian states* ([27]), introducing the *correlation matrix* as a means to efficiently simulate the system and extract information from it, concentrating on number conserving Hamiltonians. To conclude the first chapter we review, in Sec. 1.4 the concept of measurement in Quantum Mechanics ([10]), focusing on *projective measurements* and *weak measurements*, which will be used throughout this thesis.

In Chap. 2 we describe *measurement induced entanglement phase transitions*, describing the mechanism that can bring to their appearance and the main features of the related phase diagram (Sec. 2.1, 2.2). Furthermore, in Sec. 2.3, we describe more deeply the concept of *quantum trajectories*, which was already introduced in Sec. 1.4.

In Chap. 3 we study the time evolution of the entanglement entropy under unitary dynamics. We do this for the well known Hamiltonian evolution and also for *brickwork circuits*. More precisely, in Sec. 3.1, we briefly describe why it is interesting to map physical Hamiltonians to quantum circuits with the objective to carry out *quantum simulations* ([7]). Then, in Sec. 3.2, we describe the behaviour of the entanglement entropy under continuous unitary dynamics, introducing the *quasiparticle-picture* as a semi-classical interpretation of the entanglement entropy's behaviour [28]. Finally in Sec. 3.3 we prove how the brickwork circuit evolution reproduces the continuous one in a certain limit. Moreover in Sec. 3.3.1 there is the first original result of this thesis, namely the definition the quasiparticle picture for a brickwork circuit that can be mapped

onto free fermions.

At last, in Chap. 4 we introduce measurements in the dynamics of free-fermionic chains. In Sec. 4.1 we first review the entanglement entropy behaviour for a free-fermionic dynamics containing local projective measurements [24]. Since in such model there is a *crossover* and not a phase transition, we proceed studying two original models. In Sec. 4.2 we study a fermionic chain placed side by side with an ancillary fermionic chain. In this context we implement a procedure which drives the system towards a target state and which presents projective measurements on the ancillary system, demostrating how also for this model there is no phase transition, since the *volume-law* phase is not stable. Therefore in Sec. 4.3 we introduce a weak non-linear measurement on a free-fermionic chain, which seeks a stable volume-law phase. In this model, we provide results suggesting the existence of two different phases, a volume-law and an area-law phase. However, to have conclusive results, the study of the thermodynamic limit should be done, which, though, was not possible due to computational resource limitations.

Chapter 1

Background

This chapter will contain all the building blocks needed for the models that will be discussed in this thesis. As mentioned in the introduction, this work addresses the phase transition observed for the *entanglement entropy* when random measurements are introduced into the standard unitary evolution of a closed quantum system. Since the models that will be studied in this thesis are *brickwork circuits* that can be mapped onto free-fermions, in Sec. 1.2 we will describe such circuits and then we will analyze which quantum gates can be mapped onto quadratic (free) fermionic operators via the *Jordan-Wigner transformation*, explaining why it is interesting to study such models. Free fermionic system can be described as *Fermionic Gaussian States*, hence these will be defined in Sec. 1.3. Here we will explain how to take advantage of the fact that a fermionic chain can be described with this formalism. Indeed all the information about such systems is encoded in the *correlation matrix*, thus the study of its evolution permits to simulate such system efficiently on a classical computer. Moreover we will focus on how to extract the entanglement entropy and the local density from the correlation matrix, since this will be necessary in Chap. 3, 4. In addition, in Sec. 1.3.6, we will focus on the analysis of system with a Hamiltonian that conserves the number of fermions, since this is the first model that we will analyze in Chap. 3 and since it will be the basis for the other models analyzed in this thesis.

Furthermore we will introduce the concept of *measurement* in Quantum Mechanics. Here, starting from *projective measurements*, we will introduce the fundamental concept of *quantum trajectories*, which are clearer in this context, with respect to the case of *weak measurements*, that will also be introduced, since they will be widely employed in Chap. 4.

Finally we specify that throughout this thesis we will study quantum many-body systems composed of two-level systems, which are organized in a one-dimensional chain. These two level system can be viewed as spin systems, with spin 1/2, as qubits and also as fermionic states. In the following these different views will all be employed, however we will refer to the two-level systems mainly as qubits, when we will be talking about

circuit models, as for example in Sec. 1.2, and as fermions, when we will do the Jordan-Wigner transformation and when we will address fermionic Gaussian states (Sec. 1.3). Finally in Sec. 1.4 we will review the concept of measurements in quantum mechanics, focusing on the cases that are relevant for this thesis, i.e. projective measurements and generalized measurements.

1.1 Entanglement Entropy

In the following, we denote the Hilbert space by $\mathcal{H}$. To describe the quantum states we will use both the state vector formalism, i.e. we will denote states $|\psi\rangle \in \mathcal{H}$, and the density matrix formalism, i.e. $\rho \in \mathcal{S}(\mathcal{H})$, where $\mathcal{S}(\mathcal{H})$ is the space of all quantum states. We will consider quantum systems composed by N two-level systems, for which $\mathcal{H} = (\mathbb{C})^{\otimes N}$.

For a quantum system defined by a pure state, the physical quantity that determines the amount of correlation between two parts of the system is the *entanglement entropy*. Consider a quantum many-body system composed by N two-level systems (this definition applies to any composite quantum system), described by a wavefunction $|\Psi\rangle$, with corresponding density matrix $\rho_\Psi = |\Psi\rangle\langle\Psi|$. Then the system is bipartitioned into two subsystems A and B. The state of a portion of the system is described by the *reduced density matrix*. The reduced density matrix for the subsystem A id defined as

$$\rho_A = \mathrm{Tr}_B(\rho_\Psi), \tag{1.1}$$

where the Tr_B is the partial trace over subsystem B [10]. Before arriving at the definition of the entanglement entropy, we must introduce an operation that quantifies the entropy itself. Throughout this work, this quantity will be the *Von-Neumann entropy*, defined as, for a quantum state ρ:

$$S_V(\rho) = -\mathrm{Tr}[\rho \log \rho], \tag{1.2}$$

where the logarithm is usually chosen to be in base 2 or base e. The only difference between the two entropies thus defined is a multiplicative factor. Throughout these thesis we chose the base 2 for the logarithm. The Von-Neumann entropy has some important properties:

1. Let $\rho \in \mathcal{S}(\mathcal{H})$, where $\dim(\mathcal{H}) = d$. Then $0 \leq S_V(\rho) \leq \log(d)$.

2. $S_V(\rho) = 0$ if and only if ρ is a pure state, whereas $S_V(\rho) = \log(d)$ if and only if $\rho = \hat{1}/d$, namely if and only if ρ is maximally mixed.

3. The Von-Neumann entropy is additive, namely if $\rho_{AB} = \rho_A \otimes \rho_B$, $S_V(\rho_{AB}) = S_V(\rho_A) + S_V(\rho_B)$.

4. The Von-Neumann entropy satisfies concavity: $\forall\ \{p_j\}, \{\rho_j\}$, with $\sum_j p_j = 1$, $p_j \geq 0$, and $\rho_j \in \mathcal{S}(\mathcal{H})$, we have that

$$S_V\Big(\sum_j p_j \rho_j\Big) \geq \sum_j p_j S_V(\rho_j). \tag{1.3}$$

Remark. The Von-Neumann entropy can be related to the Shannon entropy. Given a classical distribution function $\{p_j\}$, the Shannon entropy is:

$$S(\{p_j\}) = -\sum_j p_j \log p_j. \tag{1.4}$$

Thus the Von-Neumann entropy is the Shannon entropy of $\{\lambda_j\}$, where $\{\lambda_j\}$ are the eigenvalues of ρ, because of the properties of the eigenvalues of a density matrix, namely $\lambda_j \geq 0\ \forall\ j$ and $\sum_j \lambda_j = 1$.

Now we can introduce the entanglement entropy, which quantifies the entanglement of a state.

Definition 1.1.1. (**Entanglement Entropy**) Let $|\psi_{AB}\rangle \in \mathcal{H}_A \otimes \mathcal{H}_B$. The entanglement entropy (EE) is defined as

$$E_{AB}(\psi_{AB}) = S_V(\rho_A). \tag{1.5}$$

Moreover, given the definition, the entanglement entropy derives the properties of the Von-Neumann entropy.

Remark. For a system in a pure state, for instance $|\Psi_{AB}\rangle$, we have that $S_V(\rho_A) = S_V(\rho_B)$, which can be easily seen using the Schmidt's decomposition. Therefore, the entanglement entropy can be computed from both ρ_A and ρ_B [10].

Remark. For a system in a mixed state, the just defined EE looses its meaning. As a matter of fact, suppose that $\rho_{AB} \in \mathcal{S}(\mathcal{H}_A \otimes \mathcal{H}_B)$ is mixed, for example let

$$\rho_{AB} = \frac{1}{2}\,|00\rangle\langle 00| + \frac{1}{2}\,|11\rangle\langle 11|\,, \tag{1.6}$$

which is a separable state, thus not entangled. However one can easily see that $\rho_A = \hat{1}/2$, hence $E_{AB} = S_V(\rho_A) = 2 \neq 0$.

1.2 Quantum Gates

Throughout this thesis we will discuss free-fermionic models that can be mapped onto quantum circuits (and vice-versa), for reasons that will be thoroughly explained i Sec. 3.1. Quantum circuit models with nearest neighbour interactions are called *brickwork*

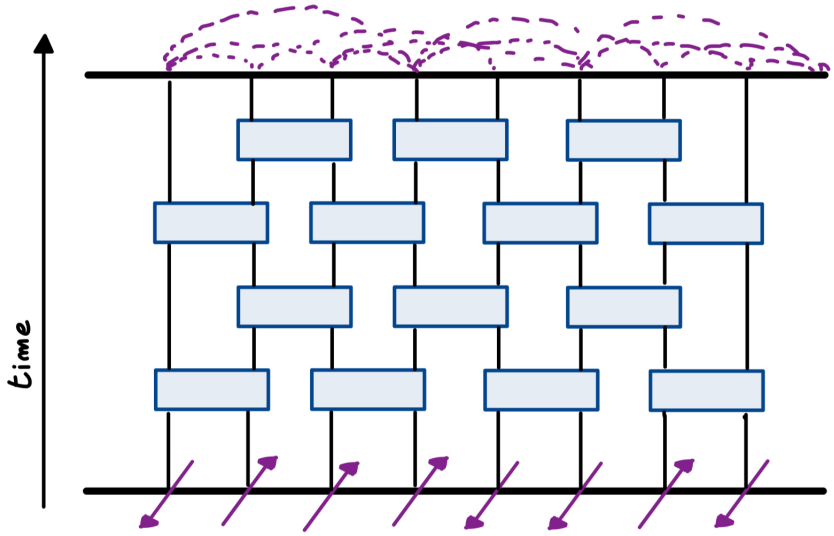

Figure 1.1: *Sketch of a brickwork circuit. Here a spin is positioned one each site of the chain. The blue boxes represent unitary operators on nearest neighbours spins, while the wires represent the evolution of the spins.*

circuits. In this models neighbouring qubits interact via a unitary operators $U_{j,j+1}$. The evolution of the whole system is done applying such unitaries in layers, namely these unitaries are applied first for all odd js in the chain, then for all even js in the chain, as shown in Fig. 1.1.

In the following, the studied quantum many-body systems will undergo the usual unitary evolution, which will then be modified introducing random measurements during the evolution. We are interested in studying free-fermionic dynamics, therefore in this section we will introduce the *Jordan-Wigner transformation*, which maps spin operators onto fermionic operators, and we will see what type of gates quadratic fermionic operators generate. Since we are interested in Hamiltonians that can be mapped onto brickwork circuits, we look at the possible one ant two-qubit operators. First of all we recall that any Hermitian one-qubit operator may be written as a linear combination of the three Pauli matrices plus the identity [10], i.e.

$$I = \begin{pmatrix} 1 & 0 \\ 0 & 1 \end{pmatrix} \quad \sigma^x \equiv X = \begin{pmatrix} 0 & 1 \\ 1 & 0 \end{pmatrix} \quad \sigma^Y \equiv Y = \begin{pmatrix} 0 & -i \\ i & 0 \end{pmatrix} \quad \sigma^Z \equiv Z = \begin{pmatrix} 1 & 0 \\ 0 & -1 \end{pmatrix}, \tag{1.7}$$

in the form

$$\mathcal{O} = \sum_{\mathcal{A}\in\{I,X,Y,Z\}} c_{\mathcal{A}}\mathcal{A} = c_I I + c_X X + c_Y Y + c_Z Z, \tag{1.8}$$

where the coefficients are given by $c_{\mathcal{A}} = \mathrm{Tr}(\mathcal{A}\mathcal{O})$. For a pair of qubits, any Hermitian operator can be written as a sum of tensor products of these operators acting on the two

qubits, for example ($Y_1 = Y \otimes I$). Since the above described operators are Hermitian, they will lead to a unitary evolution. We now see how to map these operators onto free-fermionic operators.

1.2.1 The Jordan-Wigner transformation

It is well known, from standard Quantum Mechanics, that for a single spin 1/2, the three components of the spin-operators are represented by the Pauli matrices σ^α, with $\alpha = x, y, z$. The Hilbert space for a single spin 1/2 is two-dimensional and a basis is, for instance, $\{|\uparrow\rangle, |\downarrow\rangle\}$, which is the basis of eigenstates of σ^z. If now we take a lattice with sites labelled by j, we have

$$[\sigma_j^\alpha, \sigma_{j'}^\beta] = 2i\epsilon^{\alpha\beta\gamma}\sigma_j^\gamma \delta_{jj'}. \tag{1.9}$$

Defining the raising and lowering operators

$$\sigma_j^\pm = \frac{\sigma_j^x \pm i\sigma_j^y}{2}, \tag{1.10}$$

one can easily verify that, using $\{\sigma^\alpha, \sigma^\beta\} = 2\delta^{\alpha\beta}$,

$$\{\sigma_j^+, \sigma_j^-\} = 1, \tag{1.11}$$

which is the typical fermionic anticommutation rule in second quantization. After these preliminary considerations, we can start to look at the mapping between spin operators and fermionic operators.

Take fermionic creation and annihilation operators $c_j^\dagger, c_j$ which satisfy the anticommutation rules[1]:

$$\{c_i, c_j^\dagger\} = \delta_{ij} \quad \{c_i, c_j\} = 0 = \{c_i^\dagger, c_j^\dagger\}. \tag{1.12}$$

Now, going back at the 1D chain, we can relate the vectors of the basis of the fermions to the ones of the spin 1/2, in a non-unique way [29]. For instance we take $|0\rangle \leftrightarrow |\uparrow\rangle$ and $|1\rangle = c^\dagger|0\rangle \leftrightarrow |\downarrow\rangle$ on each site. Recalling the raising and lowering operators, the fact that $\sigma^+|\downarrow\rangle = |\uparrow\rangle$, $\sigma^-|\uparrow\rangle = |\downarrow\rangle$, and that $\sigma^z = 1 - 2\sigma^-\sigma^+$, we get the *Jordan-Wigner transformations* [26]:

$$\sigma_j^+ = e^{i\pi\sum_{k<j} c_k^\dagger c_k} c_j = \prod_{k=1}^{j-1}(1 - 2c_k^\dagger c_k)c_j, \tag{1.13}$$

$$\sigma_j^- = e^{i\pi\sum_{k<j} c_k^\dagger c_k} c_j^\dagger = \prod_{k=1}^{j-1}(1 - 2c_k^\dagger c_k)c_j^\dagger, \tag{1.14}$$

$$\sigma_j^z = 1 - 2c_j^\dagger c_j. \tag{1.15}$$

[1] One can also have anti-commutation rules of the Clifford algebra, which define the *Majorana fermions*.

We can also write the *Jordan-Wigner transformations* for the operators $\sigma_j^x, \sigma_j^y, \sigma_j^z$, recalling Eq. (1.10).

$$\begin{cases} \sigma_j^x & = \prod_{k=1}^{j-1}(1-2c_k^\dagger c_k)(c_j^\dagger + c_j), \\ \sigma_j^y & = \prod_{k=1}^{j-1}(1-2c_k^\dagger c_k) i(c_j^\dagger - c_j), \\ \sigma_j^z & = 1 - 2c_j^\dagger c_j. \end{cases} \tag{1.16}$$

A question now arises naturally: what types of gates can be mapped onto operators between free fermions? Indeed, tackling quantum many-body problems is not easy. Furthermore, when one seeks a numerical solution, the number of memory required to store quantum information grows exponentially on a classical computer. For example for N spin 1/2 particles, there are 2^N basis states, thus needing 2^N complex variables to store this information. This problem with dimensionality could be solved by the rise of quantum computers, for which, in the example at hand, just N qubits are needed, thus having a linear complexity in the number of qubits, instead of an exponential one. Therefore to simulate the evolution of a many-body Hamiltonian on a quantum computer we need to be able to map the Hamiltonian into a quantum circuit. Here we will show how to map free-fermionic Hamiltonians onto gates, which are employed in quantum computers, with the Jordan-Wigner transformation. Moreover this mapping is bijective, namely we can map a spin or qubit system onto a fermionic system. This will be useful in Chap. 3, where we will try to tackle the problem of simulating a quantum circuit using the formalism of fermionic Gaussian states (which will be introduced in Sec. 1.3). Therefore we will see what types of gates a number conserving free-fermionic Hamiltonian generates, since this is the case that we will analyze in this thesis.

The most general number conserving quadratic Hamiltonian is such as:

$$H = \sum_{i,j} (\alpha_{i,j} c_i^\dagger c_j + \alpha_{i,j}^* c_j^\dagger c_i), \tag{1.17}$$

where α is a complex parameter. We will be dealing with *brikwork circuits* (Fig. 3.6). In this case Eq. (1.17) will be a sum over nearest neighbours Hamiltonians of the kind:

$$H_{i,i+1} \propto c_i^\dagger c_i + c_{i+1}^\dagger c_{i+1} + c_i^\dagger c_{i+1} + c_{i+1}^\dagger c_i. \tag{1.18}$$

To see which gates can be generated with this Hamiltonian we consider the Eq. (1.13), (1.14), (1.15), the fact that Pauli matrices are unitary and the fact that

$$\prod_{j'=1}^{j-1}(1-2n_{j'}) = \prod_{j'=1}^{j-1}\sigma_{j'}^z. \tag{1.19}$$

Hence we get that the Jordan-Wigner transformation can be written as:

$$c_j^\dagger = \Big(\prod_{j'=1}^{j-1} \sigma_{j'}^z\Big)\sigma_j^-, \tag{1.20}$$

$$c_j = \Big(\prod_{j'=1}^{j-1} \sigma_{j'}^z\Big)\sigma_j^+. \tag{1.21}$$

Now we plug these transformations into the terms of Eq. (1.18), where one can easily see how from the diagonal terms σ^z gates pop out, whereas from the non-diagonal terms combinations of σ^x and σ^y gates pop out:

$$c_i^\dagger c_i = \Big(\prod_{i'=1}^{i-1} \sigma_{i'}^z\Big)\sigma_i^-\Big(\prod_{i'=1}^{i-1} \sigma_{i'}^z\Big)\sigma_i^+ = \sigma_i^-\sigma_i^+ = \frac{1}{2}(1-\sigma_i^z) \propto \sigma_i^z, \tag{1.22}$$

$$\begin{aligned} c_i^\dagger c_{i+1} &= \Big(\prod_{i'=1}^{i-1} \sigma_{i'}^z\Big)\sigma_i^-\Big(\prod_{i'=1}^{i} \sigma_{i'}^z\Big)\sigma_{i+1}^+ = \sigma_i^-\sigma_i^z\sigma_{i+1}^+ \\ &\propto \sigma_i^x\sigma_{i+1}^x + \sigma_i^y\sigma_{i+1}^y + i(\sigma_i^x\sigma_{i+1}^y + \sigma_i^y\sigma_{i+1}^x). \end{aligned} \tag{1.23}$$

Thus we can map free fermions into the gates: σ_j^z, σ_{j+1}^z, $\sigma_j^x\sigma_{j+1}^x$, $\sigma_j^y\sigma_{j+1}^y$, $\sigma_j^x\sigma_{j+1}^y$, $\sigma_j^y\sigma_{j+1}^x$. This set of gates generates the so called *nearest neighbour matchgates*, which are defined as [23]:

Definition 1.2.1. (**Matchgate**) Let $G(A,B)$ be the two-qubit gate given by:

$$G(A,B) = \begin{pmatrix} A_{11} & 0 & 0 & A_{12} \\ 0 & B_{11} & B_{12} & 0 \\ 0 & B_{21} & B_{22} & 0 \\ A_{21} & 0 & 0 & A_{22} \end{pmatrix} \tag{1.24}$$

where

$$A = \begin{pmatrix} A_{11} & A_{12} \\ A_{21} & A_{22} \end{pmatrix} \quad B = \begin{pmatrix} B_{11} & B_{12} \\ B_{21} & B_{22} \end{pmatrix} \tag{1.25}$$

Then $G(A,B)$ is a matchgate if $\det A = \det B$.

The sets of gates $\mathcal{A}_{i,j} = \{\sigma_i^z, \sigma_j^z, \sigma_i^x\sigma_j^x, \sigma_i^y\sigma_j^y, \sigma_i^x\sigma_j^y, \sigma_i^y\sigma_j^x\}$ generate all gates $G(A,B)$ acting on qubits i,j. Free fermions generate gates in the set $\mathcal{A}_{i,i+1}$, namely free fermions generate nearest neighbours matchgates. Nevertheless, free fermions can generate multi-qubit gates when we let go of the assumption of nearest neighbour interaction. In [30] it has been shown that a circuit generated with free fermions can be implemented by a poly-sized circuit of nearest neighbours matchgates, thus it is computationally equivalent to nearest neighbours matchgates.

1.3 Fermionic Gaussian States

In the previous section we saw the mapping between spin operators and fermionic operators. We also saw how a free-fermionic dynamics can be efficiently simulated on a classical computer, thus now we will introduce the formalism needed to deal with such dynamics. Indeed *Fermionic Gaussian States* (FGS) have the handy property that all the information about the system can be extracted from the *correlation matrix*, which is a $2N \times 2N$ matrix, being N the number of sites in the 1D chain. Thus, if we want to study the evolution of a chain with N sites, which has a Hilbert space of dimension 2^N, and the evolution can be mapped into a free-fermion evolution, the dynamics is reduced to the study of the evolution of the correlation matrix, namely operations between $2N \times 2N$ square matrices, which can be computed efficiently on a classical computer. Therefore in this section we will describe *fermionic quadratic Hamiltonians*, then define what is a *fermionic Gaussian state* and the associated *correlation matrix* and how it evolves under a quadratic Hamiltonian. At a later time the technique to extract the entanglement entropy from the correlation matrix will be described. Finally we will analyze the case of a dynamics which conserves the number of fermions in the chain, since in Chap. 3 and 4 we will deal with such case.

1.3.1 Fermionic Quadratic Hamiltonians

The distruction and creation operators c_i,$c_i^\dagger$ satisfying the anti-commutation rules

$$\{c_i, c_j^\dagger\} = \delta_{ij} \quad \{c_i, c_j\} = 0 = \{c_i^\dagger, c_j^\dagger\}, \tag{1.26}$$

and they represent the action of adding and removing one fermionic mode. We can collect the Dirac operators of a system with N modes in a vector $\vec{\alpha}$ with $2N$ elements[2]:

$$\hat{\vec{\alpha}} = \begin{pmatrix} c_1 \\ \vdots \\ c_N \\ c_1^\dagger \\ \vdots \\ c_N^\dagger \end{pmatrix} \quad \hat{\vec{\alpha}}^\dagger = (c_1^\dagger, \dots, c_N^\dagger, c_1, \dots, c_N). \tag{1.27}$$

The most general *fermionic quadratic Hamiltonian* on a lattice with N sites can be written as:

$$\hat{H} = \sum_{i,j=1}^{N} \left(A_{ij} c_i^\dagger c_j - A_{ij}^* c_i c_j^\dagger + B_{ij} c_i c_j - B_{ij}^* c_i c_j^\dagger \right), \tag{1.28}$$

[2]One could also introduce the *Majorana representation*, however we will skip this, since they will not be used in this thesis.

where A is a Hermitian matrix ($A^\dagger = A$) and B is an skew-symmetric complex matrix ($B = -B^T$). Thus defining the matrix

$$\tilde{H} = \begin{pmatrix} A & -B^* \\ B & -A^* \end{pmatrix}, \tag{1.29}$$

the Hamiltonian can be written in a compact from as:

$$\hat{H} = \hat{\vec{\alpha}}^\dagger \tilde{H} \hat{\vec{\alpha}}. \tag{1.30}$$

To diagonalize the Hamiltonian we apply a canonical transformation:

$$\begin{pmatrix} c \\ c^\dagger \end{pmatrix} = \begin{pmatrix} U & V^* \\ V & U^* \end{pmatrix} \begin{pmatrix} b \\ b^\dagger \end{pmatrix}, \tag{1.31}$$

or equivalently $\hat{\vec{\alpha}} = \mathcal{S}\hat{\vec{\beta}}$. Looking at each component:

$$c_i = U_{ia} b_a + V^*_{ia} b^\dagger_a, \tag{1.32}$$

$$c^\dagger_i = V_{ia} b_a + U^*_{ia} b^\dagger_a. \tag{1.33}$$

In order for this to be a canonical transformation, the anticommutation rules must be conserved, namely

$$\{b_i, b^\dagger_j\} = \delta_{ij} \quad \{b_i, b_j\} = 0 = \{b^\dagger_i, b^\dagger_j\}. \tag{1.34}$$

This means that the transformation is unitary:

$$\mathcal{S}^\dagger \mathcal{S} = \mathcal{S}\mathcal{S}^\dagger = I. \tag{1.35}$$

From the condition $\mathcal{S}^\dagger \mathcal{S} = I$ we find that:

$$\begin{pmatrix} U^\dagger & V^\dagger \\ V^T & U^T \end{pmatrix} \begin{pmatrix} U & V^* \\ V & U^* \end{pmatrix} = \begin{pmatrix} U^\dagger U + V^\dagger V & U^\dagger V^* + V^\dagger U^* \\ V^T U + U^T V & V^T V^* + U^T U^* \end{pmatrix} = \begin{pmatrix} I & 0 \\ 0 & I \end{pmatrix}, \tag{1.36}$$

from which this conditions follow:

$$\begin{cases} U \dagger U + V^\dagger V & = I \\ U^\dagger V^* + V^\dagger U^* & = 0 \\ V^T U + U^T V & = 0 \\ V^T V^* + U^T U^* & = I. \end{cases} \tag{1.37}$$

We can also write $\hat{\vec{\beta}} = S^\dagger \hat{\vec{\alpha}}$, which gives the inverse transformations:

$$b_a = U^*_{ai} c_i + V^*_{ai} c^\dagger_i \tag{1.38}$$

$$b^\dagger_a = V_{ai} c_i + U_{ai} c^\dagger_i. \tag{1.39}$$

Now we require that the transformed Hamiltonian is diagonal, namely

$$\mathcal{S}^\dagger \tilde{H} \mathcal{S} = \mathcal{E} = \begin{pmatrix} E & 0 \\ 0 & -E \end{pmatrix}. \tag{1.40}$$

At this point the Hamiltonian is in the diagonal form:

$$H = \sum_a E_a (b_a^\dagger b_a - b_a b_a^\dagger). \tag{1.41}$$

1.3.2 Fermionic Gaussian States

We can now introduce the concept of *Fermionic Gaussian States* [27].

Definition 1.3.1. (Fermionic Gaussian States) A state ρ is a *fermionic Gaussian state* (FGS) if it can be represented as

$$\rho = \frac{e^{-H}}{Z} \tag{1.42}$$

where $Z = \mathrm{Tr}[e^{-H}]$ is a normalization constant and H is a fermionic Gaussian (quadratic) Hamiltonian (FQH).

One can see how fermionic Gaussian states have an immediate interpretation as thermal Gibbs states of the fermionic quadratic Hamiltonian. Furthermore, because of the evenness of the FQH, since FGS are exponential of FQH, fermionic Gaussian states are even operators. To better understand the handy properties of these states we look at an example.

Example 1.3.1. (Single mode Gaussian state) As a first example we consider a single mode parent Hamiltonian $H_1 = E(b^\dagger b - b b^\dagger)$. The related Gaussian state is $\rho = \exp(-H_1)/Z_1$. Its representation on the basis $\{|0\rangle, |1\rangle\}$ can be written as

$$\rho = \begin{pmatrix} f & 0 \\ 0 & 1-f \end{pmatrix} \tag{1.43}$$

where $f = \langle 0|\rho|0\rangle$ and the two off-diagonal entries are 0 because of the evenness of H_1.

Now we prove an important property of single mode fermionic Gaussian states.

Proposition 1.3.1. *A single mode fermionic Gaussian state is completely characterized by the occupation* $\langle b^\dagger b\rangle$.

Proof. We saw that in the $\{|0\rangle, |1\rangle\}$ basis the fermionic Gaussian state ρ is represented in terms of $f = \langle 0|\rho|0\rangle$ (Eq. (1.43)). Now $f = \langle 0|\rho|0\rangle = \mathrm{Tr}[\rho] - \langle 1|\rho|1\rangle$. Also $\mathrm{Tr}[\rho] = 1$ because ρ is a state, i.e. a density matrix. Since $b^\dagger b\,|0\rangle = 0$ and $b^\dagger b\,|1\rangle = 1$, we can write

$$f = 1 - \langle 0|\rho b^\dagger b|0\rangle - \langle 1|\rho b^\dagger b|1\rangle = 1 - \mathrm{Tr}[\rho b^\dagger b]. \tag{1.44}$$

Since $\mathrm{Tr}[\rho b^\dagger b] = \langle b^\dagger b\rangle$, we have

$$\langle b^\dagger b\rangle = 1 - f \tag{1.45}$$

and we can finally write

$$\rho = \begin{pmatrix} 1 - \langle b^\dagger b\rangle & 0 \\ 0 & \langle b^\dagger b\rangle \end{pmatrix}, \tag{1.46}$$

thus obtaining Eq. (1.43). □

1.3.3 Correlation Matrices

We have seen that each single mode Gaussian state is completely characterized by its occupation number. Furthermore we have also seen that a fermionic quadratic Hamiltonian can always be diagonalized. This means that the Hamiltonian will be a sum of commuting single-mode Hamiltonians, which makes possible to write

$$\rho = \frac{e^{-\sum_{k=1}^N E_k(b_k^\dagger b_k - b_k b_k^\dagger)}}{Z} = \bigotimes_{k=1}^N \frac{e^{-E_k(b_k^\dagger b_k - b_k b_k^\dagger)}}{Z_k}, \tag{1.47}$$

where $Z_k = \mathrm{Tr}[e^{-E_k(b_k^\dagger b_k - b_k b_k^\dagger)}]$. We can also write it in the from

$$\rho = \bigotimes_{k=1}^N \rho_k = \bigotimes_{k=1}^N \begin{pmatrix} f_k & 0 \\ 0 & 1 - f_k \end{pmatrix}, \tag{1.48}$$

where $f_k = \langle 0|\rho_k|0\rangle$. Thus in this last case the state is fully characterized by the set of occupation numbers $\{\langle b_i^\dagger b_i\rangle\}_{i=1}^N$. Exploiting the inverse transformations in Eq.(1.39), we see that the fermionic Gaussian state is completely characterized by the collection of the correlators $\langle c_i^\dagger c_j\rangle$, $\langle c_i c_j\rangle$, and their Hermitian conjugates, which can be collected in the so called *correlation matrix* [27].

Definition 1.3.2. (Correlation Matrix)

$$\Gamma \equiv \langle \vec{\alpha}\vec{\alpha}^\dagger\rangle = \begin{pmatrix} \Gamma^{cc^\dagger} & \Gamma^{cc} \\ \Gamma^{c^\dagger c^\dagger} & \Gamma^{c^\dagger c} \end{pmatrix}, \tag{1.49}$$

where, clarifying the indexes, $\Gamma^{c^\dagger c}_{i,j} = \langle c_i^\dagger c_j\rangle$, $\Gamma^{cc}_{i,j} = \langle c_i c_j\rangle$. Because of the fermionic anticommutation rules, $\Gamma^{cc}_{ij} = -(\Gamma^{c^\dagger c^\dagger}_{ij})^*$ and $\Gamma^{cc^\dagger}_{ij} = (I - \Gamma^{c^\dagger c})^\dagger_{ij}$. Thus Γ is Hermitian, Γ^{cc} and $\Gamma^{c^\dagger c^\dagger}$ are skew-symmetric, $\Gamma^{cc^\dagger}$ and $\Gamma^{c^\dagger c}$ are Hermitian.

Notice now that Wick's theorem states that every correlation function may be decomposed into a sum of two-point correlation functions [31]. Thus any correlation function can be expressed as a sum of elements of the correlation matrix Γ.

Example 1.3.2. Four point correlation function Let's see as an example how we can compute the four-point correlation function $\langle\psi|c_i c_j c_k c_l|\psi\rangle$ in terms of two-point correlation functions, using Wick's theorem. We have to keep in mind that fermionic operators anti-commute, so in the end:

$$\begin{aligned}\langle\psi|c_i c_j c_k c_l|\psi\rangle &= \langle\psi|c_i c_j|\psi\rangle\langle\psi|c_k c_l|\psi\rangle - \langle\psi|c_i c_k|\psi\rangle\langle\psi|c_j c_l|\psi\rangle \\ &+ \langle\psi|c_i c_l|\psi\rangle\langle\psi|c_j c_k|\psi\rangle \\ &= \Gamma^{cc}_{ij}\Gamma^{cc}_{kl} - \Gamma^{cc}_{ik}\Gamma^{cc}_{jl} + \Gamma^{cc}_{il}\Gamma^{cc}_{jk},\end{aligned} \tag{1.50}$$

thus showing how any correlator can be written as a sum of products between elements of the correlation matrix.

While discussing the entanglement entropy we will be interested in the eigenvalues of the correlation matrix. Notice how, in the case of a Gaussian state like the one in Eq. (1.48), the correlation matrix is diagonal:

$$\Gamma = \mathrm{diag}(f_1, \dots f_N, 1 - f_1, \dots, 1 - f_N). \tag{1.51}$$

Moreover, even if the parent Hamiltonian of the Gaussian state has not been diagonalized, thus yielding a correlation matrix as the one in Eq. (1.49), the correlation matrix is Hermitian, thus it exists a unitary transformation V that brings a non diagonal correlation matrix to a diagonal form as the one in Eq. (1.51).

1.3.4 Entanglement Entropy from the Correlation Matrix

We saw in Sec.1.1, that Eq. (1.5) quantifies the entanglement entropy for a pure state. In this section we have introduced fermionic Gaussian states and we now address the problem of extracting the entanglement entropy for such states. Given the fact that the Von-Neumann entropy is additive for product states, if we deal with a Gaussian state as the one in Eq. (1.48), we get:

$$S(\Gamma) \equiv S(\rho) = -\sum_{k=1}^{N}[(1 - f_k)\log(1 - f_k) + f_k \log(f_k)]. \tag{1.52}$$

What we will be studying is the *bipartite entanglement*, in a 1D chain with N sites, between a set of contiguous L qubits, which form a block of qubits that we will denote as $\mathcal{B}_L$, and the qubits in the rest of the chain, which form a block of qubits that we will call $\mathcal{B}_{\bar{L}}$. This means that we will measure the following entropy, parametrized by L:

$$S_L \equiv -\mathrm{Tr}[\rho_L \log(\rho_L)], \tag{1.53}$$

where $\rho_L = \mathrm{Tr}_{\mathcal{B}_{\bar{L}}}[\rho]$ is the reduced density matrix.

Since we are concerned with free-fermionic Hamiltonians, the states we will consider will be Gaussian states, which are completely characterized by their correlation matrix. We will thus see how to extract the entanglement entropy from the correlation matrix [32]. If the Hamiltonian has not been previously diagonalized, the corresponding correlation matrix will have the shape as the one in Eq. (1.49). To be more explicit:

$$\Gamma = \begin{pmatrix} \langle c_1 c_1^\dagger\rangle & \langle c_1 c_2^\dagger\rangle & \dots & \langle c_1 c_N^\dagger\rangle & \langle c_1 c_1\rangle & \langle c_1 c_2\rangle & \dots & \langle c_1 c_N\rangle \\ \langle c_2 c_1^\dagger\rangle & \langle c_2 c_2^\dagger\rangle & \dots & \langle c_2 c_N^\dagger\rangle & \langle c_2 c_1\rangle & \langle c_2 c_2\rangle & \dots & \langle c_2 c_N\rangle \\ \vdots & \vdots & \ddots & \vdots & \vdots & \vdots & \ddots & \vdots \\ \langle c_N c_1^\dagger\rangle & \langle c_N c_2^\dagger\rangle & \dots & \langle c_N c_N^\dagger\rangle & \langle c_N c_1\rangle & \langle c_N c_2\rangle & \dots & \langle c_N c_N\rangle \\ \langle c_1^\dagger c_1^\dagger\rangle & \langle c_1^\dagger c_2^\dagger\rangle & \dots & \langle c_1^\dagger c_N^\dagger\rangle & \langle c_1^\dagger c_1\rangle & \langle c_1^\dagger c_2\rangle & \dots & \langle c_1^\dagger c_N\rangle \\ \langle c_2^\dagger c_1^\dagger\rangle & \langle c_2^\dagger c_2^\dagger\rangle & \dots & \langle c_2^\dagger c_N^\dagger\rangle & \langle c_2^\dagger c_1\rangle & \langle c_2^\dagger c_2\rangle & \dots & \langle c_2^\dagger c_N\rangle \\ \vdots & \vdots & \ddots & \vdots & \vdots & \vdots & \ddots & \vdots \\ \langle c_N^\dagger c_1^\dagger\rangle & \langle c_N^\dagger c_2^\dagger\rangle & \dots & \langle c_N^\dagger c_N^\dagger\rangle & \langle c_N^\dagger c_1\rangle & \langle c_N^\dagger c_2\rangle & \dots & \langle c_N^\dagger c_N\rangle \end{pmatrix} \tag{1.54}$$

Since we need the reduced density matrix ρ_L for the qubit block $\mathcal{B}_L$ in order to compute the EE, we need to extract the correlation matrix for the subsystem $\mathcal{B}_L$. To achieve this we eliminate $2(N-L)$ contiguous columns and rows from the correlation matrix of Eq. (1.54), namely those corresponding to the $(N-L)$ traced out spins. This procedure gives the correlation matrix Γ_L for the state ρ_L. Take for instance the first L spins in the chain to be $\mathcal{B}_L$, then:

$$\Gamma_L = \begin{pmatrix} \langle c_1 c_1^\dagger\rangle & \dots & \langle c_1 c_L^\dagger\rangle & \langle c_1 c_1\rangle & \dots & \langle c_1 c_L\rangle \\ \vdots & \ddots & \vdots & \vdots & \ddots & \vdots \\ \langle c_L c_1^\dagger\rangle & \dots & \langle c_L c_L^\dagger\rangle & \langle c_L c_1\rangle & \dots & \langle c_L c_L\rangle \\ \langle c_1^\dagger c_1^\dagger\rangle & \dots & \langle c_1^\dagger c_L^\dagger\rangle & \langle c_1^\dagger c_1\rangle & \dots & \langle c_1^\dagger c_L\rangle \\ \vdots & \ddots & \vdots & \vdots & \ddots & \vdots \\ \langle c_L^\dagger c_1^\dagger\rangle & \dots & \langle c_L^\dagger c_L^\dagger\rangle & \langle c_L^\dagger c_1\rangle & \dots & \langle c_L^\dagger c_L\rangle \end{pmatrix}. \tag{1.55}$$

To compute the Von-Neumann entropy we need the eigenvalues of the correlation matrix. As a matter of fact, we saw that the correlation matrix is Hermitian and deleting contiguous rows and columns does not change this fact. Thus, also Γ_L is hermitian and therefore it exists a unitary matrix V that brings Γ_L in a diagonal form. Also notice that if we had already diagonalized the free fermionic Hamiltonian, we would have already a diagonal correlation matrix (see Eq. (1.48),(1.51)), from which, to get Γ_L we delete the rows and columns associated to the traced out spins.

1.3.5 Time evolution of the correlation matrix

We will now address the matter of how the correlation matrix evolves. The evolution of a quantum system is described by the evolution operator

$$U(t) = e^{-iHt}, \tag{1.56}$$

where we take H to be a quadratic Hamiltonian, thus allowing the usage of the correlation matrix for numerical simulations. A state $|\psi_0\rangle$ evolves as:

$$|\psi(t)\rangle = U(t)\,|\psi_0\rangle\,. \tag{1.57}$$

We are now interested to see how the correlation matrix is evolved by the evolution operator in Eq. (1.56). Naming C_{ij} any combination of creation and destruction operators at sites i, j, and given Eq. (1.57), the matrix elements of the correlation matrix at time t will be given by:

$$\Gamma_{i,j}(t) = \langle\psi_0|U^\dagger(t)C_{i,j}U(t)|\psi_0\rangle = \langle\psi_0|e^{\mathrm{ad}_{iHt}}C_{i,j}|\psi_0\rangle\,, \tag{1.58}$$

where $\mathrm{ad}_A(B) = [A, B]$ is the so called *adjoint action*, which is a linear operator acting on the space of operators.

Proof. Expanding the exponents, with a direct computation one finds:

$$e^{-A}Be^{A} = B + [B, A] + \frac{1}{2}[[B, A], A] + \dots \tag{1.59}$$

Defining the adjoint action as $\mathrm{ad}_A(Y) = [A, Y]$, let's compute

$$\begin{aligned} e^{\mathrm{ad}_A}(B) &= (1 + \mathrm{ad}_A + \frac{1}{2!}(\mathrm{ad}_A)^2 + \dots)(B) \\ &= B + [A, B] + \frac{1}{2!}\mathrm{ad}_A([A, B]) + \dots \\ &= B + [A, B] + \frac{1}{2}[A, [A, B]] + \dots \end{aligned} \tag{1.60}$$

Using the fact that $[-A, B] = -[A, B] = [B, A]$, we can write

$$\begin{aligned} e^{\mathrm{ad}_{-A}}(B) &= (1 + \mathrm{ad}_{-A} + \frac{1}{2!}(\mathrm{ad}_{-A})^2 + \dots)(B) \\ &= B + [-A, B] + \frac{1}{2}\mathrm{ad}_{-A}([-A, B]) + \dots \\ &= B + [B, A] + \frac{1}{2}\mathrm{ad}_{-A}([B, A]) + \dots \\ &= B + [B, A] + \frac{1}{2}[-A, [B, A]] + \dots \\ &= B + [B, A] + \frac{1}{2}[[B, A], A] + \dots, \end{aligned} \tag{1.61}$$

thus prooving that $e^{-A}Be^{A} = e^{\mathrm{ad}_{-A}}(B)$. In our specific case we have $A \equiv -iHt$ and $B \equiv C_{ij}$. □

Therefore, the time evolution of the full correlation matrix is

$$\Gamma(t) = \begin{pmatrix} \Gamma^{cc^\dagger}(t) & \Gamma^{cc}(t) \\ \Gamma^{c^\dagger c^\dagger}(t) & \Gamma^{c^\dagger c}(t) \end{pmatrix}, \tag{1.62}$$

where for each matrix element $\Gamma_{i,j}$ we apply the rule in Eq. (1.58).

1.3.6 Number Conserving Hamiltonians

The number conserving Hamiltonian for a chain with N sites is

$$\hat{H} = \sum_{i,j=1}^{N} (A_{ij} c_i^\dagger c_j + A_{ji}^* c_j^\dagger c_i), \tag{1.63}$$

because the other two terms in the general quadratic Hamiltonian (Eq. (1.28)) do not commute with the number operator $\hat{N} = \sum_i c_i^\dagger c_i$, namely $[n_i, c_j c_k] \neq 0$ and $[n_i, c_j^\dagger c_k^\dagger] \neq 0$. Moreover we can rewrite this in the following form:

$$\hat{H} = \sum_{i,j=1}^{N} (A_{ij} + A_{ji}^*) c_i^\dagger c_j = \sum_{i,j=1}^{N} H_{ij} c_i^\dagger c_j, \tag{1.64}$$

where we have defined $H_{ij} = A_{ij} + A_{ji}^*$. We can now see how the Hamiltonian operator can be represented by an $N \times N$ matrix. Indeed one can define, similarly to what we have done before, the vectors

$$\hat{\vec{\alpha}} = \begin{pmatrix} c_1, \\ \vdots \\ c_N \end{pmatrix} \quad \hat{\vec{\alpha}}^\dagger = (c_1^\dagger, \ldots, c_N^\dagger) \tag{1.65}$$

and thus the Hamiltonian is represented by the $N \times N$ matrix

$$H = A + A^\dagger, \tag{1.66}$$

thus giving

$$\hat{H} = \hat{\vec{\alpha}}^\dagger H \hat{\vec{\alpha}}. \tag{1.67}$$

Furthermore, since the Hamiltonian is Hermitian, the matrix H can be diagonalized. Let $\phi_k(i)$ be the eigenstates of H with eigenvalues ϵ_k, then the transformation to new fermionic operators

$$c_i = \sum_{k=1}^{N} \phi_k(i) a_k \tag{1.68}$$

diagonalizes $\hat{H}$:

$$\hat{H} = \sum_{k=1}^{N} \epsilon_k a_k^\dagger a_k. \tag{1.69}$$

Also the matrix representation of $\hat{H}$ becomes diagonal:

$$H^D = P^\dagger H P = \mathrm{diag}(\epsilon_1, \ldots, \epsilon_N), \tag{1.70}$$

where P is the matrix that has the eigenfunctions as columns.

As we saw in the previous section, a Gaussian state is fully characterized by its correlation matrix, namely by $\langle c_i^\dagger c_j \rangle$. The correlation matrix of a Gaussian state corresponding to a number conserving Hamiltonian, with N particles, is a $N \times N$ matrix:

$$\Gamma = \begin{pmatrix} \langle c_1^\dagger c_1 \rangle & \ldots & \langle c_1^\dagger c_N \rangle \\ \vdots & \ddots & \vdots \\ \langle c_N^\dagger c_1 \rangle & \ldots & \langle c_N^\dagger c_N \rangle \end{pmatrix}. \tag{1.71}$$

This is due to the fact that correlators of the kind $\langle c_i c_j \rangle$ and $\langle c_i^\dagger c_j^\dagger \rangle$ are zero and the correlators $\langle c_i c_j^\dagger \rangle$ can be extracted from the ones in the above matrix using the anti-commutation rules.

Furthermore, as we have seen in the previous section, when we want to extract the bipartite entanglement between a block of L spins and the rest of the chain, we will have to look at the $L \times L$ correlation matrix

$$\Gamma_L = \begin{pmatrix} \langle c_1^\dagger c_1 \rangle & \ldots & \langle c_1^\dagger c_L \rangle \\ \vdots & \ddots & \vdots \\ \langle c_L^\dagger c_1 \rangle & \ldots & \langle c_L^\dagger c_L \rangle \end{pmatrix}. \tag{1.72}$$

Furthermore $\langle c_i^\dagger c_j \rangle^\dagger = \langle c_j^\dagger c_i \rangle$, meaning that Γ_L is hermitian, therefore Γ_L can be diagonalized: $\Gamma_L^D = \mathrm{diag}(\gamma_1, \ldots, \gamma_L)$, having named the eigenvalues γ_i.

As we have already mentioned, the bipartite entanglement between a block of contiguous L spins and the rest of the chain can be quantified with the Von-Neumann entropy:

$$E_{\mathcal{B}_L \mathcal{B}_{\bar{L}}} = S(\rho_L) = -\mathrm{Tr}[\rho_L \log(\rho_L)]. \tag{1.73}$$

As we saw in the previous section, for a diagonal Gaussian Hamiltonian it stands the result of Eq. (1.48), for which

$$S(\rho) = -\sum_{k=1}^{N} [f_k \log(f_k) + (1 - f_k) \log(1 - f_k)], \tag{1.74}$$

where $f_k = \langle a_k^\dagger a_k \rangle$. We notice here that eigenvalues of the corresponding density matrix are precisely $\langle a_k^\dagger a_k \rangle$, meaning that we can calculate the Von-Neumann entropy from the eigenvalues of the correlation matrix. Thus in the case of a non-diagonal correlation matrix, to compute the entanglement entropy between the two blocks of spins $\mathcal{B}_L, \mathcal{B}_{\bar{L}}$, we can find the eigenvalues γ_i of the correlation matrix (1.72) and then compute the entanglement entropy from Eq. (1.74), namely

$$E_{\mathcal{B}_L \mathcal{B}_{\bar{L}}} = -\sum_{k=1}^{L} [\gamma_i \log(\gamma_i) + (1-\gamma_i)\log(1-\gamma_i)]. \tag{1.75}$$

Since we are interested in the time evolution of the entanglement entropy, we need to see how the correlation matrix evolves in the case of a number-conserving Hamiltonian. Of course one can use the general formula (1.58), however in this case we will find that the correlation matrix can be evolved using just matrix multiplication. Let's take the correlation matrix element $\Gamma_{ij} = \langle c_i^\dagger c_j \rangle$ of Eq. (1.71). If we let the system evolve, this matrix element will become

$$\Gamma_{ij}(t) = \langle \psi | \hat{U}^\dagger(t) c_i^\dagger c_j \hat{U}(t) | \psi \rangle \,. \tag{1.76}$$

Exploiting the unitarity of $\hat{U}(t)$,

$$\Gamma_{ij}(t) = \langle \psi | \hat{U}^\dagger(t) c_i^\dagger \hat{U}(t) \hat{U}^\dagger(t) c_j \hat{U}(t) | \psi \rangle = \langle \psi | c_i^\dagger(t) c_j(t) | \psi \rangle \,, \tag{1.77}$$

where $c_i(t) = \hat{U}^\dagger(t) c_i \hat{U}(t)$ is the destruction operator in the Heisenberg picture. We can now find an explicit expression for these operators using the Heisenberg picture:

$$\begin{aligned}
\frac{d}{dt}c_j(t) &= \frac{d}{dt}(\hat{U}^\dagger(t) c_j \hat{U}(t)) = it\hat{U}^\dagger(t)\hat{H}c_j\hat{U}(t) + it\hat{U}^\dagger(t)c_j(-\hat{H})\hat{U}(t) \\
&= -it\hat{U}^\dagger(t)[c_j, \hat{H}]\hat{U}(t) = -it\hat{U}^\dagger(t)\Big(\sum_{k,l} H_{kl}[c_j, c_k^\dagger c_l]\Big)\hat{U}(t) \\
&= -it\hat{U}^\dagger(t)\Big(\sum_{k,l} H_{kl}(\{c_j, c_k^\dagger\}c_l - c_k^\dagger\{c_j, c_l\})\Big)\hat{U}(t) \\
&= \sum_l (-itH_{jl})\hat{U}^\dagger(t)c_l\hat{U}(t) = \sum_l (-itH_{jl})c_l(t).
\end{aligned} \tag{1.78}$$

Solving this differential equation we find[30]:

$$c_j(t) = \sum_{l=1}^{n} e^{-iH_{jl}t} c_l = \sum_{l=1}^{N} U_{jl}(t) c_l. \tag{1.79}$$

With an identical procedure, we find also:

$$c_i^\dagger(t) = \sum_{k=1}^{N} e^{iH_{ik}t} c_k^\dagger = \sum_{k=1}^{N} U_{ik}^*(t) c_k^\dagger. \tag{1.80}$$

Thus, implying the convention of sum over repeated indexes, the time evolution of the correlation matrix element can be written as:

$$\Gamma_{ij}(t) = \sum_{k,l} \langle U^*_{ik}(t) c^\dagger_k U_{jl}(t) c_l \rangle = U^*_{ik}(t) \langle c^\dagger_k c_l \rangle U^T_{lj}(t) = U^*_{ik}(t) \Gamma_{kl} U^T_{lj}(t) = (U^*(t) \Gamma U^T(t))_{ij}. \tag{1.81}$$

This formula can be also derived from Fourier space. This is shown in appendix A. We here stress the fact that this formula is the basis for the implementations of most numerical simulations presented in this thesis.

Before moving on to measurements, we describe the numerical procedure we will follow to compute the time evolution of the entanglement entropy. We will do this using the so called *hopping Hamiltonian*, since this will be employed in this thesis. Indeed this is a simple quadratic Hamiltonian which acts only on nearest neighbours, thus satisfying our requirements of a Gaussian evolution that can be mapped onto a brickwork circuit.

Example: Hopping Hamiltonian We will now describe how to simulate the evolution of a chain of L free fermions and extract the bipartite entanglement as a function of time, using what just discussed in this section. In order to do a numerical simulation of the dynamics of a quantum system we need to set the initial state. Throughout the whole thesis we choose the initial state to be the so called *Néel state*:

$$|\Psi_0\rangle = |0101\ldots01\rangle = \prod_{j=1}^{L/2} c^\dagger_{2j} |0\rangle . \tag{1.82}$$

For this state the initial correlation matrix is $\Gamma_{ij} = \langle \Psi_0 | c^\dagger_i c_j | \Psi_0 \rangle = \delta_{ij}$ for i, j even.

Then we will let the system evolve under a *Hopping* Hamiltonian.

$$H = \sum_{j=1}^{L} (A_{j,j+1} c^\dagger_j c_{j+1} + A^*_{j+1,j} c^\dagger_{j+1} c_j). \tag{1.83}$$

This Hamiltonian can be defined by the circulant matrix [27]

$$A = \begin{pmatrix} 0 & A_{1,2} & 0 & \ldots & A_{1,N} \\ A_{2,1} & 0 & A_{2,3} & \ldots & 0 \\ 0 & A_{3,2} & 0 & \ldots & 0 \\ \vdots & & & \ddots & \vdots \\ A_{N,1} & 0 & 0 & \ldots & 0 \end{pmatrix}, \tag{1.84}$$

noticing that here we set periodic boundary conditions. In this way $\hat{H} = \hat{\vec{\alpha}} A \hat{\vec{\alpha}}$, as in Eq. (1.67). We also need to impose $\hat{H}$ to be Hermitian, thus $A_{ij} = A^*_{ji}$, which translates

into:

$$A = \begin{pmatrix} 0 & A_{1,2} & 0 & \dots & A_{1,N} \\ A_{1,2}^* & 0 & A_{2,3} & \dots & 0 \\ 0 & A_{2,3}^* & 0 & \dots & 0 \\ \vdots & & & \ddots & \vdots \\ A_{1,N}^* & 0 & 0 & \dots & 0 \end{pmatrix}. \tag{1.85}$$

The matrix elements $A_{i,j}$ can be taken to be random numbers, under the constraints just mentioned, or to be fixed (in the latter case we will use the Hamiltonian of Eq. (A.8)). We will let the system evolve in discrete time steps, namely at each time step we will apply

$$\hat{U} = e^{-i\hat{H}} \tag{1.86}$$

to the state of the system after the previous time step. Doing so straightforwardly will be computationally demanding for a classical computer, given the fact that the Hilbert space of the system will have dimension 2^L. However we saw that for Gaussian states the entanglement entropy can be extracted from the correlation matrix, which, in the case of number conserving Hamiltonians, is a $l \times l$ matrix (when we extract the entanglement entropy of a block of l contiguous fermions). So in each time step we will compute

$$\Gamma' = U^* \Gamma U^T, \tag{1.87}$$

where also U is an $L \times L$ matrix. Since we are interested in the bipartite entanglement of a block of l fermions, we will take, at each time step, the first l columns and l rows of the evolved correlation matrix, then we will compute the eigenvalues of Γ'_l (Eq. (1.72)), thus being able to extract the entanglement entropy using Eq. (1.75). How the entanglement entropy evolves in this setting will be thoroughly analyzed in Chap. 3.

1.4 Measurements

In Quantum Mechanics a measurement destroies the unitary evolution. Indeed a quantum system undergoes unitary evolution if the system is closed [10]. Performing a measurement means that there is an interaction between the quantum system and the measurement apparatus, which makes the system no longer closed and thus not necessarily subject to unitary evolution. In this thesis we will deal with *projective measurements* and also with more general forms of measurements, such as *weak measurements*. Furthermore, introducing random measurements during a discretized unitary evolution, will give rise to the concept of *quantum trajectories*. Therefore in this section we will begin illustrating projective measurements, which allows the expleination of the concept of quantum trajectories. Then we will introduce generalized measurements, also called *weak measurements*.

1.4.1 Projective Measurements

When an observable is described by an Hermitian operator M it admits a spectral decomposition

$$M = \sum_m m P_m, \tag{1.88}$$

where P_m is the orthogonal projector onto the eigenspace of M with eigenvalue m, since $P_m^\dagger = P_m$ and $P_m^2 = P_m$ (orthogonal projectors are Hermitian, idempotent and $P_m P_{m'} = \delta_{m,m'} P_m$). The Measurement Postulate of Quantum Mechanics for projective measurements ([10]) states that the probability to measure the eigenvalue m is

$$p(m) = \langle\psi|P_m|\psi\rangle \tag{1.89}$$

and the post-measurement state is

$$|\psi'\rangle = \frac{P_m|\psi\rangle}{\sqrt{\langle\psi|P_m|\psi\rangle}}. \tag{1.90}$$

In the language of density operators, we have that the probability that the outcome of the measurement is m is

$$p(m) = \mathrm{Tr}[\rho P_m] \tag{1.91}$$

and the post-measurement state is

$$\rho' = \frac{P_m \rho P_m}{\mathrm{Tr}[\rho P_m]}. \tag{1.92}$$

Projective measurements have some handy properties, such as a simple way to compute the mean, which will not be discussed as not relevant for the purposes of this dissertation.

Now a simple example on projective measurements will be analyzed, since it will be useful also in the expleination of quantum trajectories.

Example 1.4.1. A projective measurement on a two-level system, embedded in a quantum many-body system, will disentangle the measured subsytem. Indeed let's assume that the entire system is in the state

$$|\Psi\rangle = \frac{|00\rangle + |11\rangle}{2}. \tag{1.93}$$

Let's assume we want to measure Z_1. This has the spectral decomposition

$$Z_1 = (|0\rangle\langle 0| - |1\rangle\langle 1|) \otimes (|0\rangle\langle 0| + |1\rangle\langle 1|) = P_+ - P_-, \tag{1.94}$$

where $P_\pm$ are the projectors onto the eigenspaces of such operator:

$$P_+ = |0\rangle\langle 0| \otimes (|0\rangle\langle 0| + |1\rangle\langle 1|) \quad P_- = |1\rangle\langle 1| \otimes (|0\rangle\langle 0| + |1\rangle\langle 1|). \tag{1.95}$$

The probabilities of the outcomes ± 1 are $p_\pm = \langle\Psi|P_\pm|\Psi\rangle = 1/2$ and the post measurement states are completely disentangled: $|\Psi_+\rangle = |00\rangle$ and $|\Psi_-\rangle = |11\rangle$. Suppose now that the observer looses the result of the measurement. In this case the only thing he can infer about the system is that it will be in state $|\Psi_+\rangle$ with probability $1/2$ and in state $|\Psi_-\rangle$ with probability $1/2$. This means that the system is in a classical mixture, namely the state can be defined with the density matrix

$$\rho = \frac{1}{2}|\Psi_+\rangle\langle\Psi_+| + \frac{1}{2}|\Psi-\rangle\langle\Psi_-|, \tag{1.96}$$

which could also describe the system after an interaction with an external bath.

This simple observation allows us to introduce the concept of quantum trajectories.

Quantum Trajectories

Let's now assume to have a spin chain on which the evolution is done via unitary operations on nearest neighbours [9]. This dynamics is discrete in space and time and the application of the unitaries are divided into even and odd steps, namely one layer of unitaries $U_{j,j+1}$ is done on all odd spins and the next layer is done only on even spins. For instance we do $U_{1,2}, U_{3,4}, \ldots$ on the first layer and $U_{2,3}, U_{4,5}, \ldots$ (this is shown in Fig. 1.2 (a)).

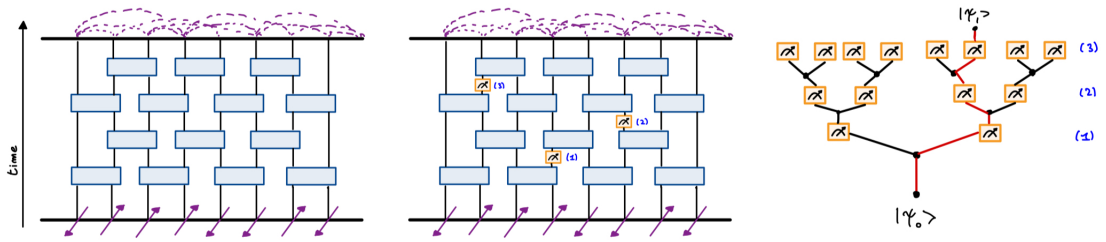

Figure 1.2: *Scheme of the unitary dynamics with the insertion of measurements. Quantum trajectories are schematically depicted in the last picture.*

As we saw in the last example, measurements modify the state of the system, and, if the number of local measurements is extensive in space and time, they fundamentally alter the dynamics of the system, as we will thoroughly see in this thesis. The example of the brickwork circuit with projective measurements is a simple case where we can see how this happens. The basic concept here is the one of *quantum trajectories*. Suppose that we make an experiment where we initialize the quantum many-body system in a pure state $|\psi\rangle$. Then we let it evolve with a circuit-like evolution, but we also do a sequence of $M \geq 1$ local measurements, at different locations and times, alternated to the unitary evolution. In order to avoid confusion, let's suppose that the sequence of

unitaries $U_{j,j+1}(t)$ are fixed in advance and in different runs of the experiment these unitaries are the same, thus leaving randomness just to the measurement outcomes. Suppose, for instance, that we do local projective measurements of Z. Therefore, if spin i is measured, the state undergoes a stochastic evolution

$$|\psi\rangle \longrightarrow \begin{cases} P_{i\uparrow}|\psi\rangle / \sqrt{p_{i\uparrow}} \text{ with probability } p_{i\uparrow} = \langle\psi|P_{i\uparrow}|\psi\rangle \\ P_{i\downarrow}|\psi\rangle / \sqrt{p_{i\downarrow}} \text{ with probability } p_{i\downarrow} = \langle\psi|P_{i\downarrow}|\psi\rangle \end{cases} . \tag{1.97}$$

In a given run of the experiment, we will obtain a random sequence $\vec{m} = (m_1, \ldots, m_M)$ of measurement outcomes, with $m_\alpha = \uparrow, \downarrow$. In general, different runs will yeld different sequences $\vec{m}$. To each measurement record $\vec{m}$, there is an associated evolving state $|\psi_{\vec{m}}(t)\rangle$ and these define a trajectory. It is important to notice that the repeated measurements do not read out a pre-existing unitary dynamics, instead they produce a new kind of dynamics, which can be seen as a random walk in the Hilbert space. If our system was made of a single spin, this would be a trajectory on the Bloch sphere, with measurement causing *quantum jumps* to the north and south pole ([33])

It is important to notice that, as long as the experimenter keeps track of the measurement outcomes $\vec{m}$, the measurement events to not introduce any classical uncertainty about the state, namely the state remains pure (as explained in Ex. 1.4.1). This is different from the interaction of the system with an external bath, where one has to work with mixed states due to this interaction. However there are formal connections between the two settings [34].

Before introducing the concept of *measurement induced phase transitions* for the entanglement entropy, which will bring us also in a deeper discussion about quantum trajectories, we will look at more general forms of measurements.

1.4.2 Generalized Measurements

One of the first lectures of any Quantum Information course, will most certainly include the topic of the *Postulates of Quantum Mechanics* (following the model of [10]). In particular, postulate 3 concerns the measurement operation:

Postulate 1.4.1. Quantum measurement are described by a set $\{M_m\}$ of *measurement operators*. They operate on the state space of the system being measured. If a system is in the state $|\psi\rangle$ before being measured, the probability that the outcome of the measure is m is

$$p(m) = \langle\psi|M_m^\dagger M_m|\psi\rangle \tag{1.98}$$

and the system is left in the state

$$|\psi'\rangle = \frac{M_m|\psi\rangle}{\sqrt{\langle\psi|M_m^\dagger M_m|\psi\rangle}}. \tag{1.99}$$

Furthermore the $\{M_m\}$ satisfy the *completeness relation*

$$\sum_m M_m^\dagger M_m = I, \tag{1.100}$$

which represents the fact that probabilities sum to one ($\sum_m p(m) = 1$). In the formalism of density matrices this translates into a probability

$$p(m) = \mathrm{Tr}[M_m \rho M_m^\dagger] \tag{1.101}$$

and a post-measurement state

$$\rho_m = \frac{M_m \rho M_m^\dagger}{p(m)}. \tag{1.102}$$

These are more general forms of measurements, since they do not require the measurement operators to be Hermitian. Sure enough, these types of operators just need to satisfy a completeness relation (Eq. (1.100)).

Any general measurement of this form may be implemented by performing a unitary interaction between the system and an ancillary system and then performing a projective measurement on the latter. Therefore any possible measurement may be derived from unitary evolution and projective measurements [10]. Since this is one of the types of measurements that we are going to employ in Chap. 4, we will here explain what just said in detail.

Generalized measurements are "projective measurements in enlarged space" Suppose we have a system $\mathcal{H}_S$ and an ancillary system $\mathcal{H}_A$. Suppose that on $\mathcal{H}_S$ we have a generalized measurement defined by the set of operators $\{M_m\}_{m=0}^R$, which satisfy the completeness condition in Eq. (1.100). Suppose also that $\mathcal{H}_A$ is the span of $\{|0\rangle, |1\rangle, \ldots, |R\rangle\}$, namely it has dimension equal to the number of measurement operators M_m.

On this system we define the operation

$$\mathcal{U} |\psi_S\rangle |0_A\rangle = \sum_{m=0}^{R} (M_m |\psi_S\rangle) \otimes |0_A\rangle, \tag{1.103}$$

namely $\mathcal{U}$ performs a measurement on $\mathcal{H}_S$. This is clearly a linear operator. Moreover it preserves the scalar product. Indeed, suppose we have the states $|\Phi\rangle = |\phi_S\rangle |0_A\rangle$ and $|\Psi\rangle = |\psi_S\rangle |0_A\rangle$, then we find that

$$\begin{aligned} \langle \Phi | \mathcal{U}^\dagger \mathcal{U} | \Psi \rangle &= \sum_{m,n=0}^{R} \langle \phi | M_m^\dagger M_m | \psi \rangle \langle m | n \rangle = \sum_{m,n=0}^{R} \langle \phi | M_m^\dagger M_m | \psi \rangle \delta_{m,n} \\ &= \sum_{m=0}^{R} \langle \phi | M_m^\dagger M_m | \psi \rangle = \langle \phi | I | \psi \rangle = \langle \phi | \psi \rangle . \end{aligned} \tag{1.104}$$

We now define a subspace $\tilde{\mathcal{H}} = \text{span}\{|\psi_S\rangle, |0_A\rangle\}$, which is a subspace of $\mathcal{H}_S \otimes \mathcal{H}_A$. Formalizing what said until now about $\mathcal{U}$, we have that

$$\begin{aligned} \mathcal{U} :\ & \tilde{H} \longrightarrow \mathcal{H}_S \otimes \mathcal{H}_A \\ & |\psi_S\rangle |0_A\rangle \mapsto \mathcal{U} |\psi_S\rangle |0_A\rangle \end{aligned} \tag{1.105}$$

and it is an *isometry*, namely

$$\langle v|\mathcal{U}^\dagger \mathcal{U}|w\rangle = \langle v|w\rangle \quad \forall\ |v\rangle, |w\rangle \in \mathcal{H}. \tag{1.106}$$

An operator having this property can be linearly extended to an operator $\mathcal{V} : \mathcal{H}_S \otimes \mathcal{H}_A \longrightarrow \mathcal{H}_S \otimes \mathcal{H}_A$ such that:

- when acting upon states in $\tilde{\mathcal{H}}$, $\mathcal{U}$ and $\mathcal{V}$ operate in the same manner, i.e.

$$\mathcal{V} |\psi_S\rangle |0_A\rangle = \mathcal{U} |\psi_S\rangle |0_A\rangle \tag{1.107}$$

- $\mathcal{V}$ is an isometry, i.e $\mathcal{V}^\dagger \mathcal{V} = I$.

Take now projective operators P_m on the ancilla system, such that $P_m = I_S \otimes |m\rangle_A \langle m|$. We can now prove that performing a generalized measurement M_m on the system $\mathcal{H}_S$ is equivalent to perform $\mathcal{V}$ and then the projective measurement P_m on $\mathcal{H}_A$, following the points of postulate 1.4.1.

Proof. Taking the state $|\psi\rangle |0\rangle$, applying $\mathcal{V}$ and then P_m we have:

$$\begin{aligned} p(m) &= \langle 0| \langle \psi|\mathcal{V}^\dagger P_m \mathcal{V}|\psi\rangle |0\rangle = \sum_{l,r} \langle l| \langle \psi|M_l^\dagger (I \otimes |m\rangle \langle m|) M_r |\psi\rangle |r\rangle \\ &= \sum_{l,r} \langle \psi|M_l^\dagger M_r|\psi\rangle \delta_{l,m}\delta_{r,m} = \langle \psi|M_m^\dagger M_m|\psi\rangle , \end{aligned} \tag{1.108}$$

which is doing a generalized measurement on $\mathcal{H}_S$. Then we need to look at the post-measurement state, which is

$$\frac{P_m \mathcal{V} |\psi\rangle |0\rangle}{\sqrt{\langle 0| \langle \psi|\mathcal{V}^\dagger P_m \mathcal{V}|\psi\rangle |0\rangle}} = \frac{M_m |\psi\rangle}{\sqrt{\langle \psi|M_m^\dagger M_m|\psi\rangle}}, \tag{1.109}$$

where we can discard the ancilla, since this is a factorized state, and recover the post-measurement state for a generalized measurement. □

Weak Measurements Generalized measurements are also called *weak measurements*. With respect to projective measurements, they perturb less the system, meanwhile extracting less information from it. Indeed suppose we have

$$M_1(\epsilon) = \sqrt{\frac{1}{2} - \epsilon}\,|0\rangle\langle 0| + \sqrt{\frac{1}{2} + \epsilon}\,|1\rangle\langle 1| \tag{1.110}$$

$$M_2(\epsilon) = \sqrt{\frac{1}{2} + \epsilon}\,|0\rangle\langle 0| + \sqrt{\frac{1}{2} - \epsilon}\,|1\rangle\langle 1|\,, \tag{1.111}$$

for which is easy to verify that $\sum_{m=1}^{2} M_m^\dagger M_m = I$. This measurement operation is projective for $\epsilon \to 1/2$, whereas for $\epsilon \to 0$, the post measurement states are close to each other [3] and we have less information about the system, because $p(0), p(1) \to 1/2$.

[3] Close in the sense that their scalar product is close to one.

Chapter 2

Measurement Induced Entanglement Phase Transitions

In this chapter we will describe *measurement induced entanglement phase transitions* (MIEPT). In Sec. 2.1 we will briefly recall the general features of phase transitions. More precisely we will highlight the differences between classical and quantum phase transitions, stressing the peculiarity of MIEPT. Then in Sec. 2.2 we will describe the mechanism that generates the MIEPT, without going into the formal details[1]. However, in order to understand this mechanism, we will explore deeper the concept of quantum trajectories, explaining some details that are crucial in the understanding of this phenomenon (Sec. 2.3).

2.1 Phase Transitions: an Overview

Classical and quantum phase transitions are processes where a system undergoes a change from one phase to another, but the two differ fundamentally in their underlying mechanisms and in the nature of the transition. Classical phase transitions are driven by thermal fluctuations, whereas quantum phase transitions occur at zero-temperature, due to the change in a non-thermal control parameter. Their common trait is that the variation of an external control parameter leads to a qualitative change in the system properties [35]. Moreover, at the critical point of quantum phase transitions, the system's properties are dominated by quantum fluctuations. Also, quantum phase transitions are characterized by a change in the ground state properties of the system [35], however, as we will see, this is not the case for MIEPT.

Classically, phase transitions are classified in *first-order phase transitions* and *second-order phase transitions*. The former involve a latent heat, they are characterized by a

[1] A Conformal Field Theory approach to MIEPT is possible, however this is not the topic of this thesis.

finite value of the correlation length and a discontinuous change of the order parameter. The latter, also called continuous phase transitions, are characterized by the absence of a latent heat, the divergence of the correlation length at the critical point and the continuous change of the order parameter. In this case, derivatives of the order parameter diverge following power laws. Furthermore, the behaviour of some quantities at the critical point is characterized by the set of *critical exponents*, which also define the *universality class* of the phase transition [36].

For the sake of completeness, we here recall that for continuous phase transitions, given the fact that the correlation length diverges, one can study the system at the critical point with more advanced approaches, such as the *renormalization group* and *Conformal Field Theory* (CFT)[36][2].

Before diving into MIEPT, we will discuss an example ([36]) of phase transitions from classical physics, because it clearly explains the competitive principles that lead to phase transitions and therefore it will help in the understanding of the mechanism behind entanglement transitions.

Example 2.1.1. Take a material in which magnetic dipoles are randomly oriented and they produce a zero-total magnetic field. However, in certain materials (*ferromagnetic*), one can observe, below a critical temperature T_c (called *Curie temperature*), that there is a non-zero total magnetic field. The system has undergone a phase transition at the temperature $T = T_c$, which, in this case, is a spontaneous magnetization, due to the alignment of the dipoles. The occurrence of this phase transition is due to the interplay of two competitive principles: *energy minimization* and *entropy maximization*. The former tends to align the spins and the minimum energy is achieved when all spins are aligned (corresponding to aligned dipoles and thus non-zero magnetic field). The latter tends to randomly orientate the spins. Indeed, from the prospective of the phase space, the number of configurations in which the spins are randomly oriented are way more than the only configuration where all spins are aligned. The control parameter, in this case the temperature, establishes which of the two principles is dominant.

Having in mind this simple example, we can now discuss MIEPT.

2.2 Measurement Induced Entanglement Transition

Entanglement phase transitions refer to changes in the entanglement properties of a quantum system, unlike common quantum phase transitions, where there are changes in the properties of the ground state of the system ([35]). Moreover MIEPT are different from other phase transitions, since there is not an evident order parameter.

[2]We will not recall more concepts of these approaches, since they are not strictly addressed in this thesis. However, in the following, some aspects of these theories may be recalled if relevant.

Before describing MIEPT, we here recall that entanglement transitions are also observed in disordered systems, where the transition from an *ergodic* phase, where the system thermalizes and the entanglement spreads extensively, to a *many-body localized* phase, where the system fails to thermalize and entanglement does not spread extensively, can be viewed as an entanglement transition [2].

Now we move to the description of *measurement induced phase transitions*. To understand how they work, we follow the example of the previous section. Let's assume that a qubit chain is in an initial state $|\psi_0\rangle$, which is a product state. Obviously, the initial entanglement is zero. Now we let the system evolve under a unitary dynamics (following the unitary operator $U = \exp(-iHt)$). If the Hamiltonian has multi-qubit terms, the system will no longer be in a product state, hence leading to a growth of entanglement, at least with respect to the initial state. Therefore we can state that the unitary dynamics brings to a growth of correlations in the system, namely a growth in the entanglement entropy, since the wavefunction that describes the system is no longer a product state. If one adjusts the system and subsystem sizes[3], respectively L and l, in order to satisfy the condition $l/L \ll 1$, one finds that the entanglement entropy saturates to a constant value, which is proportional to the volume of the subsystem size [4]. Indeed, under unitary evolution, the entanglement entropy follows a *volume-law*, meaning that the entanglement entropy saturates to a value proportional to the volume of the subsystem (in case of a qubit-chain, the volume is the number of qubits in the subsystem).

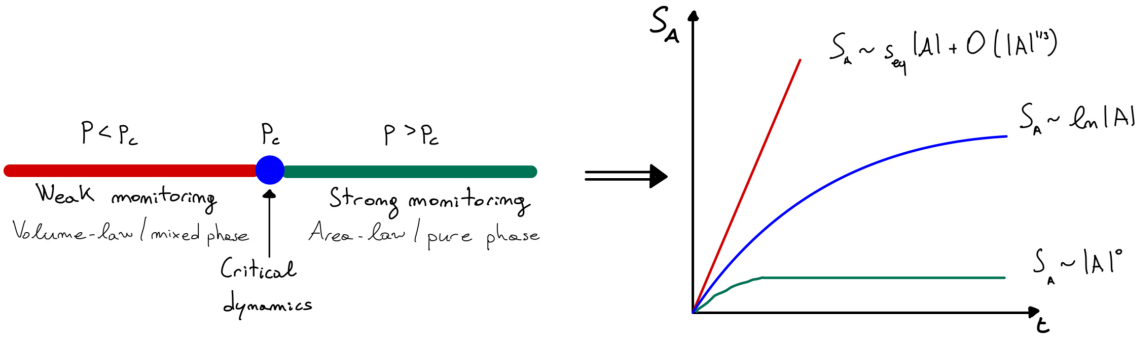

Figure 2.1: *Monitored dynamics in* $(1+1)$*-dimensions brings to a phase transition in the entanglement entropy as a function of* p*. This is schematically showed in the left picture. on the right, the scaling of the entanglement entropy for a subsystem size* $|A|$ *is displayed.*

We saw, in Example 2.1.1, that in order to have a phase transition, there has to be an interplay between two physical instances. In the case of MIEPT, the other player that gives rise to the entanglement phase transition is the measurement operation. Indeed,

[3]The subsystem is the block of spins that we take in order to compute the bipartite entanglement.
[4]See Sec. 3.2.1 for more details about this.

as discussed in Example 1.4.1, measuring a qubit disentangles it, namely one can write the system as a product state between the state of the measured qubit and the rest of the system, which may still be entangled. In order to talk about this type of phase transitions, let's put ourselves in the context of a brickwork circuit, where we assume that, after each step of unitary evolution, there is a probability p that a measurement occurs in each site of the qubit chain.

Before diving in the intermediate cases, let's focus on the case where each site of the chain is measured at every time step, namely let's assume that $p = 1$. Given an initial product state, the steps of unitary evolution will tend to generate entanglement in the system, however, since $p = 1$, after each one of such steps all the qubits are measured and therefore disentangled. Hence the system will be described by a product state throughout its evolution, yielding an entanglement entropy equal to zero after each time step (made of a unitary layer and a measurement layer). This is an example of *quantum Zeno effect* [13]. This is a first instance, although drastic, of the entanglement entropy following an *area-law*. Indeed we call area-law the case where the entanglement saturates to a value which is a constant (in this case zero).

Now we can clearly see how the probability p to perform a measurement on a given site is the external control parameter that drives the phase transition. Indeed, in order to build a phase diagram, we need to see what happens for intermediate values of p.

In Fig. 2.1 a scheme of the phase diagram of a typical MIEPT is displayed. Here we can see that for values of p (i.e. for *weak monitoring*), namely for values of $p < p_c$, where p_c is the critical probability that denotes the critical point, the entanglement entropy follows a volume-law or a mixed phase law, whereas for values of $p > p_c$ (i.e. for *strong monitoring*), the entanglement entropy follows an area-law. Instead, looking at the critical dynamics ($p = p_c$), the entanglement entropy follows a logarithmic law. This is a random but scale-invariant structure for the entanglement entropy [9].

For random circuits, the phases and the transitions can be mapped to an effective classical statistical mechanics model, where the problem is approached using, for instance, the replica trick and tensor network techniques ([14], [15], [37], [38]). This is a vast and advanced theory that we will not consider further, since its study would have been a whole other thesis.

Finally we must mention that numerical evidence of this transition has been found in several microscopic models ([12], [13], [16], [19], [39], [20], [40] etc.) and also some experimental attempts have been done. The first one ([21]) was carried out on a trapped ion quantum computer, whereas another one ([22]) was done on IBM's superconducting quantum computers.

2.3 Quantum Trajectories

Another key point in understanding MIEPT is the concept of quantum trajectories. Here we give more details, which widen the description already given in Sec. 1.4, in the paragraph about quantum trajectories. We saw that an initial pure state $|\psi(0)\rangle$, evolving under a hybrid circuit, defines a set of trajectories, labelled by the measurement outcomes $\vec{m}$:

$$|\psi_{\vec{m}}\rangle = \frac{K_{\vec{m}}\,|\psi(0)\rangle}{\sqrt{p_{\vec{m}}}}. \tag{2.1}$$

The Born probability $p_{\vec{m}} = \langle\psi(0)|K_{\vec{m}}^{\dagger}K_{\vec{m}}|\psi(0)\rangle$ of a trajectory depends on the state, making the dynamics of the monitored circuit both non-linear and non-unitary. The idea of measurement induced transitions ([12], [13], [16]) is that there is a qualitative change in the nature of the trajectories (Eq. (2.1)) as a function of the measurement rate p. One can view the MIEPT as the evolution of quantum trajectories in the Hilbert space. Indeed when p is above the threshold p_c, the stochastically evolving wavefunction is trapped in the subspace of the Hilbert space of area-law states. Instead when $p < p_c$, the wavefunction escapes this subspace and enters into the volume-low subspace of the Hilbert space.

Now let ρ_i denote the density operator for the quantum trajectory $\mathcal{T}_i$. Let $\mathcal{O}[\rho_i]$ be a general functional on the density operator[5]. We denote by $\bar{\mathcal{O}}$ the average over all quantum trajectories, which in general is:

$$\bar{\mathcal{O}} = \frac{1}{N}\sum_{i=1}^{N}\mathcal{O}[\rho_i], \tag{2.2}$$

where N is the number of quantum trajectories. Now we denote $\bar{\rho} = \sum_{i=1}^{N}\rho_i/N$ the average density operator. If and only if $\mathcal{O}$ is a linear functional of ρ, we have that $\bar{\mathcal{O}} = \mathcal{O}[\bar{\rho}]$. One must notice that if a measurement is performed, but its outcome is lost, the state is not pure and evolves as $\rho \to \sum_{a=1}^{A} K_a\rho K_a^{\dagger}$, where K_a are Kraus operators representing the measurement operation. If we consider observables that are linear functionals of the density matrix, the result of the average over a statistical mixture and the average in Eq. (2.2) coincide. In our case we are looking at the entanglement entropy (Eq. (1.5)), which is non-linear. Therefore in order to have the average over quantum trajectories we must utilize Eq. (2.2). This is the difference between *coherent trajectories* and *dissipative information loss*. Under the circuit dynamics the density matrix $\rho(0)$ evolves into $\rho_{\vec{m}} = K_{\vec{m}}\rho(0)K_{\vec{m}}^{\dagger}/p_{\vec{m}}$, with a probability $p_{\vec{m}} = \mathrm{Tr}[K_{\vec{m}}^{\dagger}K_{\vec{m}}\rho(0)]$, which is the state if the measurement outcomes $\vec{m}$ have been recorded. Instead, if this information is lost (meaning that we have classical uncertainty on the measurement outcomes), we have the trajectory average $\bar{\rho} = \sum_{\vec{m}} p_{\vec{m}}\rho_{\vec{m}}$. In the hybrid circuit dynamics $\bar{\rho}$ will tend to the

[5]In Chap. 4 we will do averages over quantum trajectories.

trivial infinite temperature density matrix [9]. Quantum trajectories are not a problem that can be tackled easily in an experimental setting, where the issue of *post-selection* arises ([21], [22]). Indeed, we need to run several experiments with the same state produced at every run, namely we need to be able to reproduce the same outcomes of all the measurements $\vec{m}$.

Chapter 3

Entanglement Entropy in the Brickwork Circuit Model

The goal of this chapter is to better explain why the study of *brickwork circuits* is crucial for the development of quantum simulations [41]. Therefore in Sec. 3.1 we will give an overview of quantum simulations, stressing how *analog quantum simulations* (AQS) are different from *digital quantum simulations* (DQS), explaining also why *brickwork circuits* are interesting for the latter type of quantum simulations. As explained in Chap. 1, we are studying systems that can be simulated on classical computers. We will therefore describe the evolution of the entanglement entropy in a fermionic chain which evolves under a *hopping Hamiltonian* in Sec. 3.2. At last, in Sec. 3.3 we will analyze the brickwork circuit that describes a system evolving under a hopping Hamiltonian and we will prove that, in this case, the entanglement entropy evolves in the same way as in the continuous model, thus showing that a fermionic chain can be simulated on a quantum computer. The theoretical proof of this is very straightforward, however we will give also a numerical proof, since the code implemented at this stage will be useful in the next chapter. Moreover, as we will explain the continuous time evolution in Sec. 3.2, we will also describe how the entanglement entropy behaves in the systems under consideration, giving also a semi-classical interpretation to the growth of the entanglement entropy. We here notice that, as explained in Chap. 1, in this thesis we are studying quantum systems that can be simulated on a classical computer, therefore all the results displayed in this chapter are obtained from classical simulations. This, however, does not affect the result of this chapter, namely that a fermion chain evolving under a hopping Hamiltonian can be simulated on a digital quantum computer.

3.1 Quantum Simulation: an Overview

With nowadays NISQ devices, the scientific community is looking foreword to quantum simulation as the mean to validate models through experiments. Indeed the goal of quantum simulation is to simulate Quantum Mechanics on quantum computers, thus overcoming the limits of such simulations on classical computers. Quantum simulation is divided in two main categories: *Analog Quantum Simulation* (AQS) and *Digital Quantum Simulation* (DQS) [7].

For AQS, a mapping between the Hamiltonian of the system and the Hamiltonian of the simulator must exist in order to do the simulation. Sometimes the mapping can be very straightforward, however this is not the case in general.

In DQS, the circuit model of quantum computation is employed. The initial state of the system $|\psi(0)\rangle$ will evolve under a Hamiltonian H_{sys} in the well known way $|\psi(t)\rangle = U(t)\,|\psi(0)\rangle = \exp(-iH_{\text{sys}}t)\,|\psi(0)\rangle$. Here the unitary $U(t)$ is a complicated many-body unitary, which in DQS must be mapped onto a sequence of one and two-qubit gates. Any unitary operation can be written in terms of universal quantum gates [10], hence any system can be simulated [42][1].

Leaving aside the problem of the *initial state preparation* and of the *measurement* of the digital quantum simulator, we will address the problem of the unitary evolution on a digital device, being this the scope of this chapter.

Unitary Evolution Let's assume that the Hamiltonian of the system we wish to simulate can be written as a sum of local interactions:

$$H = \sum_{\alpha} H_{\alpha}. \tag{3.1}$$

In this case, if $[H_{\alpha}, H_{\alpha'}] = 0 \;\forall\; \alpha, \alpha'$, then

$$U(t) = \prod_{\alpha} e^{-iH_{\alpha}t}, \tag{3.2}$$

making the decomposition into local gates very straightforward. Examples of this are the Hubbard and Ising Hamiltonians [7]. However this is not the general case. Indeed if $[H_{\alpha}, H_{\alpha'}] \neq 0$, Eq. (3.2) no longer holds. Indeed the following asymptotic approximation is at the core of quantum simulation [10]:

Theorem 3.1.1. ***(Trotter Formula)*** *Let A and B be Hermitian operators. Then, for any real t,*

$$\lim_{M\to\infty} (e^{iAt/M} e^{iBt/M})^M = e^{i(A+B)t}. \tag{3.3}$$

[1]Not any Hamiltonian can be efficiently simulated, however we will not get into this, as we will not get into many other details of quantum simulations, since it is not the goal of this thesis.

Therefore, if we assume that $H = \sum_\alpha H_\alpha$, even if $[H_\alpha, H_{\alpha'}] \neq 0$, we will have that

$$e^{-iHt} = \lim_{M\to\infty} \Big(\prod_\alpha e^{-iH_\alpha t/M} \Big)^M . \tag{3.4}$$

We are not proving this theorem, since it is a well known result in Quantum Mechanics, neither we will here give explicit examples, since in the next sections we will apply what just stated to our model.

It is now important to notice how brickwork circuit models are important for DQS. Indeed they are simple discrete-time models for many-body dynamics. In these models, a lattice of qubits (spins) evolves through the application of local unitary gates. During the unitary evolution also measurements can be applied, as we saw in Chap. 1 and as we will discuss also in Chap. 4. This discrete time structure recalls the *trotterization* of a continuous-time Hamiltonian evolution that we just discussed. However in this models the time steps are not infinitesimal, since each local operation will not be close to the identity in general [9].

3.2 Continuous Evolution

In order to compare the continuous evolution and the discrete-time evolution of the brickwork circuit, we first analyze the continuous case, which is simpler. In this setting we will also describe how the entanglement entropy behaves in a chain of L fermions and give a semi-classical interpretation to this behaviour.

It is well established that, for a closed quantum system, given an initial state $|\psi(0)\rangle$ and a Hamiltonian H, the state of the system after a time t will be $|\psi(t)\rangle = \hat{U}(t)\,|\psi(0)\rangle = \exp(-i\hat{H}t)\,|\psi(0)\rangle$. Now our goal is to study a fermionic chain, governed by the hopping Hamiltonian

$$\hat{H} = \sum_{j=1}^{L} (\alpha c_j^\dagger c_{j+1} + \alpha^* c_{j+1}^\dagger c_j). \tag{3.5}$$

This Hamiltonian conserves the number of fermions in the chain, i.e. $[\hat{H}, \hat{N}] = 0$. As we saw in Chap. 1, the entanglement entropy can be extracted from the correlation matrix and the correlation matrix evolves as described in Eq. (1.81). Being this a multiplication between $L \times L$ matrices, this system can be efficiently simulated on a classical computer, but this will not be continuous in time. Even so, this is not a problem. Indeed let's assume that the time t is discretized such as $t = \tau M$. Now at each time step τ we will apply to the system the evolution operator $\hat{U}(\tau) = \exp(-i\hat{H}\tau)$. Hence we apply $\hat{U}(\tau)$ M times:

$$|\psi(t)\rangle = \hat{U}(\tau)\hat{U}(\tau)\ldots\hat{U}(\tau)\,|\psi(0)\rangle = (\hat{U}(\tau))^M\,|\psi(0)\rangle\,. \tag{3.6}$$

This product of evolution operators is a product between exponential operators whose exponents commute (obviously $[\hat{H}, \hat{H}] = 0$), therefore

$$(\hat{U}(\tau))^M = (e^{-i\hat{H}t/M})^M = e^{-i\hat{H}t}, \tag{3.7}$$

thus proving that the discrete evolution is equal to the continuous one. Therefore the evolution of the correlation matrix can be done setting $\tau = 1$, thus

$$\Gamma' = U^\dagger \Gamma U^T, \tag{3.8}$$

where $U = e^{-iH}$. This can be directly implemented on a classical computer.

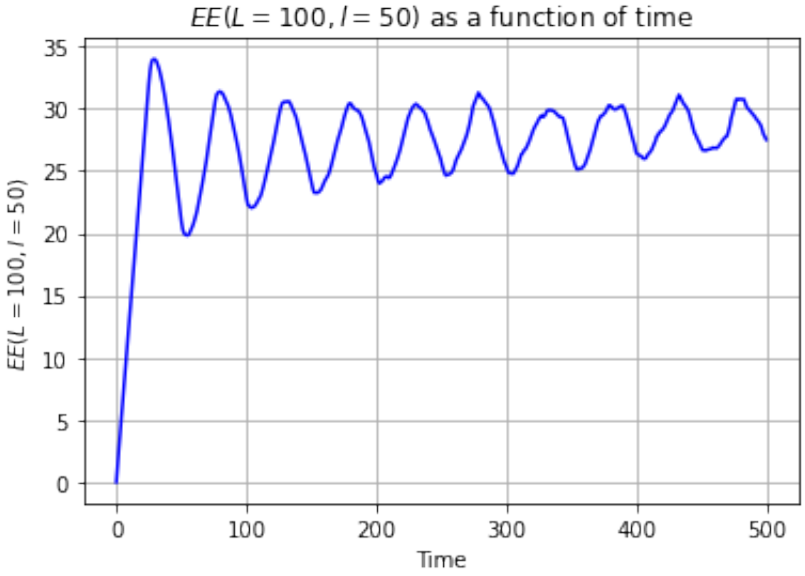

Figure 3.1: *Evolution of the entanglement entropy under a hopping Hamiltonian for a system of size* $L = 100$*, subsystem size of* $l = 50$*.*

In order to do a simulation we need to set four parameters. First of all we have to choose the value of α in Eq.(3.5). For the sake of simplicity in the topics that will follow soon, we take $\alpha = -1/2$. As explained in the example of Sec. 1.3.6, H will be a circulant matrix, with all non-zero entries equal to $-1/2$. Then we need to set L and l. As a first approach we can take them arbitrarily. For example we can look at the bipartite entanglement in a chain of $L = 100$ fermions between two subsystems of equal length $l = 50$. Finally we need to set the total evolution time. We can take $t = 50$, which, as just explained, translates into applying U 50 times to the initial correlation matrix. The initial correlation matrix depends on the initial state of the system which we choose to be the *Néel state* (for reasons that will be clear in a little while):

$$|\Psi_0\rangle = |0101\ldots01\rangle\,. \tag{3.9}$$

For this state the initial correlation matrix is $\Gamma_{ij} = \langle\Psi_0|c_i^\dagger c_j|\Psi_0\rangle = \delta_{ij}$ for i, j even. The result of the simulation is displayed in Fig. 3.1. Here we can see how the entanglement entropy grows linearly up to a certain time and then its value begins oscillating. This behaviour is called *collapse and revival* and it turns out to be due to a *finite-size* effect [43]. To understand this behaviour we introduce a semi-classical interpretation known as the *quasiparticle picture*.

3.2.1 Quasiparticle Picture

The *quasiparticle picture* is a semi-classical setting which describes how the entanglement entropy behaves in certain 1D systems, which include free fermions ([28], [43]). More precisely this is described by the classical motion of *quasiparticles* inside the system. In order to describe this we first need to briefly describe *thermalization* end the *Generalized Gibbs Ensemble*.

Stationary States and Entanglement Entropy Let us consider a quantum many-body system out of equilibrium. If the system is initially in a pure state, it will remain such during the time evolution, since the time evolution is unitary. If now we take a bipartition of the system in A, $\bar{A}$, the density matrix of the total system will be $\rho(t) = |\Psi(t)\rangle\langle\Psi(t)|$ (pure), whereas the reduced density matrix of the subsystem A will be $\rho_A(t) = \mathrm{Tr}_{\bar{A}}[\rho(t)]$, which can be mixed. It is important to notice that the physics of subsystem A is fully encoded in its reduced density matrix [28], in the sense that $\rho_A(t)$ is sufficient to determine all the correlation functions within the subsystem itself. In fact, the expectation values of a product of local operators $\prod_i O(x_i)$ with $x_i \in A$, which, by the way, are the ones accessible in experiments, is given by

$$\langle\Psi(t)|\prod_i O(x_i)|\Psi(t)\rangle = \mathrm{Tr}[\rho_A(t)O(x_i)]. \tag{3.10}$$

Now a question rises naturally: do local observables reach stationary values? In the following we will say that, after a quantum quench, an *isolated infinite system* relaxes to a stationary state, if, for all subsystems A, it exists the limit

$$\lim_{t\to\infty} \rho_A(t) = \rho_A(\infty). \tag{3.11}$$

Therefore the balancing of a closed quantum system to a statistical ensemble is tightly connected with the concept of reduced density matrices. Notice also that, in the limit procedure, the thermodynamic limit has to be taken before the infinite time limit. In fact phenomena as quantum recurrences and revivals prevent relaxation for finite systems [28] (more on this later). We also must notice that the subsystem A can be taken to be anywhere on the infinite translational invariant entire system. Also the limit of a large subsystem A can be taken, but only after the large time limit. Only the here outlined

order of the limits leads to a consistent definition of equilibrium for an isolated quantum system.

Now we can see how $\rho_A(t)$ might correspond to a statistical ensemble. A first guess would be to identify $\rho_A(t)$ with a thermal state. Nevertheless this would be valid only for thermodynamically large subsystems. Instead we will take the path outlined in [44, 45, 46, 47, 48]. Let us consider a statistical ensemble with density matrix ρ_E for the entire system. The reduced density matrix for subsystem A is

$$\rho_A = \mathrm{Tr}_{\bar{A}}[\rho_E]. \tag{3.12}$$

The stationary state is said to be described by the statistical ensemble ρ_E if, for any finite subsystem A, it holds that

$$\rho_A(\infty) = \rho_{A,E}. \tag{3.13}$$

The implication of this is that any local multi-point correlation function within A may be evaluated using ρ_E. We will be concerned with two statistical ensembles: the thermal (Gibbs) ensemble and the generalized Gibbs ensemble (GGE). We say that a non-equilibrium quantum system thermalizes after a quench when ρ_E is the Gibbs distribution

$$\rho_E = \frac{e^{-\beta H}}{Z}, \tag{3.14}$$

with $Z = \mathrm{Tr}[e^{-\beta H}]$. Notice that the inverse temperature is not a free parameter, but is fixed by the conservation of energy. Thermalization leads to the fact that all local observables will have thermal expectation values, whereas some non-local quantities will remain non-thermal for arbitrary large times. Meanwhile all non-integrable systems thermalize ([1], [49], [50], [51]), the conservation laws present in integrable models lead to a different dynamics and relaxation. Since integrable models have, by definition, an infinite number of integrals of motion in involution, rather than a thermal ensemble, the system, at large times, is expected to be described by a GGE [52], with density matrix

$$\rho_{GGE} = \frac{e^{\sum_n \lambda_n I_n}}{Z}. \tag{3.15}$$

Here the operators I_n form a complete set of integrals of motion and $Z = \mathrm{Tr}[e^{\sum_n \lambda_n I_n}]$ is the usual normalization constant. As in the Gibbs ensemble the Lagrange multipliers $\{\lambda_n\}$ are not free, but are set by the conservation laws [2].

In finite systems, when there is a maximum velocity of propagation v_M, as long as we consider times such that $v_M t < L$, where L is the linear size of the whole system,

[2] An exhaustive discussion of integrable models and their conservation laws go beyond the scope of this thesis, so they will be not treated here.

all measurements will provide the same outcome as in an infinite system (away from the boundaries) [28]. Therefore, a subsystem of linear size l can show stationary values as long as L is large enough to guarantee $l \ll v_M t < L$.

Now let us discuss a little more the bipartite entanglement of a many-body quantum system formed by many 1/2 spins on a lattice and a state which is a collection of singlets between different pairs of spins at arbitrary distances. All singlets within A or $\bar{A}$ do not contribute to the entanglement entropy S_A, whereas each share singlet contributes with a $\log_2(2)$ bit of entanglement. Thus the total entanglement entropy is $S_A = n_{A:\bar{A}} \log_2(2)$, with $n_{A:\bar{A}}$ being the number of shared singlets. In out of equilibrium many-body quantum systems the stationary value of the entanglement entropy $S_A(\infty) = -\mathrm{Tr}[\rho_A(\infty) \log(\rho_A(\infty))]$ for a thermodynamically large subsystem A is deduced from the reasoning previously outlined. In fact we saw that a system relaxes for large times to a statistical ensemble ρ_E when, for any subsystem A, $\rho_{A,E} = \rho_A(\infty)$. Therefore the stationary entanglement entropy must equal $S_{A,E} = -\mathrm{Tr}[\rho_{A,E} \log(\rho_{A,E})]$. For a large subsystem with volume V_A, $S_{A,E}$ scales like V_A, since the entropy is an extensive quantity. Hence $S_{A,E}$ equals the density of the thermodynamic entropy $S_E = -\mathrm{Tr}[\rho_E \log(\rho_E)]$ times V_A. Since $S_{A,E} = S_A(\infty)$, the stationary entanglement entropy has the same density of the thermodynamic entropy. We have thus just proved [28]:

$$s \equiv \lim_{t\to\infty} \frac{S_E}{V} = \lim_{V_A\to\infty} \frac{\lim_{V\to\infty} S_{A,E}}{V_A} = \lim_{V_A\to\infty} \frac{\lim_{V\to\infty} S_A(\infty)}{V_A}. \tag{3.16}$$

Here we must stress that this equality holds only for the extensive leading terms of the entropy. This equality has been verified analytically for non-interacting many-body systems ([3], [53] etc.).

Quasiparticle Picture for Entanglement Entropy This picture is just a simplified model, which allows us to explain the observations on the time evolution of the entanglement entropy [28]. The initial state of the system has a higher energy then the ground state of the Hamiltonian that drives the quench (for example a Néel state evolving under a hopping Hamiltonian), thus this state acts as a source of quasiparticle excitations. Particles emitted from different points on the lattice, further apart then the correlation length, are not entangled, whereas particles emitted from the same point are highly entangled. We suppose that the probability to create a pair of particles with momenta (q, q') is $f(q, q')$ and that they move classically once they separate. If the quasiparticle dispersion relation is $E(p)$, the classical velocity will be $dE(p)/dp$. We also assume that there is a maximum velocity that we set to 1, namely $|v(p)| \leq 1$. Ignoring scattering effects between these particles, a particle's position at time t will be $x(t) = x + v(p)t$. Indeed let's assume that a quasiparticle pair is produced with opposite momentum q and $-q$ at point x. At time t they will be in the positions $x' = x + v_q t$ and $x'' = x - v_q t$ and the entanglement between two subsystems l and $\bar{l}$ of the chain is related to the pairs of

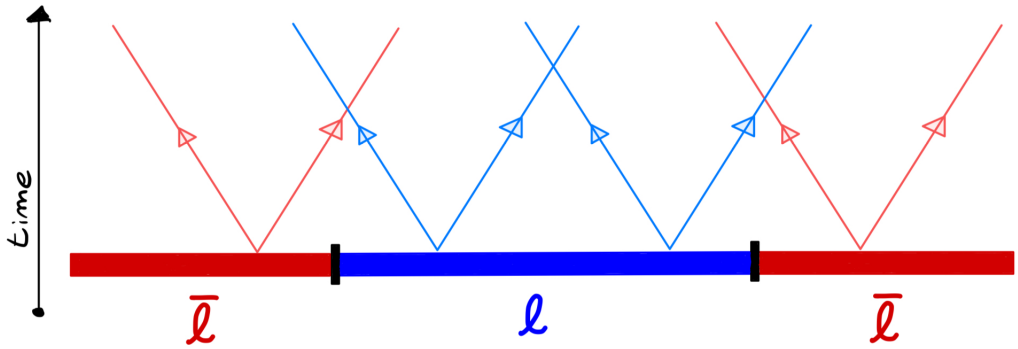

Figure 3.2: *Scheme of the propagation of quasiparticles (here l is the subsystem).*

quasiparticles shared between the two subsystems after being emitted from the arbitrary same point x. For a fixed momentum q, this is proportional to the length of the interval in x such that $x' = x \pm v_q t \in l$ and $x'' = x \mp v_q t \in \bar{l}$. The proportionality constant depends on the production rate of quasiparticle pairs with opposite momenta $(q, -q)$ and their contribution to the entanglement entropy itself. The combined result of these two effects is a function $s(q)$ which depends on the momentum q of each quasiparticle in the pair. This function encodes all the information of the initial state for the entanglement evolution. The total entanglement entropy is thus:

$$S_l(t) \approx \int_{x' \in l} dx' \int_{x'' \in \bar{l}} dx'' \int_{-\infty}^{+\infty} dx \int dq s(q) \delta(x' - x - v_q t) \delta(x'' - x + v_q t). \tag{3.17}$$

In this formula we see all the elements previously discussed:

- particles are emitted from arbitrary points (integral over all possible x);
- particles move ballistically (delta functions);
- they are forced to arrive in l or $\bar{l}$ (domain of integration of x' and x'');
- we integrate over all possible momenta with a weight $s(q)$.

In the case when l is a subsystem of finite length, the integrations on the coordinates yield [28] (the proof can be found in the Appendix B):

$$\begin{aligned} S_l(t) &\approx 2t \int_{p>0} dps(p) 2v_p \Theta(l - 2v_p t) + 2l \int_{p>0} dps(p) \Theta(2v_p t - l) \\ &= 2t \int_{2v_p t < l} dps(p) 2v_p + 2l \int_{2v_p t > l} dps(p) \end{aligned} \tag{3.18}$$

Now we can discuss the properties of this formula. First of all we notice that for $t \to \infty$ the domain of the first integral goes to zero and so the integral vanishes. Therefore the stationary value of the entanglement entropy is

$$S_l(\infty) \approx 2l \int_{p>0} dps(p) = l \int dps(p), \tag{3.19}$$

where we use the fact that $s(p) = s(-p)$ by construction. Now we assume that the velocity of the quasiparticles is limited, which is guaranteed by the Lieb-Robinson bound [54]. Calling v_M such velocity, the second integral in Eq. (3.18) vanishes as long as $t < t^* = l/2v_M$, hence, for $t < t^*$, $S_l(t)$ is linear in t. For $t > t^*$ both integrals are non vanishing. The physical interpretation of this is that while the fastest quasiparticles reach a saturation value, the slower quasiparticles continue to arrive so that the entanglement entropy slowly reaches the asymptotic value $S_L(\infty)$.

The only missing ingredients to make the result in Eq. (3.18) quantitative are v_p and $s(p)$. As for v_p, the quasiparticle velocity, one has a different velocity depending on the examined model. For non-interacting systems we identify the entangling quasiparticles with the free modes that diagonalize the Hamiltonian. Such single-particle modes have a non trivial dispersion $\epsilon(p)$ that depends on p and their velocity is given by the group velocity of the modes [28],[55]:

$$v_p = \frac{d}{dp}\epsilon(p). \tag{3.20}$$

Notice that for non-interacting systems v_p does not depend on the pre-quench state [55]. In our case, form Eq. (A.10), we get that

$$v_p = \frac{d}{dp}\Big[-\cos\Big(\frac{2\pi}{L}p\Big)\Big] = \frac{2\pi}{L}\sin\Big(\frac{2\pi}{L}p\Big). \tag{3.21}$$

We are now left with the task of identifying the entanglement content of the pair with momenta $p, -p$, which we called $s(p)$. From the analysis of the previous paragraph, $s(p)$ can be deduced from the thermodynamic entropy of the stationary state, because of the fact that the stationary entanglement entropy has the same density as the thermodynamic one.

We now consider a quench from an initial state $|\Psi_0\rangle$ which is then let evolve with the Hamiltonian of Eq. (A.10). For all this models, it has been proved that the GGE built with local conservation laws is equivalent to the one built with the mode occupation number $n_k = c_k^\dagger c_k$ [48]. The local properties of the stationary state are captured by the GGE density matrix

$$\rho_{GGE} \equiv \frac{e^{-\sum_k \lambda_k \hat{n}_k}}{Z}, \tag{3.22}$$

where $Z = \mathrm{Tr}[e^{-\sum_k \lambda_k \hat{n}_k}]$. This is true under some assumption on the initial state, namely that the initial state is a Gaussian state [56]. The thermodynamical entropy of the GGE

is $S_{TD} = -\mathrm{Tr}[\rho_{GGE} \log \rho_{GGE}]$ and with calculations analogous to the ones done in the previous sections, after taking the thermodynamic limit, we find

$$S_{TD} = L \int \frac{dk}{2\pi} H(n_k), \tag{3.23}$$

where $n_k \equiv \langle \hat{n}_k \rangle_{GGE} = \mathrm{Tr}[\rho_{GGE} \hat{n}_k]$ and

$$H(n) = -n \log n - (1-n) \log(1-n), \tag{3.24}$$

analogous to Eq. (1.52) [3]. Since n_k is an integral of motion, we can compute it on the initial state, namely $n_k = \langle \Psi_0 | \hat{n}_k | \Psi_0 \rangle$: from Eq. (A.17) we get that

$$\Gamma_{p,q}(t=0) = \frac{1}{L} \sum_{i,j} e^{i \frac{2\pi}{L}(pi - qj)} \Gamma_{i,j}(t=0), \tag{3.25}$$

where $\Gamma_{i,j}$, at $t = 0$ has non zero entries only for $\delta_{i,j}$ for i even. Taking the diagonal elements $p = q$:

$$\Gamma_{p,p}(t=0) = \frac{1}{L} \sum_{i,j} e^{i \frac{2\pi}{L} p(i-j)} \delta_{i,j}(\ i \text{ even}) = \frac{1}{L} \sum_{i \text{ even}} 1 = \frac{1}{L} \frac{L}{2} = \frac{1}{2}. \tag{3.26}$$

Hence, in the themrodynamic limit this quantity does not change, giving $n_k = 1/2$ $\forall\ k$. Therefore, a trivial calculation shows that $H(n_k) = \log_2(2) = 1\ \forall\ k$, meaning that all quasiparticle, no matter their momenta, carry an entanglement entropy of one. Plugging all what just said into Eq. (3.18), and identifying $s(p)$ with the density of the thermodynamic entropy we get

$$S_l(t) = 2t \int_{2|\epsilon'_k|t<l} \frac{dk}{2\pi} |\epsilon'_k| + l \int_{2|\epsilon'_k|t>l} \frac{dk}{2\pi}. \tag{3.27}$$

This integral can be evaluated numerically and this result can be compered to the output of the simulation in the Hilbert space. Eq. (3.27) is predictive for $L \gg l$. To prove this, in Fig. 3.3a we plot the entanglement entropy computed from the evolution of the system in the Hilbert space, as described in previous sections, and the entanglement evolution from the quasiparticle picture for a system of $L = 500$ and $l = 20$, which are values in the regime $L \gg l$. As we can see the two plots basically overlap. A more thorough analysis highlights how the entanglement entropy grows linearly up to $t \lessapprox l/2 = 10$, whereas it saturates to a value $S_l \approx l$ for large times. This is due to the boundaries of the integrals in Eq. (3.27): for $t \lessapprox l/2$ the first integral dominates, whereas for $t \gtrapprox l/2$ the second integral dominates. The slow saturation to $S_l \approx l$ can be

[3] Here the integral replaces the sum over discrete momenta that come out computing the trace.

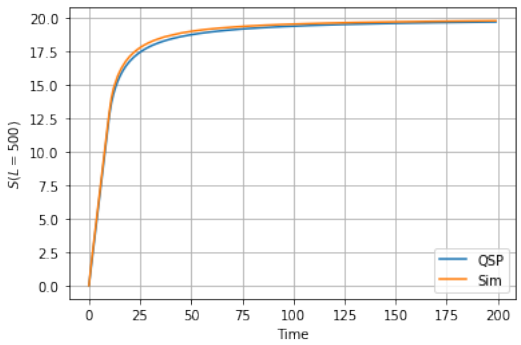

(a) *Comparison between the entanglement entropy from the evolution of the correlation matrix in the Hilbert space and the entanglement entropy form the quasiparticle picture. This is done for a system with* $L = 500$, $l = 20$, *evolving under a hopping Hamiltonian.*

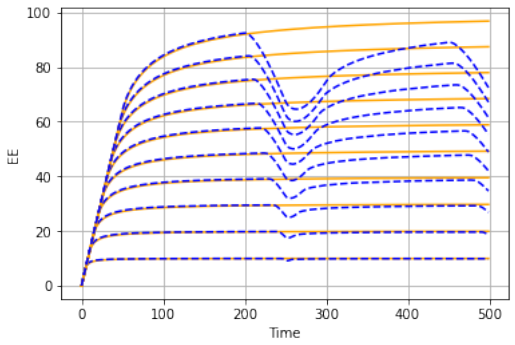

(b) *Comparison between the entanglement entropy from the evolution of the correlation matrix in the Hilbert space (dashed-blue lines) and the entanglement entropy form the quasiparticle picture (orange lines), keeping* $L = 500$ *and varying* $l \in \{10n | n \in [1, 10]\}$. l *increases from the bottom plot to the upper plot.*

Figure 3.3: *Comparisons between the entanglement entropy computed from the correlation matrix evolution in the Hilbert space and from the quasiparticle picture.*

interpreted as the arrival of the slower quasiparticles to the different domains l and $\bar{l}$ of the chain.

Moreover a numerical check allows us to verify that when l is not small enough with respect to L, the quasiparticle picture prediction, in the thermodynamic limit, does no longer hold. Indeed we can plot the entanglement entropy from the simulation and the entanglement entropy predicted by the quasiparticle picture keeping L fixed and varying l. This is shown in Fig. 3.3b, where we can see that for values of $l \lessapprox 10$, Eq. (3.27) provides a good prediction of what actually happens in the system, whereas for $l \gtrapprox 10$ this is not the case. Indeed as l increases the collapse of the entanglement entropy becomes more and more accentuated[4].

To better see this we plot (in Fig. 3.4) $S_l(t)/l$ over t/l for different subsystem sizes, keeping the system size fixed. We do this for $L = 500$ and $l \in \{10n | n \in [1, 5]\}$. As we can see from the pictures in Fig. 3.4, as l increases the agreement with the quasiparticle picture lasts for smaller times. Indeed as l increases the collapse and revivals of the entanglement entropy show up at shorter times. This is due to the finite size of the system. We also notice, from Fig. 3.4a, that also for $l = 10$, at a time $t \approx 250$ finite size

[4]To take into account the finite size of the system there are some methods, which are discussed in [43]. With some adjustments the quasiparticle pictures provides good predictions also when collapses and revivals are present.

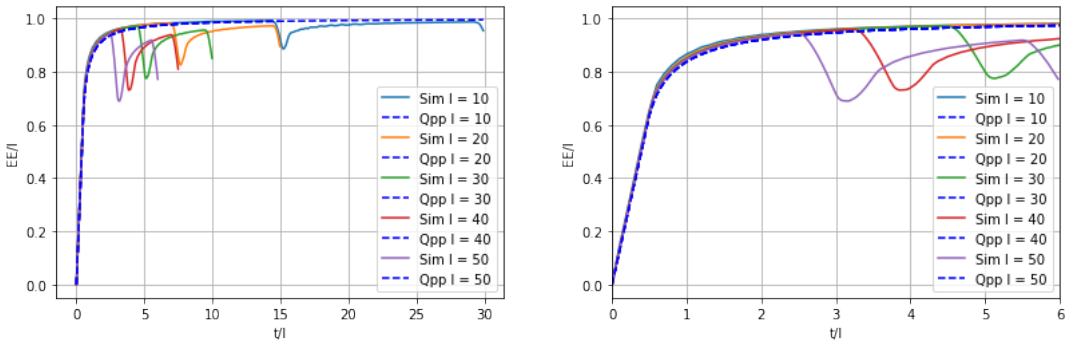

(a) *Plot in the range* $t/l \in [0, 30]$.

(b) *Plot in the range* $t/l \in [0, 6]$.

Figure 3.4: *Plot of* $S_l(t)/l$ *over* t/l *for* $L = 300$ *and* $l \in \{10n | n \in [1, 5]\}$*, extracted from the simulation in the Hilbert space (continuous lines) and from the quasiparticle picture (dashed lines).*

effect show up.

In the following, if we want to look at the entanglement entropy neglecting the finite-system effects, we should keep in mind what just said. Indeed, for a chain of length L with PBC, at a time $t = (L-l)/2$, the fastest quasiparticle ($v = 1$) that started from the boundary of the subsystem of size l, enter back in the subsystem $\mathcal{B}_l$ (the same stands for the quasiparticle starting at the boundary of $\mathcal{B}_{\bar{l}}$), causing a collapse in the entanglement entropy.

In the following we will introduce random measurements breaking out the unitary evolution. As we will see in the next chapter, introducing measurements makes the simulations more computationally challenging for the computer. Therefore we need to find a small enough L and l that avoid finite-system size effects. As an example of the reasoning behind a choice of L,l and t for a given simulation, we here take $L = 80$ and $l \in \{5n | n \in [1, 5]\}$ and thus understand up to what time the evolution does not show finite-system size effects. Looking at Fig. 3.5, we get that the best choice is to take $l = 5$ and let evolve the system until $t \approx 35$. This does not come as a surprise, because we already discuss that the smaller l with respect to L, the more we are in the limit $l/L \ll 1$, which shows a saturation of the entanglement entropy to a volume law, namely $S_l(t) \approx \alpha l$, where α is a constant. However we recall that, strictly speaking, to avoid finite size effects we must take the limits $L, l, t \to \infty$. It is thus clear how, for such system sizes, we will never be fully free of finite-size effects, as will be very manifest in the model studied in Sec. 4.3.

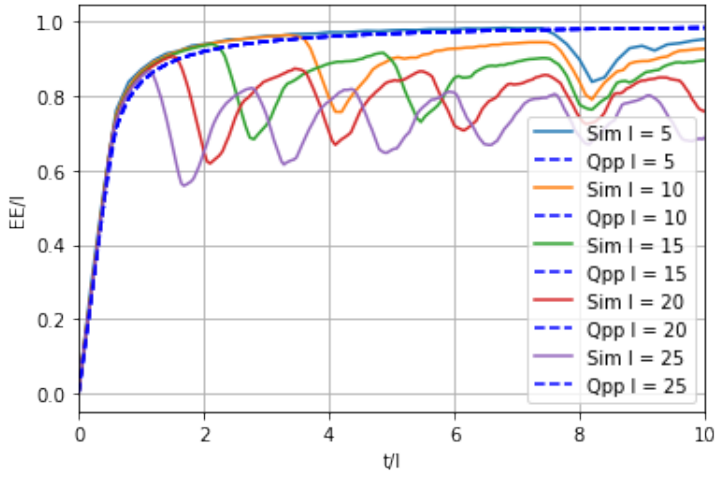

Figure 3.5: *Plot of $S_l(t)/l$ over t/l for $L = 80$ and $l \in \{5n | n \in [1, 5]\}$, extracted from the simulation in the Hilbert space (continuous lines) and from the quasiparticle picture (dashed lines).*

3.3 Brickwork Evolution

We now arrive at the main result of this chapter, namely that the dynamics described in the previous section can be simulated efficiently also on a quantum computer. Indeed the hopping Hamiltonian can be precisely mapped into a Hamiltonian for gates acting on qubits, via the Jordan-Wigner transformation (Sec. 1.2.1). Indeed, given Eq. (1.21), we have that

$$c_j^\dagger c_{j+1} = \Big(\prod_{j'=1}^{j-1} \sigma_{j'}^z\Big)\sigma_j^- \Big(\prod_{j'=1}^{j} \sigma_{j'}^z\Big)\sigma_{j+1}^+ = \sigma_j^- \sigma_j^z \sigma_{j+1}^+ = \sigma_j^- \sigma_{j+1}^+, \tag{3.28}$$

where we used the fact that $\sigma_j^- \sigma_j^z = \sigma_j^-$, and

$$c_{j+1}^\dagger c_j = \Big(\prod_{j'=1}^{j} \sigma_{j'}^z\Big)\sigma_{j+1}^- \Big(\prod_{j'=1}^{j-1} \sigma_{j'}^z\Big)\sigma_j^+ = \sigma_{j+1}^- \sigma_j^z \sigma_j^+ = \sigma_{j+1}^- \sigma_j^+, \tag{3.29}$$

where we used the fact that $\sigma_j^z \sigma_j^+ = \sigma_j^+$. It's important to notice that we can also do the inverse mapping, as shown in Appendix C.

Therefore, assuming a brickwork circuit like the one in Fig. 3.6, we have that the local unitaries are

$$U_{j,j+1} = e^{-i(\alpha \sigma_j^- \sigma_{j+1}^+ + \alpha^* \sigma_{j+1}^- \sigma_j^+)}. \tag{3.30}$$

However we will use, for the classical simulation, the fermionic Gaussian state formalism, thus the brickwork circuit can be efficiently simulated classically using local unitaries such

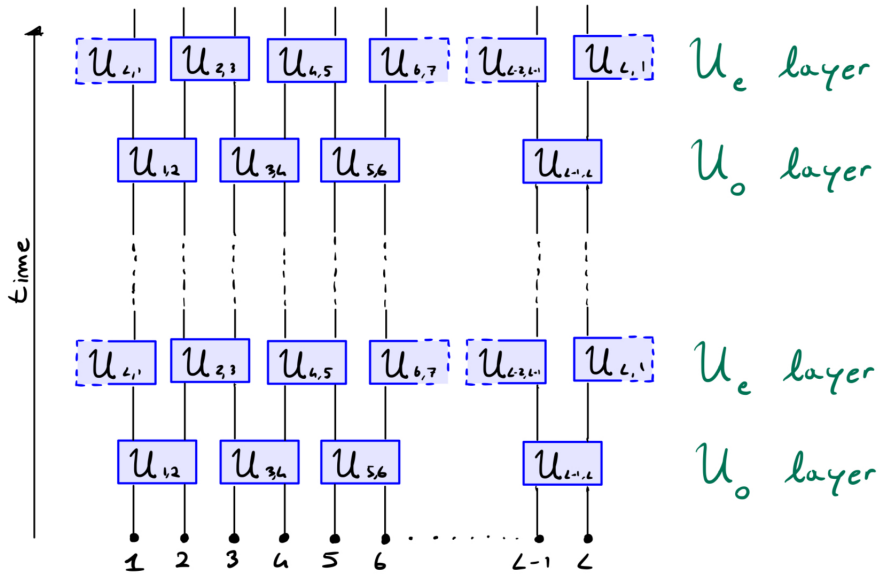

Figure 3.6: *Sketch of the brickwork circuit, where we assume L to be even and we assume PBC.*

as

$$U_{j,j+1} = e^{-i(\alpha c_j^\dagger c_{j+1} + \alpha^* c_{j+1}^\dagger c_j)}. \tag{3.31}$$

As we can see from Fig. 3.6, the evolution is divided into odd and even layers. The evolution is therefore given by:

$$|\psi'\rangle = \prod_{j \text{ even}} U_{j,j+1} \prod_{j \text{ odd}} U_{j,j+1} \cdots \prod_{j \text{ even}} U_{j,j+1} \prod_{j \text{ odd}} U_{j,j+1} |\psi_0\rangle , \tag{3.32}$$

where we apply the layers M times. However, in the multiplication, not all the operators in the exponent of the evolution operator commute. Indeed, from a direct computations, we have that

$$[c_i^\dagger c_j, c_k^\dagger c_l] = \delta_{j,k} c_i^\dagger c_l - \delta_{i,l} c_k^\dagger c_j. \tag{3.33}$$

Therefore we have that on a same layer

$$\prod_{j \text{ even/odd}} U_{j,j+1} = e^{-i \sum_{j \text{ even/odd}} (\alpha c_j^\dagger c_{j+1} + \alpha^* c_{j+1}^\dagger c_j)}, \tag{3.34}$$

but the exponents on different layers do not commute, thus we do not have an equation such as the one in Eq. (3.7). Indeed, since not all the exponents commute, we have that Eq. (3.4) stands, therefore, taking $H = \sum_j (\alpha c_j^\dagger c_{j+1} + \alpha^* c_{j+1}^\dagger c_j)$, we have that

$$e^{-iHt} = \lim_{M \to \infty} \Big(\prod_j U_{j,j+1}(\frac{t}{M}) \Big)^M. \tag{3.35}$$

We now want to prove this numerically. To do so we have to look at the evolution of the correlation matrix. This evolution can be computed in two ways, which are equivalent, but they require two different code implementations. Indeed the two approaches start from two different results of Chap. 1:

- the first one starts from the result in Eq. (1.58), as shown in App. C.1;
- the second one starts from Eq. (1.81).

Since the second one is the starting point also for the numerical simulations carried out in Sec. 3.2, 4.1, 4.2, we will follow this path, because with only a simple observation we can recycle the same code. Indeed let's focus on a single unitary of the brickwork circuit (Fig. 3.6). The Hamiltonian associated to this evolution is $H_{j,j+1} = \alpha c_j^\dagger c_{j+1} + \alpha^* c_{j+1}^\dagger c_j$, which corresponds to a single term of the sum in the Hamiltonian of Eq. (3.5). This will yield a matrix form of the Hamiltonian which has all zero entries, except for α in position $(j, j+1)$ and α^* in position $(j+1, j)$. All this said we can use Eq. (3.8), where we take $U = e^{-iH_{j,j+1}}$. We do this matrix multiplication first for all j odd and then for all j even, repeating it for a certain number of times. We thus reproduced the brickwork circuit evolution of Fig. 3.6. The entanglement entropy resulting from this simulation is compered to the one of the continuous time evolution in Fig. 3.7, where we can see how the entanglement entropy is not the same after a given time. This should not come as a surprise, since we have just showed, in Eq. (3.35), that the two evolution are equivalent in the limit of $M \to \infty$.

We therefore trotterize the evolution and we compere the entanglement entropy of the continuous evolution with the brickwork one, for different values of M. The results are displayed in Fig. 3.8, where we can see how as M increases, the entanglement entropy of the discretized dynamics reproduces better the one of the continuous dynamics.

We can now apply the quasiparticle picture to this setting.

3.3.1 Quasiparticle Picture in a Brickwork Circuit

The evolution of a brickwork circuit is described by alternating the application of unitary operators (of the kind in Eq. (3.31)) on odd and even operators. On each layer the unitary evolution is described by

$$U_o(\tau) = e^{-i\tau \sum_{j=1}^{L/2} (c_{2j-1}^\dagger c_{2j} + c_{2j}^\dagger c_{2j-1})} \tag{3.36}$$

$$U_e(\tau) = e^{-i\tau \sum_{j=1}^{L/2} (c_{2j}^\dagger c_{2j+1} + c_{2j+1}^\dagger c_{2j})} \tag{3.37}$$

In order to have a semi-classical interpretation, we need to extract the quasiparticle velocity (from the dispersion of the Hamiltonian) and the entropy density, thus combining them and obtaining the quasiparticle picture entanglement entropy from Eq. (3.18)) . Let's look at these two issues separately.

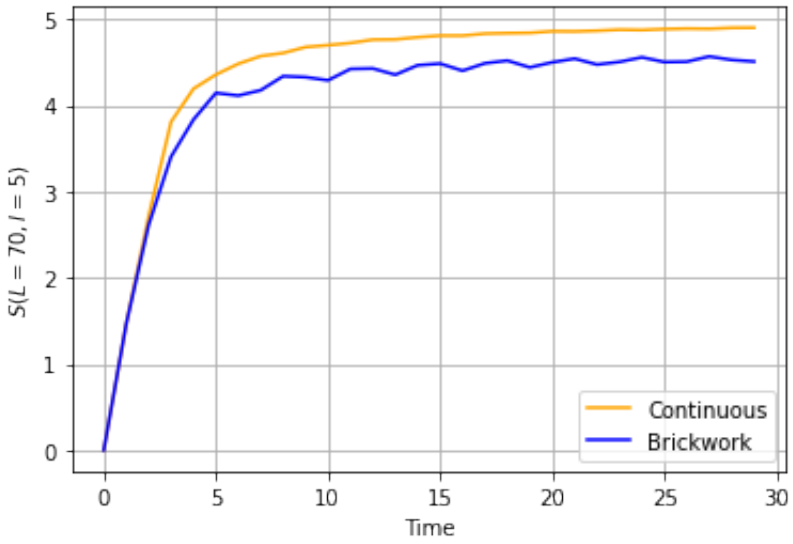

Figure 3.7: *Entanglement entropy for a system of size $L = 70$ and a subsystem size of $l = 5$. For a brickwork dynamics we can see how this does not correspond to the continuous time entanglement entropy.*

Quasiparticle Velocity The problem here is that we do not have an Hamiltonian. However we can extract it, by looking at the composition $U(\tau) = U_o(\tau)U_e(\tau)$. Indeed, looking at the exponent of $U(\tau)$, we will get the Hamiltonian. As we did in Sec. 3.2.1, the quasiparticle velocity is the derivative of the dispersion (Eq. (3.20)). Thus we need to diagonalize the Hamiltonian for the whole system. In order to find it we must look at the exponent of $U(\tau)$, which can be found using some algebra, as outlined in [57].

the first step is a Fourier transform of the fermionic operators. This has already been done in App. A, but here the period is $L/2$. Given the Fourier transform of a fermionic operator (Eq. (A.4)), we have that the term

$$\begin{aligned}\sum_{j=1}^{L/2} c_{2j-1}^\dagger c_{2j} &= \frac{1}{L}\sum_{p,q} e^{-i\frac{2\pi}{L}p(2j-1)} c_p^\dagger e^{i\frac{2\pi}{L}q2j} c_p \\ &= \sum_{p,q} e^{i\frac{2\pi}{L}p}\frac{1}{L}\sum_{j=1}^{L/2} e^{-i\frac{4\pi}{L}(p-q)j} c_p^\dagger c_q.\end{aligned} \tag{3.38}$$

Given the delta condition $\delta_{p,q+kL/2}$ (proved in App. C.2) and since the allowed values of p ore $p = 0, 1, \ldots, L-1$, the only possible integers are $k = 0, 1$. Therefore we have that

$$\frac{1}{L}\sum_{j=1}^{L/2} e^{-i\frac{4\pi}{L}(p-q)j} = \frac{1}{2}(\delta_{p,q} + \delta_{p,q+L/2}). \tag{3.39}$$

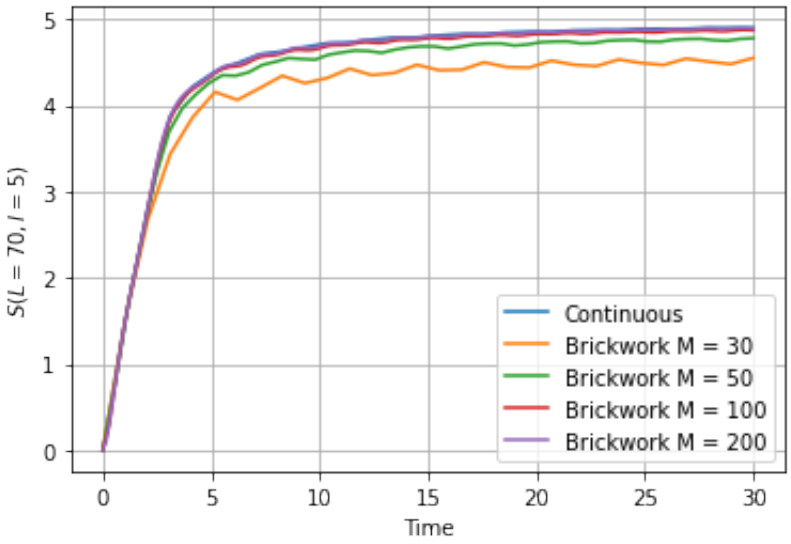

Figure 3.8: *Entanglement entropy for a system of size $L = 70$ and a subsystem size of $l = 5$. We take $M \in \{30, 50, 100, 200\}$, showing how for increasing M the entanglement entropy often brickwork circuit gets closer and closer to the one of the continuous evolution.*

Now Eq. (3.38) can be rewritten as

$$\sum_{j=1}^{L/2} c_{2j-1}^\dagger c_{2j} = \frac{1}{2}\sum_{p,q} e^{i\frac{2\pi}{L}p}(\delta_{p,q} + \delta_{p,q+L/2})c_p^\dagger c_q = \frac{1}{2}\sum_{p} e^{i\frac{2\pi}{L}p}(c_p^\dagger c_p + c_p^\dagger c_{p-L/2}). \tag{3.40}$$

We can now do the same for the other term in the exponent of the unitary at odd position, obtaining:

$$\begin{aligned}\sum_{j=1}^{L/2} c_{2j}^\dagger c_{2j-1} &= \sum_{p,q} e^{-i\frac{2\pi}{L}q}\frac{1}{L}\sum_{j=1}^{L/2} e^{-i\frac{2\pi}{L}(p-q)2j} c_p^\dagger c_q = \frac{1}{2}\sum_{p,q} e^{-i\frac{2\pi}{L}q}(\delta_{p,q} + \delta_{p,q+L/2})c_p^\dagger c_q \\ &= \frac{1}{2}\sum_{p}(e^{-i\frac{2\pi}{L}p}c_p^\dagger c_p + e^{-i\frac{2\pi}{L}(p-\frac{L}{2})}c_p^\dagger c_{p-L/2}) \\ &= \frac{1}{2}\sum_{p}(e^{-i\frac{2\pi}{L}p}c_p^\dagger c_p - e^{-i\frac{2\pi}{L}p}c_p^\dagger c_{p-L/2}).\end{aligned} \tag{3.41}$$

We can now put together the last two equations, in order to get the exponent of U_o in

Eq. (3.36). To do so we set $\alpha = \alpha^*$, i.e. we take α real. We obtain that

$$\begin{aligned}\alpha\sum_{j=1}^{L/2}(c_{2j-1}^\dagger c_{2j} + c_{2j}^\dagger c_{2j-1}) &= \alpha\sum_p\Big[\frac{e^{i\frac{2\pi}{L}p}+e^{-i\frac{2\pi}{L}p}}{2}c_p^\dagger c_p + \frac{e^{i\frac{2\pi}{L}p}-e^{-i\frac{2\pi}{L}p}}{2}c_p^\dagger c_{p-L/2}\Big]\\ &= \alpha\sum_p\Big[\cos\Big(\frac{2\pi}{L}p\Big)c_p^\dagger c_p + i\sin\Big(\frac{2\pi}{L}p\Big)c_p^\dagger c_{p-L/2}\Big].\end{aligned} \tag{3.42}$$

This is not manifestly Hermitian. Therefore we restrict $p = 0, 1, \ldots, L/2-1$. Doing so, the values of $p \in [L/2, L-1]$ get shifted as $p \to p - L/2$. Here we notice that $p - L/2 \to p - L = p$, because of the periodic boundary conditions. Doing this shift also brings $\cos(2\pi p/L) \to -cos(2\pi p/L)$ and $\sin(2\pi p/L) \to -sin(2\pi p/L)$. Therefore Eq. (3.42) becomes

$$\begin{aligned}\alpha\sum_{p=0}^{L/2-1}\Big[&\cos\Big(\frac{2\pi}{L}p\Big)c_p^\dagger c_p + i\sin\Big(\frac{2\pi}{L}p\Big)c_p^\dagger c_{p-L/2}\\ &- i\sin\Big(\frac{2\pi}{L}p\Big)c_{p-L/2}^\dagger c_p - \cos\Big(\frac{2\pi}{L}p\Big)c_{p-L/2}^\dagger c_{p-L/2}\Big].\end{aligned} \tag{3.43}$$

Doing the same for the evolution operator on even sites we get

$$\begin{aligned}\alpha\sum_{p=0}^{L/2-1}\Big[&\cos\Big(\frac{2\pi}{L}p\Big)c_p^\dagger c_p - i\sin\Big(\frac{2\pi}{L}p\Big)c_p^\dagger c_{p-L/2}\\ &+ i\sin\Big(\frac{2\pi}{L}p\Big)c_{p-L/2}^\dagger c_p - \cos\Big(\frac{2\pi}{L}p\Big)c_{p-L/2}^\dagger c_{p-L/2}\Big].\end{aligned} \tag{3.44}$$

We can now write $U_o(\tau)$ and $U_e(\tau)$ as

$$U_e(\tau) = \exp\Big[\sum_{p=0}^{L/2-1}\begin{pmatrix}c_p^\dagger & c_{p-L/2}^\dagger\end{pmatrix}A\begin{pmatrix}c_p\\ c_{p-L/2}\end{pmatrix}\Big] \tag{3.45}$$

$$U_e(\tau) = \exp\Big[\sum_{p=0}^{L/2-1}\begin{pmatrix}c_p^\dagger & c_{p-L/2}^\dagger\end{pmatrix}B\begin{pmatrix}c_p\\ c_{p-L/2}\end{pmatrix}\Big], \tag{3.46}$$

where

$$A = -i\alpha\tau\begin{pmatrix}\cos\left(\frac{2\pi}{L}p\right) & i\sin\left(\frac{2\pi}{L}p\right)\\ -i\sin\left(\frac{2\pi}{L}p\right) & -\cos\left(\frac{2\pi}{L}p\right)\end{pmatrix} = -i\alpha\tau\Big(\cos\Big(\frac{2\pi}{L}p\Big)\sigma^z - \sin\Big(\frac{2\pi}{L}p\Big)\sigma^y\Big), \tag{3.47}$$

$$B = -i\alpha\tau\begin{pmatrix}\cos\left(\frac{2\pi}{L}p\right) & -i\sin\left(\frac{2\pi}{L}p\right)\\ i\sin\left(\frac{2\pi}{L}p\right) & -\cos\left(\frac{2\pi}{L}p\right)\end{pmatrix} = -i\alpha\tau\Big(\cos\Big(\frac{2\pi}{L}p\Big)\sigma^z + \sin\Big(\frac{2\pi}{L}p\Big)\sigma^y\Big). \tag{3.48}$$

Now we wish to find the matrix C such that $e^A e^B = e^C$, thus finding the operator $U(\tau) = U_o(\tau)U_e(\tau)$. To do so we can rewrite A and B in terms of Pauli matrices, thus allowing us to exploit the properties of $SU(2)$ algebra. Indeed calculating $e^A e^B = e^C$ requires the usage of *Baker–Campbell–Hausdorff formula*, but this formula has a close form in $SU(2)$, i.e

$$\begin{aligned} e^{ia\hat{n}\cdot\vec{\sigma}}e^{ib\hat{m}\cdot\vec{\sigma}} &= I(\cos a\cos b - \hat{n}\cdot\hat{m}\sin a\sin b) \\ &+ i(\hat{n}\sin a\cos b + \hat{m}\sin b\cos a - \hat{n}\times\hat{m}\sin a\sin b)\cdot\vec{\sigma}. \end{aligned} \tag{3.49}$$

$$a = b = -\alpha\tau, \tag{3.50}$$

$$\hat{n} = (0, -\sin(2\pi p/L), \cos(2\pi p/L))^T, \tag{3.51}$$

$$\hat{m} = (0, \sin(2\pi p/L), \cos(2\pi p/L))^T. \tag{3.52}$$

Doing the direct calculations we find that

$$\begin{aligned} e^C = e^A e^B = &\Big(\cos^2(\alpha\tau) - \cos\Big(\frac{4\pi}{L}p\Big)\sin^2(\alpha\tau)\Big)I \\ &+ i\sin^2(\alpha\tau)\sin\Big(\frac{4\pi}{L}p\Big)\sigma^x + i\sin(2\alpha\tau)\cos\Big(\frac{2\pi}{L}p\Big)\sigma^z. \end{aligned} \tag{3.53}$$

We rewrite this in the following way:

$$e^C = aI + ib\sigma^x + id\sigma^z, \tag{3.54}$$

where

$$a = \cos^2(\alpha\tau) - \cos\Big(\frac{4\pi}{L}p\Big)\sin^2(\alpha\tau) \tag{3.55}$$

$$b = \sin^2(\alpha\tau)\sin\Big(\frac{4\pi}{L}p\Big) \tag{3.56}$$

$$d = \sin(2\alpha\tau)\cos\Big(\frac{2\pi}{L}p\Big). \tag{3.57}$$

Now any exponential of Pauli matrices can be written as

$$e^{i\epsilon(\hat{n}\cdot\vec{\sigma})} = \cos(\epsilon)I + i\sin(\epsilon)\hat{n}\cdot\vec{\sigma}. \tag{3.58}$$

Therefore, comparing it to Eq. (3.54) and after normalizing the vector which multiplies $\vec{\sigma}$, we have that

$$a = \cos(\epsilon), \tag{3.59}$$

$$\sqrt{b^2 + d^2} = \sin(\epsilon), \tag{3.60}$$

$$\Big(\frac{b}{\sqrt{b^2+d^2}}, 0, \frac{d}{\sqrt{b^2+d^2}}\Big)^T = \hat{n}. \tag{3.61}$$

Moreover, given the fact that the $\hat{n}$ is a normalized vector, we can rename the two non-zero components $\sin(\phi) = b/\sqrt{b^2+d^2}$, $\cos(\phi) = d\sqrt{b^2+d^2}$, thus having

$$\phi_p = \arctan\Big(\frac{b}{d}\Big). \tag{3.62}$$

Exploiting the identity

$$e^{-i\frac{\theta}{2}\sigma^y}\sigma^z e^{i\frac{\theta}{2}\sigma^y} = \cos(\theta)\sigma^z + \sin(\theta)\sigma^x, \tag{3.63}$$

we have that

$$\hat{n}\cdot\vec{\sigma} = e^{-i\frac{\phi}{2}\sigma^y}\sigma^z e^{i\frac{\phi}{2}\sigma^y}. \tag{3.64}$$

Thus, putting everything together, we get that

$$C = i\epsilon_p e^{-i\frac{\phi_p}{2}\sigma^y}\sigma^z e^{i\frac{\phi_p}{2}\sigma^y}, \tag{3.65}$$

where

$$\epsilon_p = \arctan\frac{\sqrt{b^2+d^2}}{a}. \tag{3.66}$$

Therefore we have that

$$\begin{aligned} U(\tau) &= \exp\sum_{p=0}^{L/2-1}(c_p^\dagger c_{p-\frac{L}{2}}^\dagger)C\begin{pmatrix} c_p \\ c_{p-\frac{L}{2}}. \end{pmatrix} \\ &= \exp\Big[\sum_{p=0}^{L/2-1} i\epsilon_p[\cos(\phi_p)(c_p^\dagger - c_{p-\frac{L}{2}}^\dagger) + \sin(\phi_p)(c_p^\dagger c_{p-\frac{L}{2}}^\dagger + c_{p-\frac{L}{2}}^\dagger c_p)]\Big]. \end{aligned} \tag{3.67}$$

Now the exponent of $U(\tau)$ is the Hamiltonian that drives the evolution on odd and even sites, which is diagonalized by the Bogoliubov transformation

$$\begin{pmatrix} b_p \\ b_{p-\frac{L}{2}} \end{pmatrix} = e^{i\frac{\phi_p}{2}\sigma^y}\begin{pmatrix} c_p \\ c_{p-\frac{L}{2}} \end{pmatrix}, \tag{3.68}$$

yielding

$$U(\tau) = \exp\Big[i\sum_{p=0}^{L/2-1}\epsilon_p(b_p^\dagger b_p - b_{p-\frac{L}{2}}^\dagger b_{p-\frac{L}{2}})\Big]. \tag{3.69}$$

Now we can extend the sum from $p = -L/2+1, \dots L/2-1$, obtaining

$$U(\tau) = \exp\Big[i\sum_{p=-L/2+1}^{L/2-1}\epsilon_p b_p^\dagger b_p\Big] \tag{3.70}$$

and then we can take the thermodynamic limit $L \to \infty$, getting $2\pi p/L \to k$, thus yielding

$$U(\tau) = \exp\Big[i \sum_{k=-\pi}^{\pi} \epsilon_k b_k^\dagger b_k\Big]. \tag{3.71}$$

From here we can find the quasiparticle velocity deriving the dispersion. However the continuous evolution is given by $\exp(-iHt)$, but in the above equation the time variable is not explicit. Therefore we rewrite the above equation as

$$U(\tau) = \exp\Big[i \sum_{k=-\pi/2}^{\pi/2} \tau\tilde{\epsilon_k} b_k^\dagger b_k\Big] \tag{3.72}$$

where $\tilde{\epsilon_k} = \epsilon_k/\tau$.[5]

Introducing the variables

$$a(k) = \cos^2(\alpha\tau) - \cos(2k)\sin^2(\alpha\tau) \tag{3.73}$$
$$b(k) = \sin^2(\alpha\tau)\sin(2k) \tag{3.74}$$
$$d(k) = \sin(2\alpha\tau)\cos(k), \tag{3.75}$$

we have that

$$\epsilon_k = \arctan\frac{\sqrt{b(k)^2 + d(k)^2}}{a(k)}, \tag{3.76}$$

which, upon derivation with respect to k, yields

$$v_k = \frac{d\epsilon_k}{dk} = \frac{a(k)(b(k)^2 + d(k)^2)' - 2(b(k)^2 + d(k)^2)a(k)'}{2\sqrt{b(k)^2 + d(k)^2}(a(k)^2 + b(k)^2 + d(k)^2)}, \tag{3.77}$$

where

$$a(k)' = 2\sin(2k)\sin^2(\alpha\tau) \tag{3.78}$$
$$(b(k)^2 + d(k)^2)' = 2\sin^4(\alpha\tau)\sin(4k) - \sin^2(2\alpha\tau)\sin(2k). \tag{3.79}$$

We must notice that in our final form of the evolution operator (Eq. (3.72)), we have a rescaled dispersion $\tilde{\epsilon_k}$. Therefore, in the formula for the entanglement entropy (Eq. (3.18)), we will have to use

$$\tilde{v_k} = \frac{v_k}{\tau}. \tag{3.80}$$

[5]In Appendix E, there is a comparison between the dispersion in the continuous case and in the brickwork case, where the limit $\tau \to 0$ is taken to show that, in this limit, the brickwork evolution is equivalent to the continuous one.

Entropy Density The next problem to tackle is the entropy density. We saw in the previous section that this corresponds to Eq. (3.24), thus we need to find the value of the density $\langle b_k^\dagger b_k \rangle$. To do so we first use the Bogoliubov transformation to relate this density with the correlation matrix in momentum space:

$$\begin{aligned}\langle b_p^\dagger b_p \rangle &= \cos^2 \frac{\phi_p}{2} \langle c_p^\dagger c_p \rangle + \sin^2 \frac{\phi_p}{2} \langle c_{p-L/2}^\dagger c_{p-L/2} \rangle + \cos \frac{\phi_p}{2} \sin \frac{\phi_p}{2} (\langle c_p^\dagger c_{p-L/2} \rangle + \langle c_{p-L/2}^\dagger c_p \rangle) \\ &= \cos^2 \frac{\phi_p}{2} \Gamma_{p,p} + \sin^2 \frac{\phi_p}{2} \Gamma_{p-L/2,p-L/2} + \cos \frac{\phi_p}{2} \sin \frac{\phi_p}{2} (\Gamma_{p,p-L/2} + \Gamma_{p-L/2,p}).\end{aligned} \tag{3.81}$$

Then we use the fact that for the brickwork circuit the delta condition is $\delta_{p,q+k\frac{L}{2}}$, we have that the elements of the correlation matrix in the above expression (3.81) are all equal to $1/2$, thus

$$\langle b_p^\dagger b_p \rangle = \frac{1}{2} + \frac{1}{2} \sin(\phi_p). \tag{3.82}$$

Therefore, in the thermodynamic limit, we have obtained the *Yang Yang entropy* ([58]

$$\begin{aligned}H(n_k) = &-\Big(\frac{1}{2} + \frac{1}{2}\sin(\phi_k)\Big) \log\Big(\frac{1}{2} + \frac{1}{2}\sin(\phi_k)\Big) \\ &- \Big(\frac{1}{2} - \frac{1}{2}\sin(\phi_k)\Big) \log\Big(\frac{1}{2} - \frac{1}{2}\sin(\phi_k)\Big).\end{aligned} \tag{3.83}$$

Entanglement Entropy Now we have all the ingredients to compute the entanglement entropy from Eq. (3.18), which for the brickwork evolution, upon taking the thermodynamic limit, takes the form:

$$S_l(t) = 2t \int_{2|\tilde{v_k}|t<l} \frac{dk}{2\pi} |\tilde{v_k}| H(n_k) + l \int_{2|\tilde{v_k}|t>l} \frac{dk}{2\pi} H(n_k), \tag{3.84}$$

where $H(n_k)$ is the Yang Yang entropy from Eq. (3.83), and $\tilde{v_k}$ is the quasiparticle velocity of Eq. (3.80). This integral can be evaluated numerically. In Fig. 3.9, we present the entanglement entropy computed with the trotterization of a brickwork circuit and the entanglement entropy computed with the quasiparticle picture for a system with $L = 70$, $l = 5$, $m \in \{20, 40, 60\}$. It can be noticed that the quasiparticle picture provides a good estimation of the entanglement entropy also in the case of a brickwork circuit, even though it slightly underestimates it. This is due to finite size effects, indeed the quasiparticle picture is valid in the thermodynamic limit, i.e. $L, l \to \infty$, and we had verified that, increasing their values, the accordance between the entanglement entropies computed with the two different techniques gets better. Another feature of the trend of the entanglement entropy computed from the correlation matrix evolution, is its "zig-zag" shape. This is due to the alternating application of $U_o(\tau)$ and $U_e(\tau)$ and this behaviour fades out in the limit $M \to \infty$.

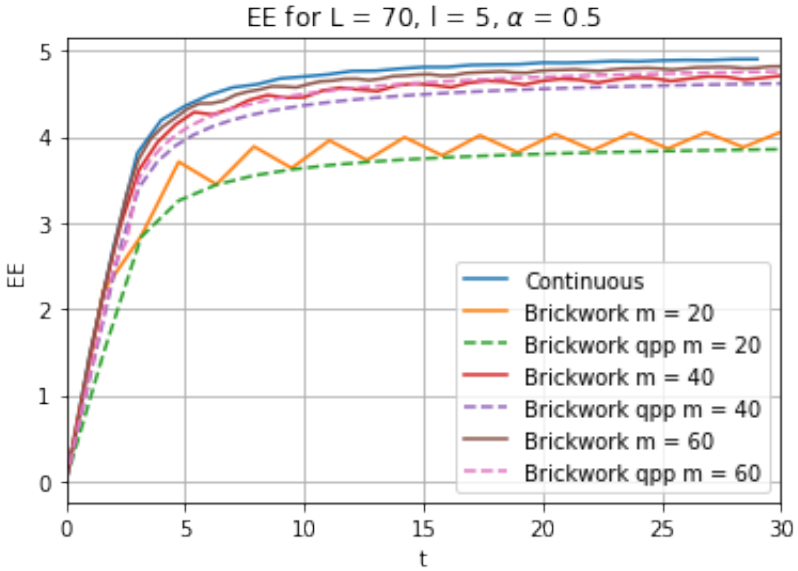

Figure 3.9: *Comparison between the entanglement entropy computed with the trotterization of a brickwork circuit and the entanglement entropy computed with the quasiparticle picture for a system with* $L = 70$, $l = 5$, $m \in \{20, 40, 60\}$.

Chapter 4

Measurements in the Dynamics

In this chapter we will introduce measurements in the free-fermionic dynamics. In this context, the measurements have to preserve the gaussianity of the state of the systems we will analyze, in order to keep simulating large systems on classical computers. First of all we will introduce local projective measurements of the density n_j (Sec. 4.1) [24]. Here we will see how the entanglement entropy behaves under different measurement rates. The research conducted by Alberton and al. ([59]) showed the presence of the MIEPT in a free-fermionic model evolving under a hopping Hamiltonian and subject to continuous monitoring of the local density. However, recent papers ([25], [60]) showed, via analytical and numerical means, that such transition is not there, instead it is a *crossover*. Indeed the volume low phase is not stable, since as soon as we introduce measurements, the entanglement entropy ceases to follow the volume-law. Therefore we moved on and studied two other models, to see if in them a phase transition is present.

The first model (Sec. 4.2), inspired by the work of O'Dea et al. ([61]), introduces an absorbing state dynamics to see if there is an entanglement and a *absorbing-state* phase transition. However, as it will be thoroughly explained in Sec. 4.2, this is not the case.

Finally, in Sec.4.3, we force a non linear measurement procedure into the hopping dynamics, to investigate if we can make the volume law phase more stable.

4.1 Entanglement Entropy Dynamics Under Local Projective Measurements

In the previous sections we evaluated the evolution of entanglement entropy over time. This evolution was unitary. Now we will perturb this unitarity inserting local projective measurements during the evolution. To do so, we take each single space-localized Hilbert space $\mathcal{H}_j$ ($j = 1, \dots, L$) and couple it randomly with the environment for a short period of time. In this time a local observable is measured via a local observable $\hat{\mathcal{O}}_j = \sum_{k=1}^{K} o_k \hat{P}_j^{(k)}$,

where o_k is a possible outcome and $\hat{P}_j^{(k)}$ is the projector on its eigenspace ($\sum_{k=1}^{K} \hat{P}_j^{(k)} = \hat{1}_j$). We take time steps dt and a characteristic rate of measurement $p = 1/\tau$. More precisely we take each time step $dt = 1$ in order to keep a discretized evolution and avoid the continuous limit ($dt \to 0$). In each time step of this kind, each single local degree of freedom is monitored independently. If such a measurement takes place, the many-body state $|\Psi\rangle$ is projected according to the Born rule:

$$|\Psi\rangle \to \frac{P_j^{(k)} |\Psi\rangle}{\sqrt{p_k}}, \tag{4.1}$$

where $p_k = \langle\Psi|P_j^{(k)}|\Psi\rangle$. In practice, this can be seen as an extraction of a random number $p \in]\,,0,1]$, and a projection onto the k-th subspace is performed if $\sum_{l=1}^{k-1} p_l < p < \sum_{l=1}^{k} p_l$. This will be exploited for the simulation of such evolution, as we will explain in a little while. Taking into account this dynamics, the evolution of the many body state $|\Psi(t)\rangle$ is conditioned by the set of measurement and their outcomes. We must remark that, if $|\Psi(0)\rangle$ is a pure state, following this protocol, it will remain pure.

As already seen in Chap. 1 and 2, depending on the placing of the random measurements and on the outcome of these measurements, the state changes, therefore we will measure averages over quantum trajectories.

4.1.1 The Procedure

We now focus on the hopping Hamiltonian of Eq. (A.8). We already saw that, since the total number operator commutes with the Hamiltonian, an initial Gaussian state will remain Gaussian and thus we can use, as previously done, the formalism of correlation matrices.

Furthermore we focus on the measurement of the local occupation numbers, namely $\hat{n}_j = c_j^\dagger c_j$. The measurement could, in principle, destroy the gaussianity of the state, however, for this type of measurement, this is not the case [24].

Claim 4.1.0.1. *Measuring the local occupation number $\hat{n}_j = c_j^\dagger c_j$, which is quadratic in the fermions operators, does not destroy the gaussianity of the state.*

Proof. If a state is Gaussian, by definition, $\rho \propto e^{\sum_{i,j} H_{i,j} c_i^\dagger c_j}$, where H is the matrix of coefficients described in Eq. (1.64). We have the spectral decomposition $\hat{n}_j = 1 \cdot \hat{P}_j^{(1)} + 0 \cdot \hat{P}_j^{(0)}$. Also $\hat{1}_j = \hat{P}_j^{(1)} + \hat{P}_j^{(0)}$. What we have just proved is that $\hat{n}_j = \hat{P}_j^{(1)}$ and $\hat{1}_j - \hat{n}_j = \hat{P}_j^{(0)}$, namely each local number operator is itself a projector. Now we can prove that these projectros can be written as limits of Gaussian operators. First of all, exploiting the fact that the local fermionic number operator has the property that $\hat{n}_j^l = \hat{n}_j \;\forall\; l = 1, \ldots, \infty$, we have that

$$\lim_{\alpha\to\infty} \frac{e^{\alpha\hat{n}_j}}{e^\alpha - 1} = \lim_{\alpha\to\infty} \Big[\frac{\hat{1}_j}{e^\alpha - 1} + \frac{(e^\alpha - 1)\hat{n}_j}{e^\alpha - 1}\Big] = \hat{n}_j.$$

Moreover

$$\lim_{\alpha\to\infty} e^{-\alpha\hat{n}_j} = \lim_{\alpha\to\infty}\left[\hat{1}_j + (e^{-\alpha}-1)\hat{n}_j\right] = \hat{1}_j - \hat{n}_j.$$

Then, finally, since when a measurement is performed the density matrix transforms as $\hat{\rho} \to \sum_{k=1}^{K} \hat{P}_j^{(k)}\hat{\rho}\hat{P}_j^{(k)}$, we have

$$e^{\pm\alpha\hat{n}_j} e^{\sum_{i,j} H_{i,j} c_i^\dagger c_j} e^{\pm\alpha\hat{n}_j} = e^{\sum_{i,j} K_{i,j}^{(\pm)} c_j^\dagger c_j},$$

where $K^{(\pm)}$ is a new matrix, whose elements are given by the Baker-Campbell-Hausdorff formula. Therefore the Gaussianity is preserved. □

An important fact, that will be exploited in the following, is that local number operators on different sites commute, thus the projecting procedure can be applied in any order. If at time t a measurement occurs on the k-th site, the post-measurement states will be

$$|\Psi(t)\rangle \to \frac{n_k\,|\Psi\rangle}{\sqrt{\langle\Psi(t)|n_k|\Psi(t)\rangle}} \text{ if outcome is 1} \tag{4.2}$$

$$|\Psi(t)\rangle \to \frac{(1-n_k)\,|\Psi\rangle}{\sqrt{\langle\Psi(t)|1-n_k|\Psi(t)\rangle}} \text{ if outcome is 0} \tag{4.3}$$

To implement this random measurement procedure we use the following recipe [24]: for each time step dt and each lattice site k we take a random number $p_k \in]0,1]$ and only if $p_k \leq dt/\tau$ we take the measurement of the occupation number n_k. In such case, we take another random number $q_k \in]0,1]$: if $q_k \leq \Gamma_{kk}(t)$, simulating outcome 1, the post measurement correlation matrix will be

$$\Gamma_{ij}(t) \to \delta_{ik}\delta_{jk} + \Gamma_{ij}(t) - \frac{\Gamma_{ik}(t)\Gamma_{kj}(t)}{\Gamma_{kk}(t)}, \tag{4.4}$$

otherwise, if $q_k(t) > \Gamma_{kk}(t)$, simulating result 0, the post-measurement correlation matrix will be

$$\Gamma_{ij}(t) \to -\delta_{ik}\delta_{jk} + \Gamma_{ij}(t) + \frac{(\delta_{ik}-\Gamma_{ik}(t))(\delta_{kj}-\Gamma_{kj}(t))}{\Gamma_{kk}(t)}, \tag{4.5}$$

where we have exploited Wick's theorem to find these expressions, whose proofs are in Appendix D.

4.1.2 Entanglement Entropy Dynamics

The bipartite entanglement entropy is affected by the random projective measurement. We already saw how to extract the entanglement entropy from Gaussian states in Sec. 1.3. In this section we will take into account combinations of L and l such that the finite-system size effects are negligible, in order to look at the limit of an infinite system.

What we will now explore is what happens when we change the measurement rate $1/\tau$. The first trivial case is when $\tau \to 0$, which means that $p_k \leq 1/\tau$ always. In such case, measurements take place everywhere at every time step, thus leaving the many-body state completely factorized, yielding a vanishing entanglement entropy. This is now as *quantum Zeno effect* [13].

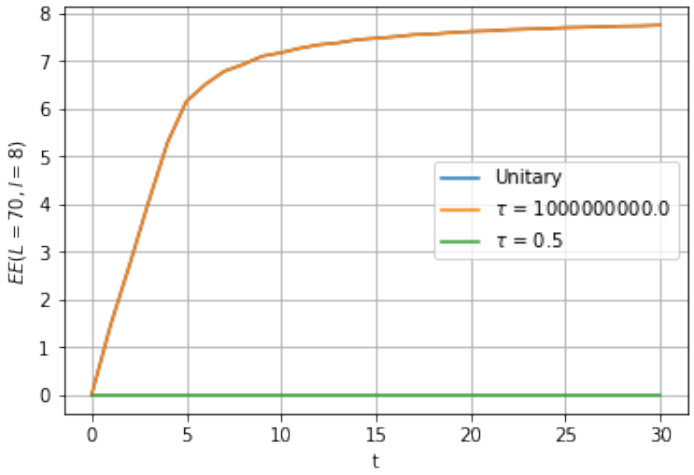

Figure 4.1: *Plot of the entanglement entropy for a system with $L = 70$, $l = 8$, when the system is not monitored and monitored everywhere at every time step.*

Next we can inspect the opposite limit, namely $\tau \to \infty$. In this case the intuition suggests that the evolution of the entanglement entropy should be equivalent to the unitary one. However in [24] it was proven that for any finite measurement rate, the volume-law is destroyed. Therefore, the volume-law phase of the unitary evolution is recovered just when no measurements occur. To ensure this some evaluations have to be done. With a system size of L, at each time step we extract L random numbers p_k. If we let the system evolve for T time steps, in order to have no measurements, it must hold that $\tau > LT$.

To verify this hypothesis we do a simulation on a chain of $L = 70$ fermions and measure the entanglement entropy with a subsystem of $l = 8$ with an evolution time $T = 30$. This values are taken in order to avoid the revivals of the entanglement entropy, as explained in Sec. 3.2.1. Furthermore, we do an average over 200 quantum trajectories in order to plot the entanglement entropy for the evolution with measurements. The result is shown in Fig. 4.1, where the entanglement entropy from the unitary evolution and the entanglement entropy from an evolution subjected to local projective measurements, with $\tau = 0.1$ and $\tau = 1 \times 10^9$ are compared. Since the measurements are very unlikely to happen for $\tau = 1 \times 10^9$, the plot of the entanglement entropy from unitary evolution and from very weak monitoring overlap, as expected. Moreover, in Fig. 4.1, also the entanglement entropy of a system where the local density is measured everywhere at

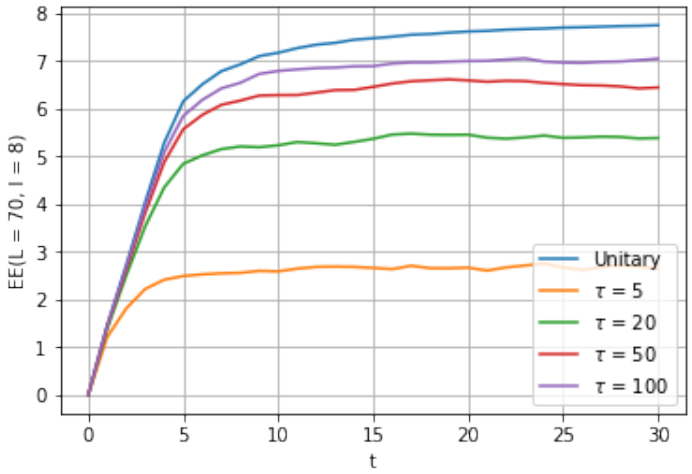

Figure 4.2: *Entanglement entropy for a system of* $L = 70$ *and* $l = 8$*, monitored with different rates* $1/\tau$*.*

every time step is plotted ($\tau = 0.1$, meaning that $dt/\tau > 1$, thus making impossible to have $p_k < dt/\tau$). As anticipated, the entanglement does not spread, namely the state of the system remains completely factorized, and the entanglement entropy is zero throughout the evolution.

We now move away from the two limiting cases and look at what happens for intermediate values of τ. To do so we simulate a system with $L = 70$ and $l = 8$, for a time $T = 30$, changing the value of $\tau \in \{5, 20, 50, 100\}$. The result is displayed in Fig. 4.2, where we can see how the entropy saturates at a different value with respect to the one of the unitary evolution. Indeed, for the unitary evolution, $S_l(t) \approx l$ for large enough times in the limit $L \to \infty$, but introducing measurements during the evolution makes the saturation value of the entropy change. Indeed, the linear growth of the entanglement entropy displayed by the unitary evolution is substituted by a slower growth, namely a logarithmic growth $S_l(t) = a_\tau \ln t + b_\tau$[24]. Thus we can say that introducing measurements during the unitary evolution allows for lower entanglement entropy, namely the two subsystems are less entangled.

We now go on analyzing what happens when we fix a value of τ and compere the entanglement entropy for different values of l, since the area law phase is featured by the fact that the entanglement entropy reaches a constant value, independent of the subsystem size.

For high enough values of τ, the entanglement entropy saturates to different values, depending on l as can be seen in Fig. 4.3a, where the entanglement entropy for $\tau = 20$ (measurement rate is 0.05) is showed.

Instead for small enough values of τ, independently from the subsystem size l, for $t > l/2$ the entanglement entropy reaches a constant value, indicating that the system

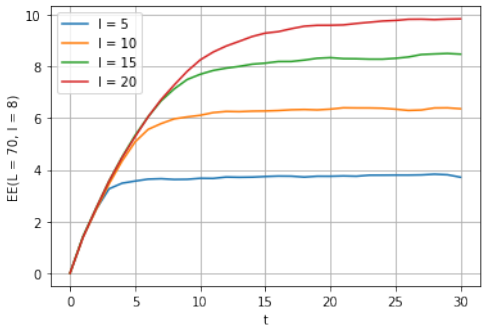

(a) *Entanglement entropy for a system monitored with a rate* $1/\tau = 1/20$.

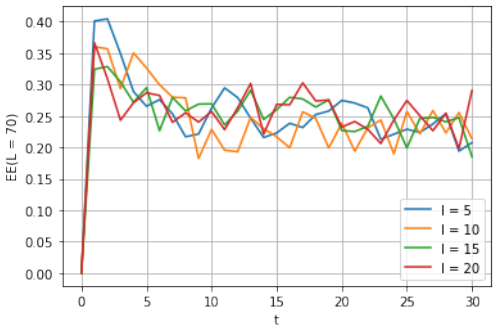

(b) *Entanglement entropy for a system monitored with* $\tau = 1.5$.

Figure 4.3: *Time evolution of the entanglement entropy for* $L = 70$ *and* $l = 5, 10, 15, 20$*, monitored with* $\tau = 20$ *(4.3a) and* $\tau = 1.5$ *(4.3b.*

is in the area-law phase. In Fig. 4.3b the entanglement entropy for various subsystem sizes is displayed for $\tau = 1.5$ (measurement rate $0.\bar{6}$). Here we can clearly see how, independently from l, the entanglement entropy saturates to a constant value. To be more precise, in Fig. 4.3b, the entanglement entropy is not stable. This is due to the fact that the plots for the various ls are the result of an average over 200 quantum trajectories. Indeed, for such a high measurement rate, the trajectories can be very different from one another, therefore yielding the plots of Fig. 4.3b[1].

Finally we here mention that in [24] it has been proven that the volume-law phase is destroyed for any finite value of the measurement rate $p = 1/\tau$. Moreover, for every size L, a critical value of τ_L^c separating the area-law and the logarithmic-law phase has been estimated, thus showing that in the limit $L \to \infty$ there is only the area-law phase.

4.2 Entanglement Entropy Dynamics in a Model with an Absorbing State

In [61], an interactive quantum dynamics with unitary evolution and measurements on a brickwork circuit has been studied. In particular the dynamics is stirred towards a target state. This is done applying the X Pauli matrix to a qubit, depending on the measurement outcome on it (this procedure is called *feedback operation*). The dynamics has been studied under two varying parameters, which are the measurement rate p_m and the rate of measurements followed by a feedback operation p_f. O'Dea at al. have shown

[1]Such plot can be improved by increasing the number of quantum trajectories of which we take the average. However this is computationally costly and, since this model was already studied in [24], we refer to this work for more precise plots.

that the phase diagram is divided into three separate phases, namely a *non-absorbing volume-law* phase, a *non-absorbing area-law* phase and an *absorbing area-law* phase.

To see if a free-fermionic model with random measurements, together with an evolution that drives the system towards a target state, could display a MIEPT, we considered a new model, in which we introduced a mechanism to stir the evolution of the system towards the target state $|00\dots0\rangle$.

4.2.1 The Procedure

The new model just described consists in a fermionic chain $\mathcal{H}_S$, initialized in the Néel state, flanked by an ancillary fermionic chain $\mathcal{H}_{S'}$, initialized in the state $|00\dots0\rangle$. The evolution follows the steps explained below:

1. Let the system $\mathcal{H}_S$ evolve under the hopping Hamiltonian.
2. We iterate along the sites of the ancillary chain and, for each site, extract a random number $p_k \in]0,1]$. Introducing a measurement rate $1/\tau$, if $p_k \leq 1/\tau$, we perform:
   (a) a hopping between $\mathcal{H}_S$ and $\mathcal{H}_{S'}$, namely we apply the unitary
   $$e^{-i\beta(c_k^\dagger c_{k'} + c_{k'}^\dagger c_k)}, \tag{4.6}$$
   where the primed indexes are for the sites on the ancillary system;
   (b) a measurement of the density on the ancillary system.
3. Measure the entanglement entropy on the system $\mathcal{H}_S$.
4. Reset the state of the ancillary system to $|00\dots0\rangle$.

Now some remarks need to be done. First of all, we notice that in this model, the number of fermions in the system $\mathcal{H}_S$ can only decrease, because, given the fact that the ancillary state is reset to $|00\dots0\rangle$, fermions can only hop from $\mathcal{H}_S$ to $\mathcal{H}_{S'}$. This tells us that there cannot be an absorbing-state transition, since there is no competitive mechanism to the destruction of fermions in $\mathcal{H}_S$. Indeed, to observe such a transition, we should introduce a mechanism that also creates fermions in $\mathcal{H}_S$.

Moreover we notice that to do the evolution we can use the same techniques already developed. Indeed the only difference here is that the system $\mathcal{H}_S \otimes \mathcal{H}_{S'}$ is described by

a $2L \times 2L$ correlation matrix of the kind:

$$\Gamma = \begin{pmatrix} \langle c_1^\dagger c_1 \rangle & \dots & \langle c_1^\dagger c_L \rangle & \langle c_1^\dagger c_{1'} \rangle & \dots & \langle c_1^\dagger c_{L'} \rangle \\ \vdots & \ddots & \vdots & \vdots & \ddots & \vdots \\ \langle c_L^\dagger c_1 \rangle & \dots & \langle c_L^\dagger c_L \rangle & \langle c_L^\dagger c_{1'} \rangle & \dots & \langle c_L^\dagger c_{L'} \rangle \\ \langle c_{1'}^\dagger c_1 \rangle & \dots & \langle c_{1'}^\dagger c_L \rangle & \langle c_{1'}^\dagger c_{1'} \rangle & \dots & \langle c_{1'}^\dagger c_{L'} \rangle \\ \vdots & \ddots & \vdots & \vdots & \ddots & \vdots \\ \langle c_{L'}^\dagger c_1 \rangle & \dots & \langle c_{L'}^\dagger c_L \rangle & \langle c_{L'}^\dagger c_{1'} \rangle & \dots & \langle c_{L'}^\dagger c_{L'} \rangle \end{pmatrix}. \tag{4.7}$$

Therefore the hopping between $\mathcal{H}_S$ and $\mathcal{H}_{S'}$ of point 2 is represented by a $2L \times 2L$ matrix with all zeros, except for the the elements $\Gamma_{k,k'}$, $\Gamma_{k',k}$, which are equal to β.

Furthermore, performing a projective measurement on the ancillary system modifies the correlation matrix above following the same rules of Eq. (4.4) and Eq. (4.5), where now the index k is substituted with the index k'. Then, once the post-measurement correlation matrix is computed, the entanglement entropy is calculated taking the reduced correlation matrix, namely taking just the first l rows and columns.

Finally, resetting the ancillary state to the state $|00\dots0\rangle$ is done replacing the entries $\Gamma_{i,j'}$, $\Gamma_{i',j}$, $\Gamma_{i',j'}$ ($\forall\ i', j' \in [1', L']$) with zeros. Before going into the discussion of the results, a remark needs to be done.

Remark. For projective measurements we let the system evolve for time $t \approx L/2$, since at this value if t the entanglement entropy has saturated and the finite-size effects are still negligible. For the model introduced in this section, the setting of the evolution time requires more thought. Indeed, if we let the system evolve for very long times, even for a small coupling β between the system and the ancilla, eventually the the system will be in the state $|\psi_S\rangle = |00\dots0\rangle$, since even for small measurement rates all the fermions will eventually hop onto the ancilla and be destroyed. This will yield an entanglement entropy equal to zero, in the long time limit, independently of the subsystem size, even for small measurement rates. Therefore we cannot talk about a saturation value of the entanglement entropy, strictly speaking, however we can fix the evolution time and take the entanglement entropy at that time and consider it its saturation value. The value of t depends on what we want to observe and in the following it will be mentioned and discussed for the different simulations.

4.2.2 Results: Entanglement Entropy and Density Dynamics

As for projective measurements, we first compare the evolution of the entanglement entropy for different values of τ. However, in this model, one can also tune the coupling strength β between $\mathcal{H}_S$ and $\mathcal{H}_{S'}$ (Eq. (4.6)).

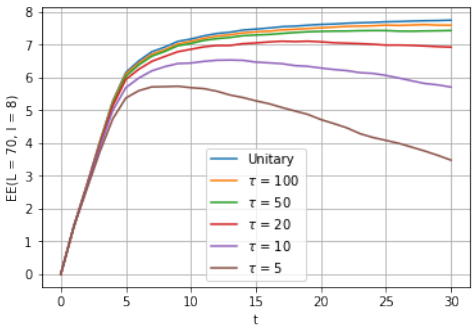

(a) *Time evolution of the entanglement entropy for some values of* τ.

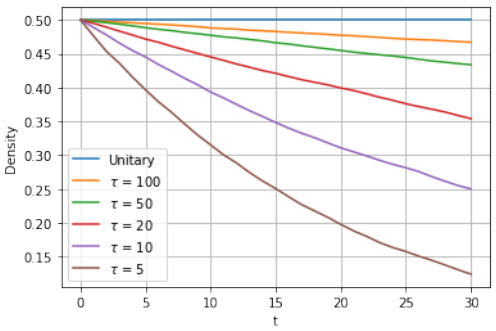

(b) *Time evolution of the density for some values of* τ.

Figure 4.4: *Time evolution of the entanglement entropy and the density for* $L = 70$, $l = 8$, *and* $\beta = 0.5$, *monitored with* $\tau \in \{5, 10, 20, 50, 100\}$.

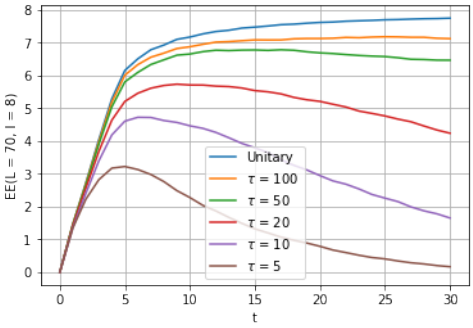

(a) *Time evolution of the entanglement entropy for some values of* τ.

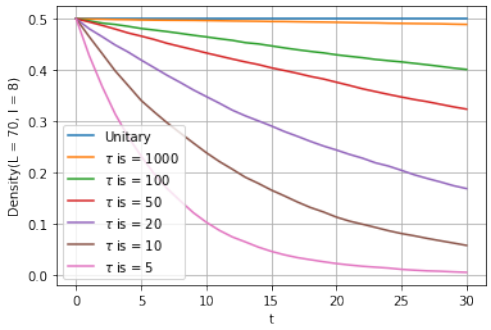

(b) *Time evolution of the density for some values of* τ.

Figure 4.5: *Time evolution of the entanglement entropy and the density for* $L = 70$, $l = 8$, *and* $\beta = 1$, *monitored with* $\tau \in \{5, 10, 20, 50, 100\}$.

In Fig. 4.4 and 4.5 the time evolution of the entanglement entropy and the density in a system with $\beta = 0.5$ and $\beta = 1$, respectively, are displayed. First of all, as one can intuitively expect, the densities, at a fixed time, are lower for a higher value of β. This reflects on the saturation value of the entanglement entropy, since the hopping between the system and the ancilla coincides with a measurement, as explained in the previous subsection. In both cases one can see how the entanglement entropy, for low enough values of τ, bends towards the zero-value, corresponding to the target state $|00\ldots0\rangle$, as discussed at the end of the previous subsection.

From Fig. 4.4a and 4.5a we can see how, depending on the measurement rate, the system displays different behaviours of the entanglement entropy. However the absence of a stable volume-law phase is obvious. Indeed, no matter the measurement rate, in the long-time limit the entanglement entropy will be zero for any subsystem size, since

the state of the system will be $|00\dots0\rangle$. Therefore there is no measurement induced entanglement phase transition in this model.

We now turn to a detailed analysis of the dependence of the dynamics on the subsystem size. To do so, we take a system with $L = 30$, since we expect no finite-size effects. Indeed, for small enough values of τ, the system will be dominated by the absorbing dynamics. Therefore we take smaller values of L, and consequently of l, since this is computationally advantageous in terms of the time required to carry out a simulation.

In Fig. 4.6a the time evolution of the entanglement entropy for different values of l is displayed and it is clear how, independently of l, the entanglement entropy saturates to a constant value, proving the existence of an area-law phase. Moreover this area-law phase is trivial. Indeed in the long-time limit the value at which the entanglement entropy saturates is 0, since the absorbing dynamics brings the system to the product state $|00\dots0\rangle$.

Since we have already proven the absence of an entanglement phase transition in this model, we do not analyze any further the entanglement entropy, instead we move to the discussion on the absence of an absorbing state transition.

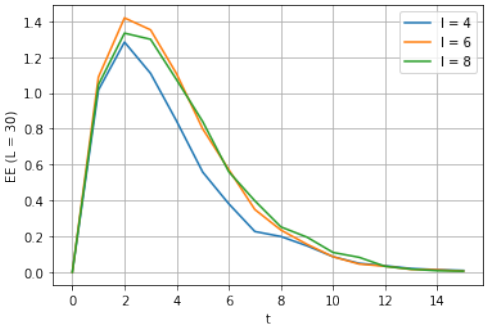

(a) *Time evolution of the entanglement entropy for some values of l.*

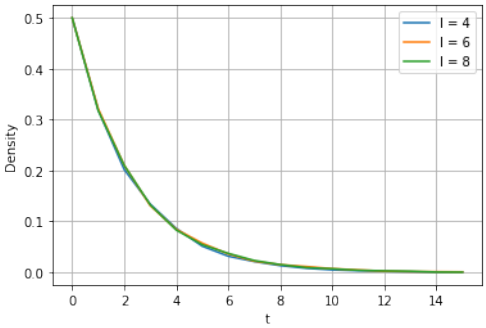

(b) *Time evolution of the density for some values of l^2.*

Figure 4.6: *Time evolution of the entanglement entropy and the density for $L = 30$, $\tau = 2$, $\beta = 1$ and $l = 4, 8, 12$.*

Results: Absence of an absorbing state transition As already mentioned in the beginning of the present section, we do not expect an absorbing state transition ,since there is no mechanism that contrasts the destruction of fermionic modes. In this paragraph we prove numerically our hypothesis.

An absorbing state transition is suggested by a discontinuity in the density when plotted in function of the measurement rate $p = 1/\tau$ [61]. Indeed, at a critical measurement rate, the density should go abruptly to zero. Moreover the critical point should be size independent. In Fig. 4.7 a plot of the asymptotic density as a function of L is

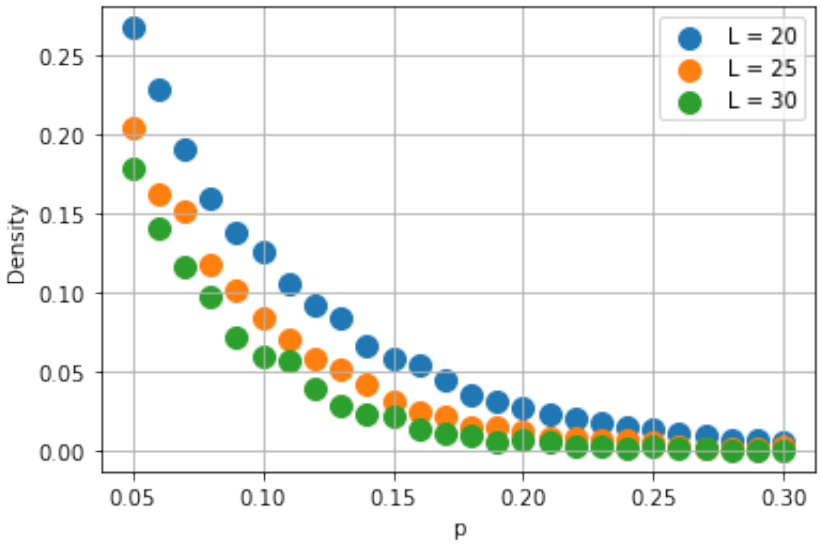

Figure 4.7: *Asymptotic density as a function of the measurement rate for different system sizes L. The system features a coupling strength of $\beta = 1$.*

displayed for different values of L. As one can see, the density goes to zero continuously, showing no signs of an absorbing state transition, as expected. To conlcude we remark that in this case the asymptotic density is taken at different times $t = L$, because for this value and the chosen range of p the density reaches zero.

4.3 Free-Fermionic Model with Non-Linear Weak Measurements

Given the results in Sec. 4.1 (as proven in [24]) and in Sec. 4.2, it is clear that there is no MIEPT in free-fermionic models, as proven in [25]. This is due to the fact that for any finite measurement rate, the system exits the volume-law phase and enters in a logarithmic phase.

Therefore we looked for a measurement procedure, to be inserted into a hopping evolution, that could make the volume law more stable. Such procedure, with the relative results, is discussed in this section.

4.3.1 Measurement Operators

For this model we use weak measurements, which were introduced in Sec. 1.4.2. We take as measurement operators[3]:

$$V_1^{(k)} = \frac{e^{-\epsilon/2}}{\sqrt{2\cosh(\epsilon)}} e^{\epsilon c_k^\dagger c_k}, \tag{4.8}$$

$$V_2^{(k)} = \frac{e^{\epsilon/2}}{\sqrt{2\cosh(\epsilon)}} e^{-\epsilon c_k^\dagger c_k}. \tag{4.9}$$

It is manifest how the strength of these operators is given by the parameter ϵ. For instance, for $\epsilon = 0$, V_1 and V_2 are proportional to the identity, thus not disturbing the state they are measuring.

Furthermore, the parameter ϵ is the means by which we introduce a non-linearity in the evolution. Indeed we will take

$$\epsilon \to \epsilon_k = J\Big(\frac{1}{2} - n_k\Big), \tag{4.10}$$

where $n_k = \langle\psi|\hat{n}_k|\psi\rangle$ is the local density and J is a coupling strength. We choose such formula for ϵ, because, as explained in Chap. 3, the density is $1/2$ when the entanglement entropy saturates to a value approximately equal to l. Therefore in this scenario, ϵ_k will become very small, leading to very weak measurements that could make the volume-law more stable.

Remark. By *non-linearity* we mean that there is a non-linearity, with respect to the density matrix, in the measurement outcomes. Indeed, for traditional generalized measurements, the probability of a measurement outcome is given by Eq. (1.101), which is linear in ρ. Instead, in the present case, we have that the measurement operators are $M = M(\rho)$, given the dependency of ϵ_k on the local density. Therefore the probability of a measurement outcome is non-linear in ρ.

We also mention that the experimental realization of such measurements is non trivial, given the fact that, before performing a measurement (described in Eq. (4.8), (4.9)), one also has to measure the local density.

4.3.2 QR-Decomposition

For projective measurements, we worked with the correlation matrix formalism. Namely its unitary evolution is given by Eq. (1.81) and the post-measurement state of the system is described by the correlation matrix of Eq. (4.4), (4.5).

For the type of weak measurements we have now introduced we employ a different technique, i.e. the *QR-decomposition*, which was first suggested in [18] and also used

[3]In appendix we show that they follow the completeness rule of Eq.(1.100).

in [25]. This approach presents some subtleties. First of all this technique works if the initial state is a *domain wall* (DW) state, namely, for a chain with L sites, with L even, the domain wall state is filled up to the site $L/2$, i.e. $|\psi_{\text{DW}}\rangle = |11\dots100\dots0\rangle$. However we are considering a system whose initial state is a Néel state. Therefore we need a matrix that brings the DW state into the Néel state. This can be done by a "permutation" unitary U_0. Therefore

$$|\psi_{\text{DW}}(0)\rangle = U_0\,|\psi_{\text{Néel}}(0)\rangle\,. \tag{4.11}$$

Given this fact we have that to go from the correlation matrix for the DW to the correlation matrix of the Néel state, we have to perform a change of basis, namely

$$\Gamma_{\text{DW}}(0) = U_0^{-1}\Gamma_{\text{Néel}}(0)U_0 = \text{diag}(1,\dots,1,0,\dots,0), \tag{4.12}$$

where the ones are until the diagonal element indexed by $L/2$. With this approach, the initial state is represented by the unitary U_0 and the state evolved under a Hamiltonian H is represented by $U(t) = \mathcal{U}(t)U_0$[4]. Therefore, to get the evolved correlation matrix, from which we can extract the entanglement entropy we do the change of basis $\Gamma(t) = U(t)\Gamma_{\text{DW}}(0)U(t)^{-1}$.

Following what proved in [25], the evolution of the correlation matrix under a measurement operator such as the ones in Eq. (4.8), (4.9), is done via the QR decomposition. More precisely, given a pure state $|\psi\rangle$, which is the evolution of an initial DW state, the post-measurement state $|\psi'\rangle = \mathcal{V}\,|\psi\rangle$ is given by

$$|\psi'\rangle = \mathcal{Q}\,|\psi\rangle\,, \tag{4.13}$$

where $\mathcal{Q}$ is the matrix Q from the QR-decomposition of the matrix $\mathcal{VU}$, namely $\mathcal{VU} = \mathcal{QR}$. We notice that $\mathcal{Q}$ is a unitary matrix and $\mathcal{R}$ is an upper triangular matrix[5].

As for the unitary evolution, at a time t, the state of the system is represented by the matrix $\tilde{U}(t) = \mathcal{Q}(t)U_0$. Therefore, to get the correlation matrix at time t, we do the change of basis $\Gamma(t) = \tilde{U}(t)\Gamma_{\text{DW}}(0)\tilde{U}(t)^{-1}$ [6].

4.3.3 Measurement Procedure

Having formalized the QR decomposition, we can now describe how to simulate the measurement on a classical computer. Similarly to what we have done in Sec. 4.1, we iterate on the sites of the fermionic chain. We always measure the system, after a unitary

[4] In this section we use capital letters for the matrices representing the states and calligraphic letters for the matrices representing operators on the many-body space.

[5] The QR decomposition is unique only if R has all positive entries on the diagonal.

[6] The entanglement entropy extracted from the procedure outlined in Sec. 4.3.2 has been compered to the one described in Sec. 1.3. The two approaches yield the same results.

step, but we must decide whether to apply $V_1^{(k)}$ or $V_2^{(k)}$. To do so we need to compute the probabilities of outcome 1 and 2 (look at App. F for the details):

$$p_k(1) = \langle\psi|V_1^{(k)\dagger}V_1^{(k)}|\psi\rangle = \frac{e^{-\epsilon_k}}{2\cosh(\epsilon_k)}\big(1 + (e^{2\epsilon_k} - 1)\Gamma_{k,k}\big), \tag{4.14}$$

$$p_k(2) = \langle\psi|V_2^{(k)\dagger}V_2^{(k)}|\psi\rangle = \frac{e^{\epsilon_k}}{2\cosh(\epsilon_k)}\big(1 + (e^{-2\epsilon_k} - 1)\Gamma_{k,k}\big). \tag{4.15}$$

Moreover we have that ϵ_k depends on the local density $n_k = \Gamma_{k,k}$. Therefore, before doing the measurement, we record the values of $\Gamma_{k,k}\ \forall\ k \in [1, L]$. Then for each k we extract a random number $q_k \in (0, 1]$. If $q_k \leq p_k(1)$ we apply $V_1^{(k)}$, otherwise we apply $V_2^{(k)}$, using the QR decomposition described in the previous subsection.

To be more precise, if $q_k \leq p_k(1)$ we apply the QR decomposition on $V_1^{(k)}\mathcal{U}$, where $V_1^{(k)}$ is a diagonal matrix with entries equal to $e^{-\epsilon/2}/\sqrt{2\cosh(\epsilon)}$, except for the k-th diagonal element, which is equal to $e^{-\epsilon/2}\epsilon/\sqrt{2\cosh(\epsilon)}$. This is due to the fact that the matrix representation of $c_k^\dagger c_k$ is a matrix with all zeros expect for the k-th diagonal element.

4.3.4 Results

For this model with non-linear weak measurements we will analyze the time evolution of the entanglement entropy, looking for a measurement induced entanglement phase transition. More precisely we will be looking for a stable volume-law phase. To do so we stress the fact that the control parameter for the hypothetical entanglement transition is the parameter J in Eq. (4.10). Indeed the magnitude of this constant affects the strength of the weak measurement. J is therefore the equivalent of the measurement rate $p = 1/\tau$ of the previous two models. In analogy with those, is natural to ask ourselves if there is a volume-law phase or mixed phase for small values of J and an area-law phase for big enough values of J. To be more precise we expect to have an area-law phase, in analogy to the weak monitoring regime of the previous analyzed models, but we are looking for a more stable volume law for the model at hand.

First Qualitative Analysis To start to understand the behaviour of this non-linear model, the first thing we do is to plot the time evolution of the entanglement entropy for different values of J. As one can see in Fig. 4.8, for $J \lessapprox 0.1$, the monitored evolution seems to resemble the unitary one, whereas for grater values of J it does not. Then, for $1 \lessapprox J \lessapprox 4$, the entanglement entropy saturates at a value smaller than the unitary case. Finally for $J \gtrapprox 5$ there is a similarity with the area-law behaviour of the projective measurement case, namely the entanglement entropy peaks and then decreases, saturating to a certain value.

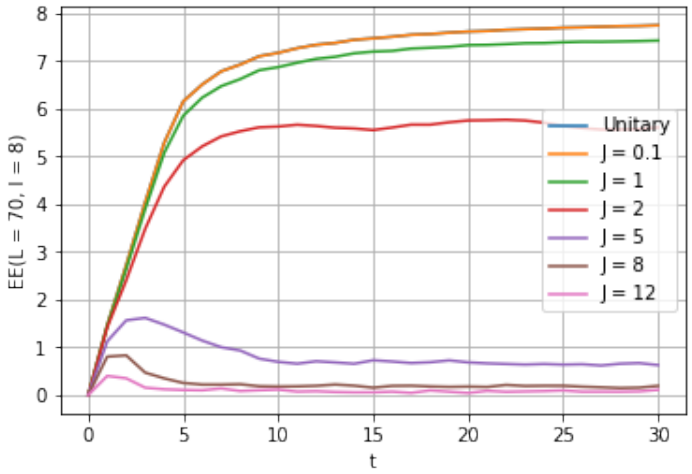

Figure 4.8: *Time evolution of the entanglement entropy for a system with* $L = 70$, $l = 8$ *and a varying parameter* J.

This preliminary discussion does not allow us to determine whether a transition exists. Indeed, for a quantitative precise estimation, one should fix J and take the saturation value of the entanglement entropy for every possible l, given a fixed (large enough) L. Then one should extrapolate EE/l for $l \to \infty$. Doing this $\forall$ J, one should then plot the entanglement entropy over l, in the large l limit, as a function of J to extract the critical value of J.

However finite size effects need to be considered. Indeed, having fixed L, one has a limited choice for l. Indeed, as l increases, the time t at which a collapse of the entanglement entropy shows up decreases. Moreover, in the volume-law phase, as l increases, the entanglement entropy reaches a saturation value $S_l(\infty) \approx \alpha l$ (where α is a constant). However, finite-size effect make this value lower for increasing ls if we normalize the entanglement entropy with l.

To reduce finite-size effects, we should simulate a larger system than the ones we have considered in this thesis, however our computational resources do not allow us to reliably analyze the effect of finite sizes. Therefore we will do a qualitative analysis with the data we can collect from the evolution, up to $t = 30$, of a system with $L = 70$ and subsystem sized $l = 2, 3, 4, 5$. Indeed these are the dimensions of the subsystem and the evolution time for which finite sizes are more negligible.

Small-J Regime The model discussed in the present section was introduce to see if there is a type of measurement that gives a stable volume-law phase in non-interacting fermionic. As explained above, to find if the measure we introduced yields a volume-law phase we need to do an asymptotic analysis.

In this model we measure every fermionic mode at every time step and we measure

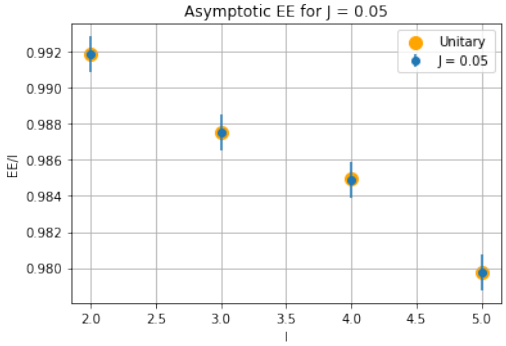

(a) *Asymptotic analysis of the entanglement entropy for* $J = 0.05$ *(with standard deviation).*

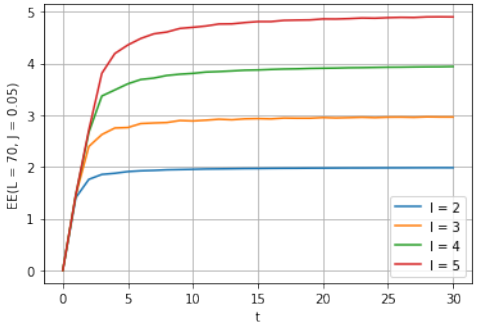

(b) *Evolution of the entanglement entropy for a system with* $L = 70$*,* $J = 0.05$ *and different values of the subsystem size* l*.*

Figure 4.9: *Asymptotic analysis of the entanglement entropy and the entanglement entropy evolution on a system with* $J = 0.05$ *and* $L = 70$ *for* $l = 2, 3, 4, 5$*.*

$V_1^{(k)}$ or $V_2^{(k)}$ (Eq. (4.8), (4.9)) depending on a random number, as described in Sec. 4.3.3. Therefore we need to do an average over quantum trajectories.

In Fig. 4.9a we plot the asymptotic value of the entanglement entropy in the unitary case and in a weak monitoring non-linear dynamics with $J = 0.05$. We can here see how the asymptotic value of the entanglement entropy in the monitored case overlaps with the unitary one, thus suggesting a stable volume-law phase. Indeed, looking at Fig. 4.9b, one can see how the values of the entanglement entropy at time $t = 30$ are equally spaced for different values of l, suggesting a volume law phase $S_l(\infty) \approx \alpha l$, where α is a constant[7]. This becomes more manifest if we compare this behaviour with the one of the entanglement entropy of a system subjected to projective measurements. For instance, in Fig. 4.3a we can clearly see how this constant spacing is not there and indeed, in the case of projective measurements, the free-fermionic chain evolving under a hopping Hamiltonian does not have a stable volume-law phase.

Large-J Regime As for the volume-law phase, a rigorous analysis is not possible due to our computational resources. However we can still give evidence of the existence of an area-law phase, at least in systems with finite sizes. Looking at the time evolution entanglement entropy in a system with $L = 70$ for different subsystem sizes $l = 2, 3, 4, 5$ in a non-linear strong monitoring regime (Fig. 4.10), we can see how the entanglement entropy saturates at a constant value, independently from l.

[7]To be precise, as l gets larger, $S_l(\infty)/l$ decreases, as one can see from Fig. 4.9a. This is due to finite size effects, therefore what we are here saying is subject to this limitation, as already stressed.

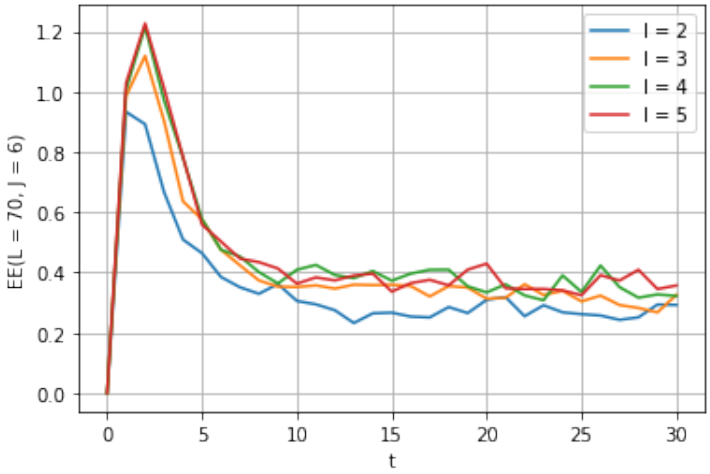

Figure 4.10: *Time evolution of the entanglement entropy for* $J = 6$ *and* $l = 2, 3, 4, 5$.

Remark. Fluctuations of the entanglement entropy: as one can see in Fig. 4.10, the entanglement entropy fluctuates very much in the area-law regime. This is due to the fact that the quantum trajectories can be very different from each other in this regime, yielding very different averages.

Conclusions and Outlook

The main results of this thesis are three and they are here listed.

1. In Sec. 3.9: the application of the quasiparticle picture on a brickwork circuit with local unitaries that can be mapped onto free fermionic unitaries.

   We indeed prove that we can find an effective Hamiltonian for the brickwork dynamics, which, once diagonalized (Eq. (3.72)), yields the values of the quasiparticle velocity (Eq. (3.80)) and of the Yang-Yang entropy (Eq. (3.83) that. After putting them together in the quasiparticle picture,they yield a prediction for the unitary evolution of the entanglement entropy (Fig. 3.9).

2. In Sec. 4.2: the absence of a measurement induced phase transition in a free-fermionic model with a dynamics that drives the system towards a target state monitored with weak measurements.

   Here we introduce an ancillary system on which, after a hopping between the system and the ancilla, local projective measurements are performed, which is equivalent to apply weak measurements on the system (Sec. 1.4.2). The hopping brings the system towards an absorbing state, which is the state without fermionic excitations. In this case we have that there is no absorbing state transition, given the fact that there is no mechanism that contrasts the distruction of fermionic excitations in the system. Moreover, the volume-law phase of the entanglement entropy is proven to be unstable, thus there is no entanglement transition, as for the projective measurement case.

3. In Sec. 4.3: the results here presented suggest the presence of a measurement induced entanglement phase transition for a free fermionic model monitored with weak measurements (Eq. (4.8), (4.9)), whose strength is given by a non-linear parameter J (Eq. (4.10)).

   Guided by the fact that the volume-law is unstable for free fermionic dynamics that conserves the number of fermions, we introduced a measurement procedure that could stabilize the volume-law. To do so we noticed that, when the entanglement entropy saturates, the local density is 0.5 on all sites of the system. Therefore we

draw up a local weak measurement, whose strength depends on the local density (Eq. (4.10)), such that, the measurement is very weak when the density is close to 0.5, i.e. when the entanglement entropy saturates (Sec. 4.3.1).

As explained in Sec. 4.3.4, while we have simulated systems of $L = 70$, in order to have more precise results one should simulate larger systems. This however proves to be very time demanding for a regular personal computer. Therefore a first spin-off of this thesis could be the simulation of larger systems on more powerful hardware, matched with an optimization of the code used for the numerical results, that could also involve parallelization techniques. This will allow to avoid finite-size effects and extrapolate the critical value of J in the thermodynamic limit, where we could find a rigorous phase diagram.

Besides, we could also map all the measurement procedures described in Chap. 4 onto a brickwork circuit. Indeed, as done in Chap. 3, the continuous free-fermionic dynamics is reproduced by a brickwork circuit, with appropriate gates. Therefore we could insert the projective and weak measurements of Chap. 4 into this discretized evolution and analyze the results.

Appendix A

Fourier-Space for Fermions

We can investigate the time evolution of the correlation matrix also in Fourier space. To do so we do a discrete Fourier transform of the fermionic creation and annihilation operators:

$$b_p = \frac{1}{\sqrt{L}} \sum_{j=1}^{L} e^{-i\frac{2\pi}{L}pj} c_j, \quad b_p^\dagger = \frac{1}{\sqrt{L}} \sum_{j=1}^{L} e^{i\frac{2\pi}{L}pj} c_j^\dagger. \tag{A.1}$$

The inverse Fourier transform is:

$$c_j = \frac{1}{\sqrt{L}} \sum_{p} e^{i\frac{2\pi}{L}pj} b_p, \quad c_j^\dagger = \frac{1}{\sqrt{L}} \sum_{p} e^{-i\frac{2\pi}{L}pj} b_p^\dagger. \tag{A.2}$$

Now we set periodic boundary conditions, namely

$$c_j = c_{j+N} \Rightarrow p = 0, 1, \ldots, L-1. \tag{A.3}$$

Therefore:

$$c_j = \frac{1}{\sqrt{L}} \sum_{p=0}^{L-1} e^{i\frac{2\pi}{L}pj} b_p, \quad c_j^\dagger = \frac{1}{\sqrt{L}} \sum_{p=0}^{L-1} e^{-i\frac{2\pi}{L}pj} b_p^\dagger. \tag{A.4}$$

Form now on, when we write the sums, the allowed values for the momenta are understood.

From here, using the anticommutation rules for the fermionic creation and annihilation operators, it is straightforward to see that:

$$\{b_p, b_q\} = 0 = \{b_p^\dagger, b_q^\dagger\} \tag{A.5}$$

$$\{b_p, b_q^\dagger\} = \delta_{p,q}. \tag{A.6}$$

Looking at Eq. (1.77), we see that we need the expression of the creation and annihilation operators in the Heisenberg picture. The Fourier transform of these is:

$$c_j(t) = \frac{1}{\sqrt{L}} \sum_{p} e^{i\frac{2\pi}{L}pj} b_p(t), \quad c_j^\dagger(t) = \frac{1}{\sqrt{L}} \sum_{p} e^{-i\frac{2\pi}{L}pj} b_p^\dagger(t). \tag{A.7}$$

Hence we need to find the expression for $b_p(t), b_p^\dagger(t)$. To do so we follow the same procedure of Eq.(1.78). In order to be able to do that we must find the expression of the Hamiltonian in terms of the Fourier transformed operators. In the following we will be considering the Hopping Hamiltonian:

$$H = -\frac{1}{2}\sum_{j=1}^{L}(c_j^\dagger c_{j+1} + c_{j+1}^\dagger c_j). \tag{A.8}$$

By substituting the corresponding Fourier transforms of Dirac operators we find:

$$\begin{aligned}
H &= -\frac{1}{2}\sum_{j=1}^{N}\Big[\frac{1}{L}\sum_{p,q} e^{-i\frac{2\pi}{L}pj}e^{i\frac{2\pi}{L}q(j+1)}b_p^\dagger b_q + \frac{1}{L}\sum_{p,q} e^{-i\frac{2\pi}{L}p(j+1)}e^{i\frac{2\pi}{L}qj}b_p^\dagger b_q\Big] \\
&= -\frac{1}{2}\Big(\sum_{p,q} e^{i\frac{2\pi}{L}q}b_p^\dagger b_q \frac{1}{L}\sum_{j=1}^{N} e^{i\frac{2\pi}{L}j(q-p)} + \sum_{p,q} e^{-i\frac{2\pi}{L}p}b_p^\dagger b_q \frac{1}{L}\sum_{j=1}^{N} e^{i\frac{2\pi}{L}j(q-p)}\Big) \\
&= -\frac{1}{2}\Big(\sum_{p,q} e^{i\frac{2\pi}{L}q}b_p^\dagger b_q \delta_{p,q} + \sum_{p,q} e^{-i\frac{2\pi}{L}p}b_p^\dagger b_q \delta_{p,q}\Big) \\
&= -\frac{1}{2}\sum_{p}(e^{i\frac{2\pi}{L}p} + e^{-i\frac{2\pi}{L}p})b_p^\dagger b_p \\
&= -\sum_{p}\cos\Big(\frac{2\pi}{L}p\Big)b_p^\dagger b_p.
\end{aligned} \tag{A.9}$$

The Hamiltonian is thus diagonal in momentum space and can be written as:

$$H = \sum_p \epsilon_p b_p^\dagger b_p, \quad \epsilon_p = -\cos\Big(\frac{2\pi}{L}p\Big). \tag{A.10}$$

Now we can find the expression for $b_p(t)$ and $b_p^\dagger(t)$ following the same procedure of Eq.(1.78), namely:

$$\begin{aligned}
\frac{d}{dt}b_q(t) &= -iU^\dagger(t)t\Big(\epsilon_p\sum_p[b_q, b_p^\dagger b_p]\Big)U(t) \\
&= -iU^\dagger(t)t\Big(\epsilon_p\sum_p(\{b_q, b_p^\dagger\}b_p - b_p^\dagger\{b_q, b_p\})\Big)U(t) \\
&= -i\epsilon_q t b_q(t),
\end{aligned} \tag{A.11}$$

and solving the differential equation we get and (identical procedure for the hermitian conjugate):

$$b_p(t) = e^{-i\epsilon_p t}b_p, \quad b_p^\dagger(t) = e^{i\epsilon_p t}b_p^\dagger. \tag{A.12}$$

Thus we get

$$c_j(t) = \frac{1}{\sqrt{L}} \sum_p e^{i\frac{2\pi}{L}pj} e^{-i\epsilon_p t} b_p, \tag{A.13}$$

$$c_j^\dagger(t) = \frac{1}{\sqrt{L}} \sum_p e^{-i\frac{2\pi}{L}pj} e^{i\epsilon_p t} b_p^\dagger. \tag{A.14}$$

We have now all the instruments to look at the correlation matrix. Let's start from the static case. From Eq.(A.4), we get that the matrix elements of the correlation matrix can be written as:

$$\Gamma_{j,k} = \langle c_j^\dagger c_k \rangle = \langle \frac{1}{L} \sum_p e^{-i\frac{2\pi}{L}pj} b_p^\dagger \sum_q e^{i\frac{2\pi}{L}qk} b_q \rangle. \tag{A.15}$$

Defining

$$\Gamma_{p,q} \equiv \langle b_p^\dagger b_q \rangle, \tag{A.16}$$

we can write the correlation matrix elements as:

$$\Gamma_{j,k} = \frac{1}{L} \sum_{p,q} e^{-i\frac{2\pi}{L}(pj-qk)} \Gamma_{p,q}. \tag{A.17}$$

The time evolution of the correlation matrix can be found using the operators in Eq.(A.14) we thus find:

$$\Gamma_{j,k}(t) = \frac{1}{L} \sum_{p,q} e^{it[\epsilon_p - \epsilon_q]} e^{-i\frac{2\pi}{L}(pj-qk)} \Gamma_{p,q}. \tag{A.18}$$

To be more explicit, we do the inverse fourier transform of $\Gamma_{p,q}$:

$$\Gamma_{p,q} = \frac{1}{L} \sum_{m,n=1}^{L} e^{i\frac{2\pi}{L}(pm-qn)} \Gamma_{m,n}. \tag{A.19}$$

Therefore, putting this together with Eq.(A.17), we get that

$$\Gamma_{j,k}(t) = \sum_{m,n=1}^{L} \frac{1}{L} \sum_{p=0}^{L-1} e^{i\frac{2\pi}{L}p(m-j)} e^{i\epsilon_p t} \Gamma_{m,n} \frac{1}{L} \sum_{q=0}^{L-1} e^{-i\frac{2\pi}{L}q(n-k)} e^{-i\epsilon_q t}. \tag{A.20}$$

Defining

$$R_{k,n}(t) \equiv \frac{1}{L} \sum_{q=0}^{L-1} e^{-i\frac{2\pi}{L}q(n-k)} e^{-i\epsilon_q t} \tag{A.21}$$

and thus

$$R^*_{j,m} = \frac{1}{L}\sum_{p=0}^{L-1} e^{i\frac{2\pi}{L}p(m-j)} e^{i\epsilon_p t}, \tag{A.22}$$

we get

$$\Gamma_{j,k}(t) = \sum_{m,n=1}^{L} R^*_{j,m}\Gamma_{m,n}R_{n,k} = R^*_{j,m}\Gamma_{m,n}R^T_{n,k}, \tag{A.23}$$

which is equivalent to Eq.(1.81).

What is left to do is to see if our code, which follows the evolution in Hilbert space, is consistent. Therefore we compare the matrix elements of correlation matrices (at each time step for a trotterized evolution) calculated with the formula for the Hilbert space and with the fast Fourier transforms provided by Python. As one can see in Fig. A.1, the two approaches are equivalent. Indeed there is no difference in the matrix elements of the two approaches. by the way, the simulations are done on a system of size $L = 6$ and the matrix elements are chosen randomly. Moreover we plot the real part for $\Gamma_{5,5}$ and the imaginary part for $\Gamma_{4,5}$ because these are non-zero.

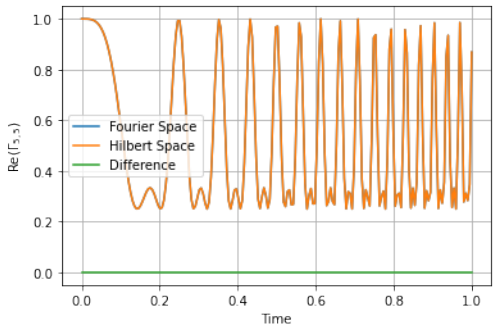

(a) *Time evolution of the real part of the matrix element* $\Gamma_{5,5}$ *in the Fourier space and in the Hilbert space.*

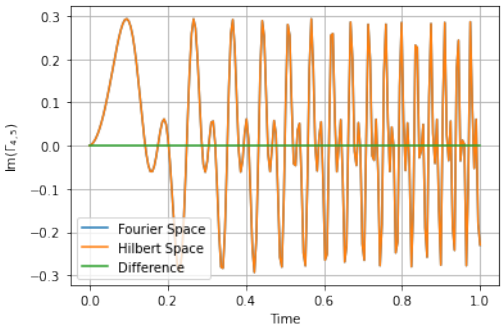

(b) *Time evolution of the imaginary part of the matrix element* $\Gamma_{4,5}$ *in the Fourier space and in the Hilbert space.*

Figure A.1: *Time evolution of the real and imaginary parts of selected matrix elements of the correlation matrix in the Fourier space and in the Hilbert space. The green line is the maximum difference between corresponding matrix element (in that time step of the evolution) calculated in Fourier space and in the Hilbert space.*

Appendix B

Entanglement Entropy from the Quasiparticle Picture

Starting from Eq. (3.17), we have, first of all, to set the integration regions. We are taking into account the whole real axis and we set the region A to be the segment of length L such that $x' \in [0, L]$. Now since we are looking at the whole real axis, the contribution to the entanglement entropy from the sub-region of $\bar{A}$ to the left of A, is equal to the one on the right, thus we have

$$\int_{x' \in A} dx' \to \int_0^L dx', \qquad \int_{x'' \in \bar{A}} dx'' \to 2 \int_L^{+\infty} dx''. \tag{B.1}$$

Thus, reordering the integrals, we have to calculate

$$\begin{aligned} S_L(t) &= 2 \int dps(p) \int_0^L dx' \int_L^{+\infty} dx'' \int_{-\infty}^{+\infty} dx \delta(x' - x - v_p t) \delta(x'' - x + v_p t) \\ &= 2 \int dps(p) \int_0^L dx' \int_L^{+\infty} dx'' \delta(x'' - x' + 2 v_p t). \end{aligned} \tag{B.2}$$

Now we exploit the fact that the delta function is the derivative of the Heaviside step function, getting

$$S_L(t) = 2 \int dps(p) \int_0^L dx' \Theta(2 v_p t - L - x'). \tag{B.3}$$

The step function is different from zero just when $x' < 2 v_p t - l$. Now if $2 v_p t > L$ we have the integration region from 0 to L, whereas if $2 v_p t < L$ the integration region is from 0 to $2 v_p t$, thus giving the final result

$$S_L(t) \approx 2t \int_{2 v_p t < L} dps(p) 2 v_p + 2l \int_{2 v_p t > L} dps(p). \tag{B.4}$$

Appendix C

Inverse Jordan-Wigner Mapping

Suppose we have a chain of L qubits as shown in Fig. 3.6, where we assume L to be even and we assume periodic boundary conditions. We let the system evolve under local unitaries of the kind

$$U_{j,j+1} = e^{-i\alpha(\sigma_j^- \sigma_{j+1}^+ + \sigma_{j+1}^- \sigma_j^+)}. \tag{C.1}$$

Our goal is to prove that this evolution, local in time and in space, can be mapped onto the evolution of a fermionic chain under a hopping Hamiltonian, thus yielding to the same behaviour of the entanglement entropy. To do so we map the spin operators to fermionic operators using the JW transformation. We obtain, with a direct calculation:

$$\sigma_j^- \sigma_{j+1}^+ = c_j^\dagger (1 - 2n_j) c_{j+1} = c_j^\dagger c_{j+1}, \tag{C.2}$$

because $c_j^\dagger n_j c_{j+1} = c_j^\dagger c_j^\dagger c_j c_{j+1} = 0$ and

$$\sigma_{j+1}^- \sigma_j^+ = c_{j+1}^\dagger (1 - 2n_j) c_j = c_{j+1}^\dagger c_j, \tag{C.3}$$

because $c_{j+1}^\dagger n_j c_j = c_{j+1}^\dagger$ and $c_j^\dagger c_j c_j = 0$.

C.1 Brickwork Evolution of the Correlation Matrix

Following the result in Eq. (1.58), adapted for discrete-time evolution, we find how the correlation matrix evolves for a fixed j, then we can do it for all js in the system. We showed in a previous sections that, in general, the correlation matrix evolves, for discrete time steps, as:

$$\Gamma'_{i,j} = \langle \psi_0 | e^{ad_{iH}} c_i^\dagger c_j | \psi_0 \rangle \,. \tag{C.4}$$

In the present case we have a local evolution. Let's look at the general case of the evolution of $\Gamma_{a,b}$ under $U_{j,j+1}$, i.e. we look at the effect of a local evolution on generic indexes of the correlation matrix.

$$\Gamma'_{a,b} = \langle \psi_0 | U_{j,j+1}^\dagger c_a^\dagger c_b U_{j,j+1} | \psi_0 \rangle \,. \tag{C.5}$$

We know that

$$e^A B e^{-A} = B + [A, B] + \frac{1}{2}[A, [A, B]] + \dots \tag{C.6}$$

where $A = i\alpha(c_j^\dagger c_{j+1} + c_{j+1}^\dagger c_j)$ and $B = c_a^\dagger c_b$. Using the anticommutation rules of the fermionic operators we get:

$$[A, B] = i\alpha(-\delta_{a,j+1} c_j^\dagger c_b + \delta_{b,j} c_a^\dagger c_{j+1} - \delta_{a,j} c_{j+1}^\dagger c_b + \delta_{b,j+1} c_a^\dagger c_j) \tag{C.7}$$

and $[A, [A, B]] = 0$ which makes all the other nested commutators equal to zero as well. Therefore

$$\begin{aligned} e^{i\alpha(c_j^\dagger c_{j+1} + c_{j+1}^\dagger c_j)} c_a^\dagger c_b e^{-i\alpha(c_j^\dagger c_{j+1} + c_{j+1}^\dagger c_j)} &= c_a^\dagger c_b + \\ &+ i\alpha(-\delta_{a,j+1} c_j^\dagger c_b + \delta_{b,j} c_a^\dagger c_{j+1} - \delta_{a,j} c_{j+1}^\dagger c_b + \delta_{b,j+1} c_a^\dagger c_j). \end{aligned} \tag{C.8}$$

This yelds to the following correlation matrix evolution

$$\Gamma'_{a,b} = \Gamma_{a,b} - i\alpha\delta_{a,j+1}\Gamma_{j,b} + i\alpha\delta_{b,j}\Gamma_{a,j+1} - i\alpha\delta_{a,j}\Gamma_{j+1,b} + i\alpha\delta_{b,j+1}\Gamma_{a,j}. \tag{C.9}$$

Now we can iterate this for all j.

C.2 Delta Condition for a Fourier Transform on Half Period

Looking at the last row of Eq. (3.38), we now need to see for which p, q we have that

$$\frac{1}{L}\sum_{j=1}^{L/2} e^{-i\frac{4\pi}{L}(p-q)j} \neq 0. \tag{C.10}$$

For a geometric series

$$\sum_{j=1}^{N} r^j = r\frac{1-r^N}{1-r}. \tag{C.11}$$

In this case we have that $r = \exp(-i4\pi(p-q)/L)$ and $N = L/2$, then

$$\sum_{j=1}^{L/2} e^{-i\frac{4\pi}{L}(p-q)j} = e^{-i\frac{4\pi}{L}(p-q)}\frac{1 - e^{-i\frac{4\pi}{L}(p-q)\frac{L}{2}}}{1 - e^{-i\frac{4\pi}{L}(p-q)}}. \tag{C.12}$$

From this expression we can find the delta condition. Indeed, imposing the denominator to be equal to zero, we find that

$$p - q = k\frac{L}{2}, \tag{C.13}$$

where k is an integer.

Appendix D

Correlation matrix after a local measurement

If the outcome of the measurement is 1, the post-measurement state will be

$$\frac{n_k \left|\Psi\right\rangle}{\sqrt{\langle\Psi(t)|n_k|\Psi(t)\rangle}}, \tag{D.1}$$

therefore the correlation matrix, which is obtained by averaging over this state, will be:

$$\Gamma_{i,j}(t) = \frac{\langle c_k^\dagger c_k c_i^\dagger c_j c_k^\dagger c_k\rangle}{\langle c_k^\dagger c_k\rangle}. \tag{D.2}$$

The denominator of this expression is simply the correlation matrix element $\Gamma_{k,k}$, whereas the numerator can be evaluated using Wick's theorem.

$$\begin{aligned}\langle c_k^\dagger c_k c_i^\dagger c_j c_k^\dagger c_k\rangle = {} & \langle \overbracket{c_k^\dagger c_k} \overbracket{c_i^\dagger c_j} \overbracket{c_k^\dagger c_k}\rangle + \langle \overbracket{c_k^\dagger \overbracket{c_k c_i^\dagger} c_j c_k^\dagger} c_k\rangle + \langle \overbracket{c_k^\dagger \overbracket{c_k c_i^\dagger} c_j} \overbracket{c_k^\dagger c_k}\rangle \\ & + \langle \overbracket{c_k^\dagger c_k} \overbracket{c_i^\dagger \overbracket{c_j c_k^\dagger} c_k}\rangle + \langle \overbracket{c_k^\dagger \overbracket{c_k c_i^\dagger} \overbracket{c_j c_k^\dagger} c_k}\rangle + \langle \overbracket{c_k^\dagger \overbracket{c_k \overbracket{c_i^\dagger c_j} c_k^\dagger} c_k}\rangle.\end{aligned} \tag{D.3}$$

Now we can evaluate all this contractions, keeping in mind that we are dealing with fermionic operators and thus anti-commutation rules have to be taken into account:

1.

$$\langle \overbracket{c_k^\dagger c_k} \overbracket{c_i^\dagger c_j} \overbracket{c_k^\dagger c_k}\rangle = \langle c_k^\dagger c_k\rangle\langle c_i^\dagger c_j\rangle\langle c_k^\dagger c_k\rangle = \Gamma_{k,k}^2\Gamma_{i,j}; \tag{D.4}$$

2.

$$\begin{aligned}\langle \overbracket{c_k^\dagger \overbracket{c_k c_i^\dagger} \overbracket{c_j c_k^\dagger} c_k}\rangle &= (-1)^6\langle c_k^\dagger c_k\rangle\langle c_k c_k^\dagger\rangle\langle c_i^\dagger c_j\rangle = \Gamma_{k,k}(1-\langle c_k^\dagger c_k\rangle)\Gamma_{k,k} \\ &= \Gamma_{k,k}\Gamma_{i,j} - \Gamma_{k,k}^2\Gamma_{i,j};\end{aligned} \tag{D.5}$$

3.

$$\begin{aligned}\langle c_k^\dagger c_k c_i^\dagger c_j c_k^\dagger c_k\rangle &= (-1)^2\langle c_k^\dagger c_j\rangle\langle c_k c_i^\dagger\rangle\langle c_k^\dagger c_k\rangle = \Gamma_{k,j}(\delta_{i,k-\Gamma_{i,k}})\Gamma_{k,k} \\ &= \Gamma_{k,k}\Gamma_{k,j}\delta_{i,k} - \Gamma_{k,k}\Gamma_{i,k}\Gamma_{k,j};\end{aligned} \tag{D.6}$$

4.

$$\begin{aligned}\langle c_k^\dagger c_k c_i^\dagger c_j c_k^\dagger c_k\rangle &= (-1)^2\langle c_k^\dagger c_k\rangle\langle c_i^\dagger c_k\rangle\langle c_j c_k^\dagger\rangle = \Gamma_{k,k}\Gamma_{i,k}(\delta_{j,k} - \Gamma_{k,j}) \\ &= \Gamma_{k,k}\Gamma_{i,k}\delta_{j,k} - \Gamma_{k,k}\Gamma_{i,k}\Gamma_{k,j};\end{aligned} \tag{D.7}$$

5.

$$\begin{aligned}\langle c_k^\dagger c_k c_i^\dagger c_j c_k^\dagger c_k\rangle &= (-1)^4\langle c_k^\dagger c_k\rangle\langle c_k c_i^\dagger\rangle\langle c_j c_k^\dagger\rangle = \Gamma_{k,k}(\delta_{i,k} - \Gamma_{i,k})(\delta_{j,k} - \Gamma_{k,j}) \\ &= \Gamma_{k,k}\delta_{i,k}\delta_{j,k} + \Gamma_{k,k}\Gamma_{i,k}\Gamma_{k,j} - \Gamma_{k,k}\Gamma_{i,k}\delta_{j,k} - \Gamma_{k,k}\Gamma_{k,j}\delta_{i,k};\end{aligned} \tag{D.8}$$

6.

$$\begin{aligned}\langle c_k^\dagger c_k c_i^\dagger c_j c_k^\dagger c_k\rangle &= (-1)^3\langle c_k^\dagger c_j\rangle\langle c_k c_k^\dagger\rangle\langle c_i^\dagger c_k\rangle = -\Gamma k, j(1 - \Gamma_{k,k})\Gamma_{i,k} \\ &= -\Gamma_{i,k}\Gamma_{k,j} + \Gamma_{k,k}\Gamma_{i,k}\Gamma_{k,j}.\end{aligned} \tag{D.9}$$

Thus

$$\langle c_k^\dagger c_k c_i^\dagger c_j c_k^\dagger c_k\rangle = 1) + 2) + 3) + 4) + 5) + 6) = \Gamma_{k,k}\Gamma_{i,j} + \Gamma_{k,k}\delta_{i,k}\delta_{j,k} - \Gamma_{i,k}\Gamma_{k,j}. \tag{D.10}$$

Plugging all just said in Eq. (D.2), we get the correlation matrix after the measurement, if the outcome of the measurement is 1:

$$\Gamma_{i,j}(t) = \delta_{ik}\delta_{jk} + \Gamma_{ij}(t) - \frac{\Gamma_{ik}(t)\Gamma_{kj}(t)}{\Gamma_{kk}(t)}. \tag{D.11}$$

On the other hand, if the outcome of the measurement is 0, the post-measurement state will be:

$$\frac{(1 - n_k)\,|\Psi(t)\rangle}{\sqrt{\langle\Psi(t)|(1 - n_k)|\Psi(t)\rangle}}. \tag{D.12}$$

Hence, the correlation matrix obtained averaging over this state will be:

$$\Gamma_{i,j}(t) = \frac{\langle(1 - c_k^\dagger c_k)c_i^\dagger c_j(1 - c_k^\dagger c_k)\rangle}{\langle 1 - c_k^\dagger c_k\rangle}. \tag{D.13}$$

As before, the denominator is very straightforward: $\langle(1-c_k^\dagger c_k)\rangle = 1-\Gamma_{k,k}$. The numerator can be written as:

$$\langle(1 - c_k^\dagger c_k)c_i^\dagger c_j(1 - c_k^\dagger c_k)\rangle = \langle c_i^\dagger c_j\rangle - \langle c_i^\dagger c_j c_k^\dagger c_k\rangle - \langle c_k^\dagger c_k c_i^\dagger c_j\rangle + \langle c_k^\dagger c_k c_i^\dagger c_j c_k^\dagger c_k\rangle. \tag{D.14}$$

Here, the first term of the sum is trivial, and the last term is the one in Eq. (D.10). For the other two terms we use Wick's theorem:

1.

$$\begin{aligned}\langle c_i^\dagger c_j c_k^\dagger c_k\rangle &= \langle \overbrace{c_i^\dagger \overbrace{c_j \overbrace{c_k^\dagger c_k}}}\rangle + \langle \overbrace{c_i^\dagger}\overbrace{c_j \overbrace{c_k^\dagger}}\overbrace{c_k}\rangle \\ &= (-1)^2\langle c_i^\dagger c_k\rangle\langle c_j c_k^\dagger\rangle + \langle c_i^\dagger c_j\rangle\langle c_k^\dagger c_k\rangle \\ &= \Gamma_{i,k}(\delta_{j,k}-\Gamma_{k,j}) + \Gamma_{i,j}\Gamma_{k,k} = \Gamma_{i,k}\delta_{j,k} - \Gamma_{i,k}\Gamma_{k,j} + \Gamma_{i,j}\Gamma_{k,k};\end{aligned} \tag{D.15}$$

2.

$$\begin{aligned}\langle c_k^\dagger c_k c_i^\dagger c_j\rangle &= \langle \overbrace{c_k^\dagger}\overbrace{c_k \overbrace{c_i^\dagger}}\overbrace{c_j}\rangle + \langle \overbrace{c_k^\dagger \overbrace{c_k \overbrace{c_i^\dagger c_j}}}\rangle \\ &= \langle c_k^\dagger c_k\rangle\langle c_i^\dagger c_j\rangle + (-1)^2\langle c_k^\dagger c_j\rangle\langle c_k c_i^\dagger\rangle \\ &= \Gamma_{k,k}\Gamma_{i,j} + \Gamma_{k,j}(\delta_{i,k}-\Gamma_{i,k}) = \Gamma_{k,k}\Gamma_{i,j} + \Gamma_{k,j}\delta i,k - \Gamma_{k,j}\Gamma_{i,k}.\end{aligned} \tag{D.16}$$

Putting everything together we get

$$\langle(1-c_k^\dagger c_k)c_i^\dagger c_j(1-c_k^\dagger c_k)\rangle = \Gamma_{i,j}-\Gamma_{i,k}\delta_{j,k}-\Gamma_{k,j}\delta_{i,k}+\Gamma_{i,k}\Gamma_{k,j}-\Gamma_{k,k}\Gamma_{i,j}+\Gamma_{k,k}\delta_{i,k}\delta_{j,k}. \tag{D.17}$$

Adding and subtracting $\delta_{i,k}\delta_{j,k}$ to this expression we get

$$\langle(1-c_k^\dagger c_k)c_i^\dagger c_j(1-c_k^\dagger c_k)\rangle = (1-\Gamma_{k,k})\Gamma_{i,j}-(1-\Gamma_{k,k})\delta_{i,k}\delta_{j,k}+(\delta_{i,k}-\Gamma_{i,k})(\delta_{j,k}-\Gamma_{j,k}). \tag{D.18}$$

Therefore the correlation matrix if the outcome of the measurement is zero is:

$$\Gamma_{i,j}(t) = \Gamma_{i,j}(t) - \delta_{i,k}\delta_{j,k} + \frac{(\delta_{i,k}-\Gamma_{i,k})(\delta_{j,k}-\Gamma_{k,j})}{1-\Gamma_{k,k}} \tag{D.19}$$

Appendix E

Continuous limit of the Brickwork Circuit

E.1 Dispersion and Quasiparticle Velocity

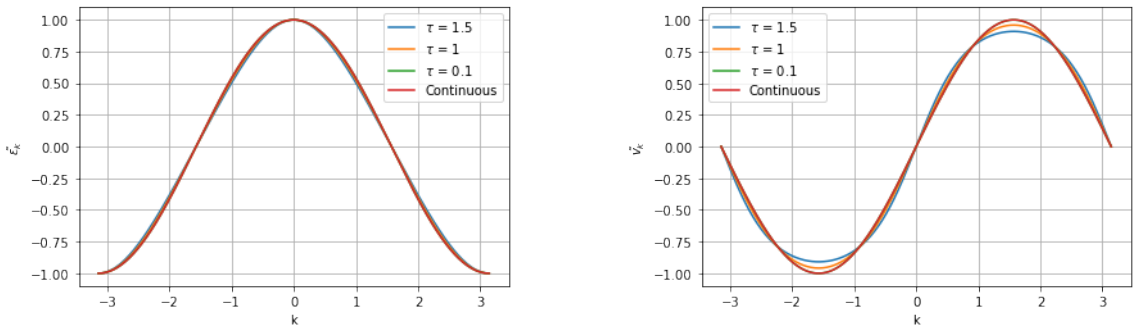

(a) *Dispersion of the brickwork evolution for* $\tau \in \{0.1, 1, 1.5\}$ *compared to the one of a continuous evolution for* $t = 30$.

(b) *Quasiparticle velocity of the brickwork evolution for* $\tau \in \{0.1, 1, 1.5\}$ *compared to the one of a continuous evolution for* $t = 30$.

Figure E.1: *Comparison between the dispersion and the quasiparticle velocity of the brickwork evolution and the continuous evolution.*

In Sec. 3.3 we have introduced the brickwork evolution. We then trotterized this evolution (Eq. (3.35)) and proved that, in the limit of $M \to \infty$, this is equivalent to the Hamiltonian evolution in Sec. 3.2.

In Sec. 3.2.1 we introduced a semi-classical interpretation for the entanglement entropy evolution, which proved itself to be a good instrument to estimate the entanglement entropy. Therefore in Sec. 3.3.1 we tried to apply this interpretation also to the brick-

work evolution. However this was not immediate. Indeed in the continuous evolution we have an explicit Hamiltonian, which can be diagonalized to extract the quasiparticle velocity. This is not true in the brickwork case, where the evolution is governed by the evolution operators Eq. (3.37), (3.36). Hence we had to find a global evolution operator (Eq. (3.70)) and reintroduce a time variable (Eq. (3.72)) in order to extract an effective Hamiltonian to diagonalize and thus get the dispersion (Eq. (3.76)) and the quasiparticle velocity (Eq.(3.77)). Since $\tau = t/M$, if everything has been done correctly, in the limit $\tau \to 0$, i.e. $M \to \infty$, we have that $\tilde{\epsilon_k} = \epsilon_k/\tau$ and $\tilde{v_k} = v_k/\tau$ should tend to their counterparts of the continuous case (Eq. (A.10), (3.21)).

This is shown in Fig. E.1, where it is clear how for $\tau \to 0$ both the dispersion and the quasiparitcle velocity tend to the one of the continuous case.

E.2 Yang-Yang Entorpy

In Sec. 3.2.1 we showed that the Yang-Yang entropy for the continuous case is $H(n_k) = 1$ $\forall\ k \in [-\pi, \pi]$, whereas in Sec. 3.3.1 we showed that this is not the case for the brickwork evolution, where the Yang-Yang entropy takes is the one in Eq. (3.83). However this quantity must converge to 1. τ appears in the Yang-Yang entropy via ϕ_p (Eq. (3.62)), thus we study the limit $\tau \to 0$ for this quantity:

$$\begin{aligned} \phi_p &= \arctan \frac{\sin^2(\alpha\tau)\sin(2k)}{\sin(2\alpha\tau)\cos(k)} = \arctan\Big(\frac{\sin^2(\alpha\tau)}{2\sin(\alpha\tau)\cos(\alpha\tau)}\frac{2\sin(k)\cos(k)}{\cos(k)}\Big) \\ &= \arctan\Big(\tan(\alpha\tau)\sin(k)\Big) \xrightarrow{\tau\to 0} \arctan(0) = 0. \end{aligned} \tag{E.1}$$

Thus Eq. (3.83) yields $H(n_k) = 1\ \forall\ k \in [-\pi, \pi]$ in the limit $\tau \to 0$.

E.3 Final Benchmark

Finally, to see that all is consistent, we compare the entanglement entropy with the quasiparticle picture from the continuous and the brickwork case. If all has been done well, for a large enough M, the two plots should overlap. This is done in a system with $L = 70$, $l = 5$, setting $\alpha = 1/2$. The result is displayed in Fig. E.2, showing how the brickwork quasiparticle picture is consistent with the continuous one in the limit of large M.

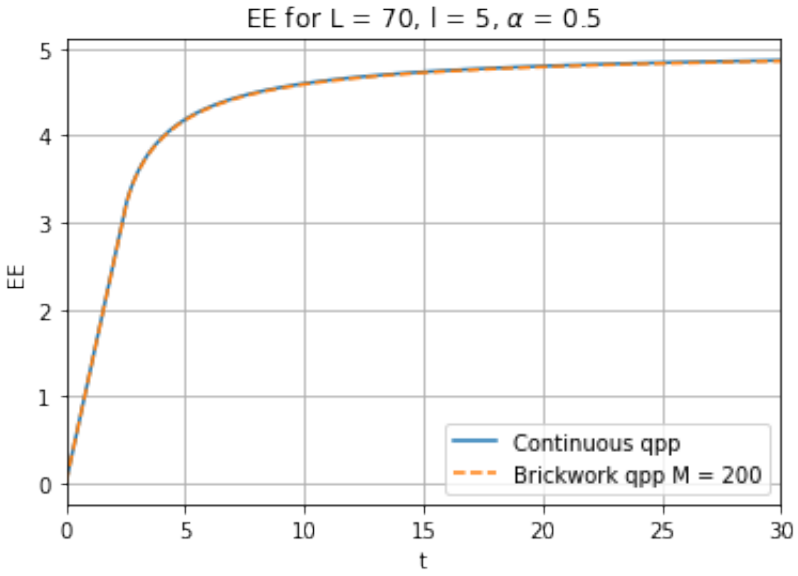

Figure E.2: *Comparison between the entanglement entropy computed with the quasiparticle picture in the continuous and in the brickwork evolution, for* $M = 200$.

Appendix F

Measurement Operators

In this appendix we give the proofs of some formulas appearing in Sec. 4.3.

Completeness relation of the measurement operators We start with the proof that $V_1^{(k)}$ and $V_2^{(k)}$ (Eq. (4.8),(4.9)) are good measurement operators, namely that

$$V_1^{(k)\dagger} V_1^{(k)} + V_2^{(k)\dagger} V_2^{(k)} = I. \tag{F.1}$$

Proof. This is a direct computation (we omit the indexes k):

$$V_1^\dagger V_1 + V_2^\dagger V_2 = \frac{e^{-\epsilon}}{2\cosh(\epsilon)} e^{2\epsilon c^\dagger c} + \frac{e^{\epsilon}}{2\cosh(\epsilon)} e^{-2\epsilon c^\dagger c}.$$

We can now use the fact that the matrix representation of $c_k^\dagger c_k$ is an $L \times L$ matrix C, where L is the number of sites in the chain, with all zero entries, except for the matrix element $C_{k,k} = 1$. Since this matrix is diagonal, its exponential will also be diagonal, with $\exp[\pm 2\epsilon C] = \mathrm{diag}(1, \ldots, 1, e^{\pm 2\epsilon}, 1, \ldots, 1)$, where the diagonal element different from one is in row k and column k. For the sake of readability, let's assume $k = 1$, but the following steps hold true $\forall\ k \in [1, L]$.

$$\begin{aligned} V_1^\dagger V_1 + V_2^\dagger V_2 &= \frac{e^{-\epsilon}}{2\cosh(\epsilon)} \begin{pmatrix} e^{2\epsilon} & & & \\ & 1 & & \\ & & \ddots & \\ & & & 1 \end{pmatrix} + \frac{e^{\epsilon}}{2\cosh(\epsilon)} \begin{pmatrix} e^{-2\epsilon} & & & \\ & 1 & & \\ & & \ddots & \\ & & & 1 \end{pmatrix} \\ &= \frac{2}{2(e^\epsilon + e^{-\epsilon})} \begin{pmatrix} e^\epsilon + e^{-\epsilon} & & & \\ & e^\epsilon + e^{-\epsilon} & & \\ & & \ddots & \\ & & & e^\epsilon + e^{-\epsilon} \end{pmatrix} \\ &= I \end{aligned}$$

□

Outcome probabilities Here we prove Eq. (4.14).

Proof. Following the measurement postulate Eq. (1.98), using the formal definition of the exponential function and the fact that $(c^\dagger c)^n = c^\dagger c \;\forall\; n \in [1, \infty)$, we have that (omitting the index k):

$$\begin{aligned} p(1) &= \langle\psi|V_1^\dagger V_1|\psi\rangle = \langle\psi|\frac{e^{-\epsilon}}{2\cosh(\epsilon)}e^{2\epsilon c^\dagger c}|\psi\rangle = \frac{e^{-\epsilon}}{2\cosh(\epsilon)}\langle\psi|\sum_{n=0}^{\infty}\frac{(2\epsilon c^\dagger c)^n}{n!}|\psi\rangle \\ &= \frac{e^{-\epsilon}}{2\cosh(\epsilon)}\langle\psi|1 + (2\epsilon)c^\dagger c + \frac{(2\epsilon)^2}{2!}c^\dagger c + \ldots|\psi\rangle \\ &= \frac{e^{-\epsilon}}{2\cosh(\epsilon)}\langle\psi|1 - c^\dagger c + c^\dagger c + (2\epsilon)c^\dagger c + \frac{(2\epsilon)^2}{2!}c^\dagger c + \ldots|\psi\rangle \\ &= \frac{e^{-\epsilon}}{2\cosh(\epsilon)}\langle\psi|1 - c^\dagger c + \sum_{n=0}^{\infty}\frac{(2\epsilon)^n}{n!}c^\dagger c|\psi\rangle \\ &= \frac{e^{-\epsilon}}{2\cosh(\epsilon)}\big(\langle\psi|\psi\rangle + (e^{2\epsilon} - 1)\langle\psi|c^\dagger c|\psi\rangle\big). \end{aligned} \tag{F.2}$$

Reintroducing the index k we get:

$$p_k(1) = \frac{e^{-\epsilon}}{2\cosh(\epsilon)}\big(1 + (e^{2\epsilon} - 1)\Gamma_{k,k}\big). \tag{F.3}$$

For the operator $V_2^{(k)}$ the calculations are analogous. □

Bibliography

[1] L. D'Alessio, Y. Kafri, A. Polkovnikov, and M. Rigol, From quantum chaos and eigenstate thermalization to statistical mechanics and thermodynamics, *Advances in Physics* **65** 239 (2016).

[2] D. A. Abanin, E. Altman, I. Bloch, and M. Serbyn, Colloquium : Many-body localization, thermalization, and entanglement, *Reviews of Modern Physics* **91** (2019).

[3] M. Fagotti and P. Calabrese, Evolution of entanglement entropy following a quantum quench: Analytic results for the XY chain in a transverse magnetic field, *Physical Review A* **78** (2008).

[4] A. C. Potter and R. Vasseur. In: Entanglement Dynamics in Hybrid Quantum Circuits. 211. (Springer International Publishing, 2022). ISBN: 9783031039980, DOI: 10.1007/978-3-031-03998-0_9, URL: http://dx.doi.org/10.1007/978-3-031-03998-0_9.

[5] P. Calabrese and J. Cardy, Evolution of entanglement entropy in one-dimensional systems, *Journal of Statistical Mechanics: Theory and Experiment* **2005** P04010 (2005).

[6] P. Calabrese and J. Cardy, Entanglement entropy and conformal field theory, *Journal of Physics A: Mathematical and Theoretical* **42** 504005 (2009).

[7] I. M. Georgescu, S. Ashhab, and F. Nori, Quantum simulation, *Reviews of Modern Physics* **86** 153 (2014).

[8] J. Preskill, Quantum Computing in the NISQ era and beyond, *Quantum* **2** 79 (2018).

[9] M. P. Fisher, V. Khemani, A. Nahum, and S. Vijay, Random Quantum Circuits, *Annual Review of Condensed Matter Physics* **14** 335 (2023).

[10] M. A. Nielsen and I. L. Chuang. Quantum Computation and Quantum Information: 10th Anniversary Edition. (Cambridge University Press, 2011).

[11] M. Rigol, V. Dunjko, and M. Olshanii, Thermalization and its mechanism for generic isolated quantum systems, *Nature* **452** 854 (2008).

[12] B. Skinner, J. Ruhman, and A. Nahum, Measurement-Induced Phase Transitions in the Dynamics of Entanglement, *Physical Review X* **9** (2019).

[13] Y. Li, X. Chen, and M. P. A. Fisher, Quantum Zeno effect and the many-body entanglement transition, *Physical Review B* **98** (2018).

[14] C.-M. Jian, Y.-Z. You, R. Vasseur, and A. W. W. Ludwig, Measurement-induced criticality in random quantum circuits, *Physical Review B* **101** (2020).

[15] Y. Bao, S. Choi, and E. Altman, Theory of the phase transition in random unitary circuits with measurements, *Physical Review B* **101** (2020).

[16] Y. Li, X. Chen, and M. P. A. Fisher, Measurement-driven entanglement transition in hybrid quantum circuits, *Physical Review B* **100** (2019).

[17] A. Chan, R. M. Nandkishore, M. Pretko, and G. Smith, Unitary-projective entanglement dynamics, *Physical Review B* **99** (2019).

[18] X. Cao, A. Tilloy, and A. De Luca, Entanglement in a fermion chain under continuous monitoring, *SciPost Physics* **7** (2019).

[19] A. Zabalo, M. J. Gullans, J. H. Wilson, S. Gopalakrishnan, D. A. Huse, and J. H. Pixley, Critical properties of the measurement-induced transition in random quantum circuits, *Physical Review B* **101** (2020).

[20] A. Zabalo, M. J. Gullans, J. H. Wilson, R. Vasseur, A. W. W. Ludwig, S. Gopalakrishnan, D. A. Huse, and J. H. Pixley, Operator Scaling Dimensions and Multifractality at Measurement-Induced Transitions, *Physical Review Letters* **128** (2022).

[21] C. Noel et al., Measurement-induced quantum phases realized in a trapped-ion quantum computer, *Nature Physics* **18** 760 (2022).

[22] J. M. Koh, S.-N. Sun, M. Motta, and A. J. Minnich, Measurement-induced entanglement phase transition on a superconducting quantum processor with mid-circuit readout, *Nature Physics* **19** 1314 (2023).

[23] D. J. Brod, Efficient classical simulation of matchgate circuits with generalized inputs and measurements, *Physical Review A* **93** (2016).

[24] M. Coppola, E. Tirrito, D. Karevski, and M. Collura, Growth of entanglement entropy under local projective measurements, *Physical Review B* **105** (2022).

[25] M. Fava, L. Piroli, D. Bernard, and A. Nahum, *A tractable model of monitored fermions with conserved* U(1) *charge*, 2024, arXiv: 2407.08045 [cond-mat.stat-mech], URL: https://arxiv.org/abs/2407.08045.

[26] F. Franchini. An Introduction to Integrable Techniques for One-Dimensional Quantum Systems. (Springer International Publishing, 2017). DOI: 10.1007/978-3-319-48487-7, URL: http://dx.doi.org/10.1007/978-3-319-48487-7.

[27] J. Surace and L. Tagliacozzo, Fermionic Gaussian states: an introduction to numerical approaches, *SciPost Physics Lecture Notes* (2022).

[28] P. Calabrese, Entanglement spreading in non-equilibrium integrable systems, *SciPost Physics Lecture Notes* (2020).

[29] G. B. Mbeng, A. Russomanno, and G. E. Santoro, *The quantum Ising chain for beginners*, 2020, arXiv: 2009.09208 [quant-ph].

[30] R. Jozsa and A. Miyake, Matchgates and classical simulation of quantum circuits, *Proceedings of the Royal Society A: Mathematical, Physical and Engineering Sciences* **464** 3089 (2008).

[31] L. G. Molinari, *Notes on Wick's theorem in many-body theory*, 2023, arXiv: 1710.09248.

[32] G. Vidal, J. I. Latorre, E. Rico, and A. Kitaev, Entanglement in Quantum Critical Phenomena, *Physical Review Letters* **90** (2003).

[33] M. B. Plenio and P. L. Knight, The quantum-jump approach to dissipative dynamics in quantum optics, *Reviews of Modern Physics* **70** 101 (1998).

[34] A. J. Daley, Quantum trajectories and open many-body quantum systems, *Advances in Physics* **63** 77 (2014).

[35] M. Vojta, Quantum phase transitions, *Reports on Progress in Physics* **66** 2069 (2003).

[36] G. Mussardo. Statistical field theory: an introduction to exactly solved models in statistical physics. (Oxford Univ. Press, New York, NY, 2010).

[37] A. Nahum, S. Roy, B. Skinner, and J. Ruhman, Measurement and Entanglement Phase Transitions in All-To-All Quantum Circuits, on Quantum Trees, and in Landau-Ginsburg Theory, *PRX Quantum* **2** (2021).

[38] M. Fava, L. Piroli, T. Swann, D. Bernard, and A. Nahum, Nonlinear Sigma Models for Monitored Dynamics of Free Fermions, *Physical Review X* **13** (2023).

[39] Y. Li, X. Chen, A. W. W. Ludwig, and M. P. A. Fisher, Conformal invariance and quantum nonlocality in critical hybrid circuits, *Physical Review B* **104** (2021).

[40] M. Szyniszewski, A. Romito, and H. Schomerus, Entanglement transition from variable-strength weak measurements, *Physical Review B* **100** (2019).

[41] F. R., Simulating Physics with Computers, *Int. J. Theor. Phys. 21* 467 (1982).

[42] S. Lloyd, Universal Quantum Simulators, *Science* **273** 1073 (1996).

[43] R. Modak, V. Alba, and P. Calabrese, Entanglement revivals as a probe of scrambling in finite quantum systems, *Journal of Statistical Mechanics: Theory and Experiment* **2020** 083110 (2020).

[44] T. Barthel and U. Schollwöck, Dephasing and the Steady State in Quantum Many-Particle Systems, *Physical Review Letters* **100** (2008).

[45] M. Cramer, C. M. Dawson, J. Eisert, and T. J. Osborne, Exact Relaxation in a Class of Nonequilibrium Quantum Lattice Systems, *Phys. Rev. Lett.* **100** 030602 (2008).

[46] M. Cramer and J. Eisert, A quantum central limit theorem for non-equilibrium systems: Exact local relaxation of correlated states, *New Journal of Physics* **12** (2010).

[47] P. Calabrese, F. H. L. Essler, and M. Fagotti, Quantum quenches in the transverse field Ising chain: II. Stationary state properties, *Journal of Statistical Mechanics: Theory and Experiment* **2012** P07022 (2012).

[48] M. Fagotti and F. H. L. Essler, Reduced density matrix after a quantum quench, *Phys. Rev. B* **87** 245107 (2013).

[49] J. M. Deutsch, Quantum statistical mechanics in a closed system, *Phys. Rev. A* **43** 2046 (1991).

[50] M. Srednicki, Chaos and quantum thermalization, *Physical Review E* **50** 888 (1994).

[51] M. Rigol and M. Srednicki, Alternatives to Eigenstate Thermalization, *Physical Review Letters* **108** (2012).

[52] M. Rigol, V. Dunjko, V. Yurovsky, and M. Olshanii, Relaxation in a Completely Integrable Many-Body Quantum System: An Ab InitioStudy of the Dynamics of the Highly Excited States of 1D Lattice Hard-Core Bosons, *Physical Review Letters* **98** (2007).

[53] L. Bucciantini, M. Kormos, and P. Calabrese, Quantum quenches from excited states in the Ising chain, *Journal of Physics A: Mathematical and Theoretical* **47** 175002 (2014).

[54] E. H. Lieb and D. W. Robinson, The finite group velocity of quantum spin systems, *Commun. Math. Phys.* **28** 251 (1972).

[55] V. Alba, B. Bertini, M. Fagotti, L. Piroli, and P. Ruggiero, Generalized-hydrodynamic approach to inhomogeneous quenches: correlations, entanglement and quantum effects, *Journal of Statistical Mechanics: Theory and Experiment* **2021** 114004 (2021).

[56] S. Sotiriadis and P. Calabrese, Validity of the GGE for quantum quenches from interacting to noninteracting models, *Journal of Statistical Mechanics: Theory and Experiment* **2014** P07024 (2014).

[57] E. Vernier, B. Bertini, G. Giudici, and L. Piroli, Integrable Digital Quantum Simulation: Generalized Gibbs Ensembles and Trotter Transitions, *Physical Review Letters* **130** (2023).

[58] B. Bertini, M. Fagotti, L. Piroli, and P. Calabrese, Entanglement evolution and generalised hydrodynamics: noninteracting systems, *Journal of Physics A: Mathematical and Theoretical* **51** 39LT01 (2018).

[59] O. Alberton, M. Buchhold, and S. Diehl, Entanglement Transition in a Monitored Free-Fermion Chain: From Extended Criticality to Area Law, *Physical Review Letters* **126** (2021).

[60] M. Fava, L. Piroli, T. Swann, D. Bernard, and A. Nahum, Nonlinear Sigma Models for Monitored Dynamics of Free Fermions, *Phys. Rev. X* **13** 041045 (2023).

[61] N. O'Dea, A. Morningstar, S. Gopalakrishnan, and V. Khemani, Entanglement and absorbing-state transitions in interactive quantum dynamics, *Physical Review B* **109** (2024).